IAAST INT'L CONFERENCE

International Conference on Biotechnology, Nanotechnology and Environmental Engineering (ICBNE'15)

April 22-23, 2015 Bangkok (Thailand)

EDITORS:
Prof. Dr. Md. Aminur Rahman
Prof. Dr. Akos Lakatos

ISBN 978-93-84468-21-7

Organized By

International Academy of Arts, Science & Technology
www.iaast.org

Suwarto

IAAST Int'l Conference Proceedings

of

International Conference on Biotechnology, Nanotechnology and Environmental Engineering (ICBNE'15)

April 22-23, 2015

Bangkok (Thailand)

Editors:

Prof. Dr. Md. Aminur Rahman

Prof. Dr. Akos Lakatos

ISBN 978-93-84468-21-7

Organized By:

International Academy Of Arts, Science & Technology

www.iaast.org

Program Committee (ICBNE'15)

Conference Chair

Prof. Bülent TOPCUOGLU, Akdeniz University, Vocational School of Technical Sciences, Antalya, Turkey

Prof. Dr. Jimmy (C.M.) Kao, Distinguished Professor, National Sun Yat-Sen University, National Science Council, Taiwan

Prof. Dr. Akos Lakatos, University of Debrecen, Faculty of Engineering, Debrecen, Hungary

Dr. Md. Aminur Rahman, Institute of Bioscience, Universiti Putra Malaysia (UPM),Selangor Darul Ehsan, Malaysia

Co-Chair

Dr. Yogesh Kumar Gupta, Professor and Head Department of Chemistry, B. K. Birla Institute of Engineering and Technology, PILANI, India

Prof. Dr. Heecheul Kim, Dept. of Architectural Engineering , Kyung Hee University, Deogyeong-daero, Giheung-gu, Gyeonggi-do, Korea

Prof. Dr. Jagmohan Oberoi, Director, Ganpati Group Of Institutions Bilaspur (Yamuna Nagar) Haryana, India

Prof. Dr. Parvinder S. Sandhu, Rayat-Bahra University, India

Dr. Saji Baby, Environmental Manager (Research and Consultation) & Principal Scientist, GEO Environmental Consultation, Kuwait

Technical Committee

Prof. Dr. Ming-Hsiang Shih, Professor, Department of Civil Engineering, National Chi Nan University, Taiwan

Dr. V. Duraipandiyan, Division of Ethnopharmacology, Entomology Research Institute, Loyola College, Chennai, India

Dr. Bulent Acma, Anadolu University, Department of Economics, Eskisehir, Turkey

Asso. Prof. Dr. Yu-Kuang Zhao, Department of Refrigeration, Air Condition and Energy Engineering, National Chin-Yi University of Technology, Taiwan

Dr. Zetty Norhana Balia Yusof, Faculty of Biotechnology and Biomolecular Sciences, Universiti Putra Malaysia, UPM, Serdang, Malaysia

Dr. C. Arunachalam, Department of Botany and Microbiology, College of Science, King Saud University, Riyadh, Kingdom of Saudi Arabia

Assoc. Prof. Dr. Jagadish H Patil, Associate Professor, R V College Of Engineering, Bangalore, India

Mohammad Hadi Bazrkar, Lecturer in Azad University, Iran

Dr. Imene Yahyaoui, Departamento Ingenieria de Automatica y Sistemas (ISA), Escuela de Ingenieria Industriale, Sede Mergelina, Valladolid, Espana

Prof. Sudhakar YEDLA, Professor, Indira Gandhi Institute of Development Research (IGIDR), Mumbai, India

Dr. Emhemmed Abdullah Alhibshi, Faculty of Science, Aljabel Algharbi University, Libya

Program Committee (ICBNE'15) Contd.

Dr. Mohammad Jawad Al-Jassani, Lecturer, Babylon University, Iraq

Assist. Prof. Dr. Benouis Khedidja, University of Djillali Liabes – Sidi Bel Abbes - Algeria

Assoc. Prof. Dr.G.P.Ganapathy, VIT University, India

Dr. ABHILASH, Scientist, CSIR-National Metallurgical Laboratory, Jamshedpur, INDIA

Assoc. Prof. Dr. Shih- Heng Tung, Associate Professor, Department of Civil and Environmental Engineering, National University of Kaohsiung, Taiwan

Dr. Qusaie Ebrahim Karam, Kuwait Institute for Scientific Research, Kuwait

Associate Professor Dr. Neha Mathur, Govt. P.G. College, Dausa (Rajasthan), India

Associate Professor Fawzi Irshaid, Al al-bayt University, Al-Mafraq, Jordan

Dr. Hussein Oleiwi Muttaleb Al-Dahmoshi, Babylon University, Iraq

Assoc. Prof. Dr. Zawawi Bin Daud, Faculty of Civil and Environmental Engineering, Universiti Tun Hussein Onn Malaysia (UTHM), Parit Raja, Batu Pahat Johor, Malaysia

Dr. Ayman Batisha, International Sustainability Institute, Egypt

Loren Grace F. Jaranilla, Instructor 3, Father Saturnino Urios University, Butuan City, Philippines

PREFACE

Dear Distinguished Delegates, Colleagues and Guests,

The IAAST Organizing Committee warmly welcomes our distinguished delegates and guests at International Conference on Biotechnology, Nanotechnology and Environmental Engineering (ICBNE'15) scheduled on *April 22-23, 2015 Bangkok (Thailand).* The main themes and track of ICBNE'15 are Biotechnology, Nanotechnology and Environmental.

These conferences are managed and sponsored by International Academy of Arts, Science & Technology (IAAST) and assisted by University of Johannesburg and University of Quebec. IAAST is striving hard to compile the research efforts of scientists, researchers and academicians across the broad spectrum of Science, Engineering and Technology. These conferences are aimed at discussing the wide range of problems encountered in present and future high technologies among the research fraternity.

The conferences are organized to bring together the members of our international community at a common platform, so that, the researchers from around the world can present their leading-edge work. This will help in expansion of our community's knowledge and provide an insight into the significant challenges currently being addressed in that research. The conference Program Committee is itself quite diverse and truly international, with membership from the America, Australia, Europe, Asia and Africa.

The conference has solicited and gathered technical research submissions related to all aspects of major conference themes and tracks. This proceeding records the fully refereed papers presented at the conference.

All the submitted papers in the proceeding have been peer reviewed by the reviewers drawn from the scientific committee, external reviewers and editorial board depending on the subject matter of the paper. Reviewing and initial selection were undertaken electronically. After the rigorous peer-review process, the submitted papers were selected on the basis of originality, significance, and clarity for the purpose of the conference. The main goal of these events is to provide international scientific forums for exchange of new ideas in a number of fields that interact in-depth through discussions with their peers from around the world.

The program has been structured to favor interactions among attendees coming from many diverse horizons, scientifically, geographically, from academia and from industry. We would like to thank the program chairs, organization staff, and the members of the program committee for their work. We like to thank and show gratitude to Editors from IAAST. We are grateful to all those who have contributed to the success of IAAST *April 22-23, 2015(Bangkok (Thailand))* Conference. We hope that all participants and other interested readers benefit scientifically from the proceedings and also find it stimulating in the Process in their quest of achieving greater

heights. Finally, we would like to wish you success in your technical presentations and social networking.

We hope you have a unique, rewarding and enjoyable week at IAAST Conferences at vibrant Bangkok (Thailand).

With our warmest regards,

Organizing Committee

April 22-23, 2015
Bangkok (Thailand)

INDEX

International Conference on Biotechnology, Nanotechnology and Environmental Engineering (ICBNE'15) April 22-23, 2015 Bangkok (Thailand)

SECTION-I

SECTION-I

International Conference on Biotechnology, Nanotechnology and Environmental Engineering (ICBNE'15)

Production of Organic Matter *In Situ* for Sustainability High Productivity on Cassava Field

Suwarto

Abstract— Real productivity of cassava in Indonesia is 16.6-21.4 tons/ha whereas the potential productivity is 24.8-30.4 tons/ha. The low productivity has been a problem in developing cassava-based industries. Formation and enlargement of cassava tubers need loose, fertile and high C-organic of soil. C-organic of the soil should be not less than 2%. To increase C-organic of the soil at about 2-4% will be needed organic fertilizers of 20-40 tons/ha. Organic matter produced 'in situ' of the cassava field was 5.92-21.28 tons/ha (1.60-5.28 tons/ha in dry weight) which contributed average at 0.5% in increasing soil C-organic. Besides, the organic matter contains some important nutrients such are N, P, K, Ca, Mg. All nutrients produced 'in situ' were sufficient for Adira-1. All nutrients were also sufficient for Adira-4, except K. Nutrient of P and K were insufficient for Malang-4 and UJ-5. Nutrient of P and Mg were only sufficient Adira-1 and Adira-4.

Keywords— *organic matter, production, cassava, in situ, sustainability.*

I. Introduction

Cassava is one of the crops for food, feed and industry. The harvested area of cassava Indonesia in 2012 was 1,129,688 ha with a production of 24,177 million tons and productivity of 21.402 ton/ha (BPS 2013). Cassava is a plant that still can grow well in poor soils when other plants are not able to grow and produce. However, to obtain high yields and sustainable, fertilizing should be done correctly. Fertilizers can be provided either inorganic or organic.

Cassava plants require optimum growing medium to grow and produce maximally. Fertile soil is the optimum growing media and organic matter plays an important role in determining the fertility of the soil. Observations made by [1], cassava 'Ratim' (the local name in West Halmahera) produces 15 kg of tubers per plant when organic matter content reaches 3:17%, if the soil organic matter content below 2% only produce tubers 5 kg per plant.

To increase soil organic C content of at least 2%, organic material needs to be added is 20-40 tons/ha. The problem is the supply of organic material and its application in cassava cultivation is not easy. One alternative is to produce organic materials 'in situ'. According to [2] Production of organic material 'in situ' would facilitate its application and cost-saving and environmentally friendly. Organic material 'in situ' can be obtained from the leaves, stems and roots of major crops and intercropped. Legumes such as yam bean (Pachyrhizus erosus (L) Urban) can be intercropped with cassava [3]. Yam can be a source of organic matter and have a positive impact on the environment, which are (1) high efficiency of nitrogen fixation and increase the vigor of the plants in surrounding areas (especially in poor soil), (2) tolerance to drought, (3) effectively control soil erosion [4]. This study has been conducted to determine the production of organic matter of some varieties of cassava monoculture and intercropping with yam.

Suwarto is Lecturer, Department of Agronomy and Agriculture, Faculty of Agriculture, Bogor Agricultural University, Indonesia

II. Materials And Methods

The experiment was conducted using a split plot design. The main plots were four varieties of cassava (Adira-1, Adira-4, Malang-4, and UJ-5). The subplots were monoculture cropping systems and intercropping with yam bean. Each treatment was repeated four times so that there were 32 experimental plots. The size of each experimental plot was 4 m x 10 m with a population of 40 plants. In each plot were determined five plants as a plant sample. Spacing of cassava is 1 m × 1 m. Cassava plants fertilized with a dose of 67.5 kg N, 54 kg P2O5 and 60 kg K2O per hectare [5]. At 3 months old of cassava, yam bean grown between the cassava with a spacing of 20 cm x 20 cm. The distance between the first yam bean and cassava is 30 cm. There were 9 yam beans and 1 cassava in the area of one square meter in intercropping systems. Yam bean fertilized with a dose of 59 kg N, 14 kg P2O5, and 30 kg K2O per hectare. Weed control was done once a month during the growing season. Pest and disease control was done as needed.

Variables measured were: (1) number of attached leaves at 2, 4, 5, 7 months after planting (MAP), (2) dry weight of leaves fall a month at 3, 4, 5, 6, 7 MAP, (3) total number and dry weight of leaves fall, (4) fresh and dry weight of cassava biomass at harvest, (5) dry weight biomass of yam bean, (6) fresh weight of cassava tubers per plant, (7) fresh weight of cassava tubers per plot, (8) weight of yam bean tubers per plot, (9) weight of dry biomass of yam bean, and (10) soil properties. The cassava and yam bean biomass mean all part of the plant without tubers.

cassava tubers per plot, (8) weight of yam bean tubers per plot, (9) weight of dry biomass of yam bean, and (10) soil properties. The cassava and yam bean biomass mean all part of the plant without tubers.

The collected data were analyzed using analysis of variance (F-test). Then, continued using Duncan's Multiple Range Test at 5% level to determine significantly effect of the treatments.

III. Results And Discussion

Organic Matter Production, Soil C-Organic, and Soil Nutrient Supply

Sources of organic matter in situ on cassava field were plant biomass. Production of organic matter differs between varieties. Adira-1 produces the highest biomass, followed by Adira-4, UJ-5, and Malang-4. The amount of biomass produced will determine the amount of organic material that can be restored to the land. Reference [6] explains that when cassava stem is returned to the land, the total uptake of N that can be returned to the ground will be a lot due to the accumulation of nutrients in the stems reach 76% of the total uptake of N. According [7] organic fertilizer is a slow-release and can improve the availability of nutrients in the soil.

The biomass of the cassava field consisted of 60% of stem and of all attached leaves on the stem at harvest and leaves fall during the growing season. At harvest time, the weight of fresh and dry biomass of Adira-1 was the highest. In monoculture were 2.23 kg/plant and 0.54 kg/plant and in intercropping were 2.66 kg and 0.66 kg/plant (Table 1). In contrast, the weight of fresh and dry biomass of Malang-4 was the lowest; in monoculture were 0.74 kg/plant and 0.20 kg / plant and in intercropping were 0.94 kg/plant and 0.26 kg/plant. The weight of fresh biomass that was resulted per hectare was estimated to range between 5.92-21.28 tons.

TABLE I
BIOMASS PRODUCTION OF CASSAVA AT HARVEST

Variety	Cropping System	Biomass Weight			
		Fresh	Dry	Fresh	Dry
		.....kg/plant.... (a)		....ton/ha*)..... (b)	
Adira-1	Mnc	2.23a	0.54a	17.8a	4.32a
	Intc	2.66a	0.66a	21.3a	5.28a
Adira 4	Mnc	1.42b	0.34b	11.4b	2.72b
	Intc	1.56b	0.44b	12.5b	3.52b
Malang-4	Mnc	0.74c	0.20c	5.92c	1.60c
	Intc	0.94c	0.26c	7.52c	2.08c
UJ-5	Mnc	1.23b	0.34b	9.84b	2.72b
	Intc	1.27b	0.36b	10.2b	2.86b

Note: figure in the same column followed by the same alphabet is not significantly different at DMRT 5%; Mnc= monoculture, Intc=intercropping. *) estimated by formula: b= 0.8*10000*a/1000

In addition to stem and leaf biomass at harvest, the organic matter in the cassava field derived from fallen leaves during the growing season. The fallen leaves were determined by the number of attached leaves. The number of attached leaves at 2, 4, 5, and 7 MAP is showed in Table 2. There was a relationship between the number of attached leaves and the number of fallen leaves. The number and the weight of fallen leaves during the age of 2-7 MAP can be seen in Table 3. The number and dry weight of leaf fall was influenced by the characteristics of the variety. According to the description of variety [8], Adira-1 has branching and produce more leaves than others.

TABLE II
NUMBER OF ATTACHED LEAVES OF CASSAVA

Varieties	Cropping Sys	Attached Leaves/Plant			
		2 MAP	4 MAP	5 MAP	7 MAP
Adira-1	Mnc	54.8	118.2a	153.9a	243.0a
	Intc	54.0	122.3a	153.3a	279.7a
Adira 4	Mnc	49.4	102.5b	78.0b	140.7b
	Intc	45.4	102.6b	89.7b	145.9b
Malang-4	Mnc	46.2	90.4c	60.8c	80.7c
	Intc	50.6	99.8c	62.3c	82.7c
UJ-5	Mnc	49.8	91.3c	76.0b	86.0c
	Intc	51.1	92.7c	77.4b	91.5c

Note: figure in the same column followed by the same alphabet is not significantly different at DMRT 5%; Mnc= monoculture, Intc=intercropping. *) estimated by formula: b= 0.8*10000*a/1000

According to the description of varieties [8], Adira-1 has branching and produce more leaves than others. As a result, the number and dry weight of fallen leaves of Adira-1 was higher than others.

TABLE III
NUMBER AND WEIGHT OF FALLEN LEAVES OF CASSAVA

Varieties	Cropping Sys	Leaves Fall During 2-7 MAP		
		Number of leaves	Dry Weight	
			....kg/plant...	...tons/ha*)...
Adira-1	Mnc	401.10a	0.259a	2.072a
	Intc	390.85a	0.237a	1.896a
Adira 4	Mnc	202.33b	0.212b	1.696b
	Intc	204.20b	0.201b	1.608b
Malang-4	Mnc	168.25c	0.162c	1.296c
	Intc	179.48c	0.197c	1.576c
UJ-5	Mnc	148.15d	0.175c	1.400c
	Intc	148.18d	0.178c	1.424c

Note: figure in the same column followed by the same alphabet is not significantly different at DMRT 5%; Mnc= monoculture, Intc=intercropping. *) estimated by formula: b= 0.8*10000*a/1000

C-organic of the soil showed increase at range of 0.00-0.96% due to the organic matter 'in situ' of fallen leaves (Table 4). The average C-organic of the soil increase was 0.50 % due to the average of fallen leaves of 1.62 tons/ha. If the all of organic matter 'in situ' which average were 3.14 tons/ha returned to the land, the soil C-organic is estimated will increase about 0.94%. Finally, C-organic of the soil is

predicted more than 2% and will be suitable for cassava tuber formation and enlargement.

TABLE IV
CHANGE OF SOIL-C ORGANIC DUE TO FALLEN LEAVES OF CASSAVA

Cassava Age (MAP)	Soil C-organic				
	Adira 1	Adira 4	Malang 4	UJ 5	Average
	.....%.....				
2	1.27	1.75	1.43	1.43	1.47
7	2.23	1.75	1.75	2.15	1.97
(+/-)	+0.96	0	+0.32	+0.72	+0.5

The total of organic materials production and nutrient content '*in situ*' from the biomass at harvest and the biomass of fallen leaves during the growing seasons is shown in Table 5. The nutrient content is calculated based on the nutrient content of cassava biomass [9]. N is the highest nutrient produced 'in situ', followed by Ca, K, P and Mg.

TABLE V
PRODUCTION OF ORGANIC MATTER AND ESTIMATED NUTRIENTS CONTENT

Varieties	Cropping System	Organic Matter and Nutrient Content					
		Organic Matter (tons/ha)	Nutrient*) (kg/ha)				
			N	P	K	Ca	Mg
Adira-1	Mnc	6.39a	361	43	182	209	42
	Intc	7.18a	406	48	205	235	47
Adira 4	Mnc	4.42b	250	30	126	145	29
	Intc	5.13b	290	34	146	168	33
Malang-4	Mnc	2.90c	164	19	83	95	19
	Intc	3.66c	207	24	104	120	24
UJ-5	Mnc	4.12b	233	28	118	135	27
	Intc	4.28b	242	29	122	140	28

Note: figure in the same column followed by the same alphabet is not significantly different at DMRT 5%; Mnc= monoculture, Intc=intercropping. *) counted base on nutrient content of [Puttacharoen et.al, 1998]

IV. NUTRIENT SUFFICIENCY

Reference [10] estimated the amount of nutrients absorbed by cassava plants to produce fresh tubers at about 30 tons/ha were 200 kg of K, 164 kg of N, 80 kg of Ca, 31 kg of P, 31 kg of Mg, 6 kg of S, 3.6 kg of Fe, 1.35 kg of Zn and 0.14 kg of Cu. Because of the differences of tubers yields, nutrients uptake among the varieties were different (Table 6). Adira-1 produced the lowest tubers and uptake the lowest nutrients. UJ-5 was on the contrary.

TABLE VI
TUBERS YIELD AND NUTRIENT UPTAKE OF CASSAVA

Variety	Cropping System	Tubers Yield and Nutrient Uptake					
		Tubers Yield (Ton ha-1)	Nutrient Uptake (kg ha^{-1})				
			N	P	K	Ca	Mg
Adira-1	Mnc	10.84^{c}	59.3	11.2	72.3	28.9	11.2
	Intc	10.25^{c}	56.0	10.6	68.3	27.3	10.6
Adira 4	Mnc	26.03^{b}	142.3	26.9	173.5	69.4	26.9
	Intc	27.28^{b}	149.1	28.2	181.9	72.7	28.2
Malang-4	Mnc	21.75^{b}	118.9	22.5	145.0	58.0	22.5
	Intc	25.38^{b}	138.7	26.2	169.2	67.7	26.2
UJ-5	Mnc	28.85^{a}	157.7	29.8	192.3	76.9	29.8
	Intc	35.19^{a}	192.4	36.4	234.6	93.8	36.4

Note: figure in the same column followed by the same alphabet is not significantly different at DMRT 5%; Mnc= monoculture, Intc=intercropping. *) estimated by formula: b= 0.8*10000*a/1000

If the amount of nutrients produced 'in situ' (Table 5) is compared to the nutrient uptake (Table 6), there was varies in nutrient sufficiency among the varieties (Table 7). All nutrients produced 'in situ' were sufficient for Adira-1. All nutrients were also sufficient for Adira-4, except K. Nutrient of P and K were insufficient for Malang-4 and UJ-5. Nutrient of P and Mg were only sufficient for the varieties of Adira-1 and Adira-4.

TABLE VII
TUBERS YIELD AND NUTRIENT 'IN SITU' SUFFICIENCY

Variety	Cropping System	Tubers Yield and Nutrient Sufficiency					
		Tubers Yield (Ton ha-1)	Nutrient Sufficeincy (kg ha^{-1})				
			N	P	K	Ca	Mg
Adira-1	Mnc	10.84^{c}	301.7	31.8	109.7	180.1	30.8
	Intc	10.25^{c}	350.0	37.4	136.7	207.7	36.4
Adira 4	Mnc	26.03^{b}	107.7	3.1	-47.5	75.6	2.1
	Intc	27.28^{b}	140.9	5.8	-35.9	95.3	4.8
Malang-4	Mnc	21.75^{b}	45.1	-3.5	-62.0	37.0	-3.5
	Intc	25.38^{b}	68.3	-2.2	-65.2	52.3	-2.2
UJ-5	Mnc	28.85^{a}	75.3	-1.8	-74.3	58.1	-2.8
	Intc	35.19^{a}	49.6	-7.4	-112.6	46.2	-8.4

High tuber production requires high nutrient uptake. Nutrient of K was absorbed more than N, P, Ca, and Mg. The nutrient of K that was produced '*in situ*' was not enough for all varieties, except Adira-1. Nutrients deficiency was suspected to be fullfilled from the fertilizer applied and the nutrients available in the soil. The fertilizer dose 60 kg of K per hectare will fulfill almost all the need of K for all varieties, except UJ-5. Although the nutrient of N and P produced 'in situ' will be sufficient for all varieties, fertilizing of the nutrient must still be done in supporting the first growing of cassava plant. Besides, the nutrient of Mg needs to be given in planting of cassava, especially for high yielding varieties such as Malang-4 and UJ-5.

V. Intercropped Yam Bean

All the data of the biomass production and tuber yield of cassava were not influenced by the yam bean intercropped. The yam bean that has been planted on the 3 months old of the cassava planting was not growing well. Light intensity needed for the growth of yam bean was lack because of shading of the cassava canopy. Analog to [11], light use efficiency of the yam bean in the intercropping will be lower. As a result, the produced biomass of yam bean was very little (Table 8).

TABLE VIII
TUBERS AND BIOMASS PRODUCTION OF YAM BEAN INTERCROPPED WITH CASSAVA

Variety of Cassava	Yam Bean Tubers and Biomass	
	Tubers (kg/ha)	Biomass (kg/plot)
Adira-1	4.8b	0.7c
Adira-4	163.4ab	11.1b
Malang-4	354.4a	22.2a
UJ-5	182.3b	9.1b

Note: figure in the same column followed by the same alphabet is not significantly different at DMRT 5%

The variety of Adira-1 which has the most number of leaf (Table 3) caused the growth of yam bean was the lowest. The produced tuber and biomass of the yam bean were lower than intercropped with other varieties.

According to [12] some nutrients are contained in the biomass of yam bean. Those are 54.68% of C, 3.79% of N, and 0.17% of P. Therefore, if the produced biomass of the yam bean is increased, it will be important to contribute in increasing the production of organic matter 'in situ' of the cassava field.

One way to increase the biomass of yam bean 'in situ' is by regulating planting time of the yam bean in intercropping with cassava. Yam bean may be planted earlier or at the same time with the time of cassava planting to give more light which is needed by the yam bean.

VI. Conclusion

Organic matter 'in situ' could increase the C-soil organic content at average of 0.5% due to the leaf fallen only. The increasing estimated to be 0.94% if all of the biomass returned to the soil and the soil C-organic content will be more than 2%.

Organic matter 'in situ' could contribute to supply macro nutrients needed by cassava especially Nitrogen, Phosphorous, and Potassium at the various sufficient level. Nitrogen was sufficient for the all varieties. Phosphorous was sufficient for Adira-4 and Adira-4. Potassium was only sufficient for Adira-4.

Yam bean still did not contribute significantly to the organic matter production 'in situ'.

Suggestion

Besides of applying chemical fertilizer, in the purpose to maintain soil fertility and to reach high tubers yield, it is suggested the biomass produced 'in situ' should be returned to the soil. The biomass that is permitted to be removed from the field is only the stem for planting material.

References

[1] Bogor Agric.Univ. Research Team. Feasibility Study on Nursery and Cassava Plantation Development in North Halmahera. Coopertion of IPB and Hallagro Ltd. 2012

[2] Sudiarto and Gusmaini. Utilization of organic materials in situ for efficiency and sustainability of ginger cultivation. Journal of Agricultural Research, Indonesia. 2004. vol 23 (2): 37-45.

[3] Karuniawan A.. *Cultivation Status and Genetic Diversity of Yam Bean (Pachyrhizus erosus* (L.) Urban*) in Indonesia*. Göttingen (ID): Cuvillier Verlag. 2004.

[4] Sørensen M, Hoof WCH van. Plant resources of south-east asia No.9. *In*: Flach M, Rumawas F, editor. *Pachyrhizus erosus* (L.) Urban. Bogor (ID): Prosea Fondation. 1996.

[5] Suwarto, Yahya S, Handoko, Chozin MA. Competition of corn and cassava in intercropping systems. 2005. Bul Agron 33 (2): 1-7.

[6] Adjei-Nsiah S, Kuyper TW, Leeuwis C, Abekoe MK, Giller KE. Evaluating sustainable and proftable cropping sequences with cassava and four legume crops: Effects on soil fertility and maize yields in the forest/savannah transitional agro-ecological zone of Ghana. 2007. *Field Cros Reseacrh* 103: 87-97.

[7] Yuniwati ED. 2011. Determination of soil quality index in cassava as a key technology for the maintenance of land (land husbandry). Periodic Biological Research. 2011. Special Edition 7F: 47-54.

[8] [CRILT]. Description of Cassava Varieties. Crops Research Institute for Legumes and Tubers. Malang. 2001. Indonesia.

[9] S. Puttacharoen, R.H Howeler, S. Jantawat, and V. Vichukit. Nutrient uptake and soil erosion losses in cassava and six other crops in Psamment in Eastern Thailand. 1998. Field Crops Research 57:113-126.

[10] M.J.T. Norman, C.J Pearson, and P.G.E. Searle. The Ecology of Tropical Food Crops 2nd Ed. Melbourne (AU). 1995. Cambridge University Press.

[11] Suwarto. Changes in chlorophyll, specific leaf area, and light use efficiency of cassava in intercropping systems with maize. 2013. Bul Agrohorti 1 (1): 135-139. Bogor Agricultural University.

[12] R. Adawiyah. Effect of planting yam bean, sentro and return of biomass and nitrogen fertilizer on the growth and production of corn. [dissertation]. 2004. Bogor [ID]: Bogor Agricultural University.

About Author (s):

The importance to produce organic matter 'in situ' for improving sustainability high tuber yield of cassava in Indonesia.

Intestinal Controlled Delivery of Diclofenac Sodium through pH- Sensitive Hydrogel Beads

Tapan Kumar Giri

***Abstract*—**pH-sensitive hydrogel beads of hydrolyzed polyacrylamide (PAAm) grafted locust bean gum (LBG) and carboxymethyl cellulose (CMC) were prepared by ionotropic gelation and covalent cross-linking method for the controlled delivery of diclofenac sodium. The developed hydrogel beads are to survive the harsh acidity of stomach and preferably release drugs in intestine. The results showed that hydrogel beads are pH responsive. The release of diclofenac sodium (DS) from hydrogel beads was slower for the pH 1.2 solution than that of the pH 6.8 buffer solution. It has been observed that an increase in alluminium chloride (AlCl3) concentration causes a decrease in the drug release from the hydrogel beads. Moreover, hydrogel beads developed showed a consistent swelling pattern, high entrapment efficiency and promoting sustained release profiles of the drug.

***Keywords*—** pH sensitive, locust bean gum, hydrogel, graft copolymer, in-vitro release, controlled delivery.

I. Introduction

DICLOFENAC sodium is a non-steroidal drug having a effective anti-inflammatory, analgesic, and antipyretic effect. It is used for the relief of pain and inflammation in circumstances such as osteoarthritis, rheumatoid arthritis, acute gout, ankylosing spondylitis, and subsequent surgical procedures [1]. It has a short biological half-life of 1-2 h and the most common side effects are gastritis and peptic ulceration [2]. Controlled release drug delivery systems have the prospective of solving these tribulations. Controlled release systems are the methods that can attain therapeutically useful concentration of drug in the systemic circulation over an extensive period of time with improved patient conformity [3]-[5]. Therefore, it is advantageous to develop diclofenac sodium controlled release dosage forms to decrease the unpleasant effects on upper gastrointestinal tract, to lengthen a half-life and to improve patient conformity.

One method of formulating controlled release dosage forms and releasing the drug in the lower gastrointestinal tract is by the inclusion of the drug in a matrix containing pH-receptive hydrogel. pH-receptive hydrogels are three dimensional cross-linked hydrophilic polymers which swell exclusive of dissolving with water or other biological fluids [6]-[7]. Both synthetic and natural polymers have been used in the preparation of pH-responsive hydrogel [8]-[9]. However, hydrogels based on natural polymers have been extensively used for controlled release of drug.

In the present work, pH-sensitive hydrogel beads of hydrolyzed PAAm grafted LBG and carboxymethyl cellulose was prepared. The main purpose of grafting and hydrolysis of graft copolymer was to increase the number of carboxylic groups in the backbone matrix that is required for the development of Al^{3+}cross-linked hydrogel beads. These carboxylic groups are likely to take part in minimizing the swelling at upper gastrointestinal tract (pH 1.2) and maximizing the swelling at lower gastrointestinal tract (pH 6.8).

Tapan Kumar Giri is with NSHM College of Pharmaceutical Technology, NSHM Knowledge Campus, Kolkata Group of Institutions, 124 BL Saha Road, Kolkata-700053, India. tapan_ju01@rediffmail.com

II. Materials And Methods

A. Materials

Diclofenac sodium was obtained as gift sample from Arti Pharmaceutical Company, Orissa, India. LBG was purchased from Victory Essence Mart, Bangalore, India. AAm and methanol were purchased from Loba Chemie, Mumbai, India. CAN was purchased from Universal Fine Chem, India. Gluteraldehyde (GA) was purchased from SD Fine-Chem. Ltd., Mumbai, India as 25 % v/v aqueous solution. All other reagents were of analytical grades and used as received.

B. Methods

1. Synthesis of Graft Copolymer

Requisite quantity (175 mg) of LBG was dissolved in 25 ml of distilled water. 700 mg of acrylamide was dissolved in 5 ml of distilled water and mixed with LBG solution. The reaction temperature was kept constant 70°C.At this stage 5 ml ceric ammonium nitrate solution ($10x10^{-3}$ mol/L) was added and the reaction was continued to 60 min. The polymer was precipitated by addition of excess of methanol at the end of the reaction. It was then dried at 40°C to a constant weight.

2. Alkaline Hydrolysis of Graft Copolymer

500 mg of graft copolymer was dissolved in 25 ml of sodium hydroxide solution (0.9M) and stirred at 70°C for 60 minutes. The solution was then cooled and poured in excess methanol. The hydrolyzed product was separated by filtration and washed repeatedly with methanol. Then the resultant product was dried overnight at 40°C.

3. Preparation of Hydrogel Beads

Weighed quantity of DS corresponding to 20% of dry mass of the polymer was dispersed in an aqueous solution of hydrolyzed LBG-grafted-AAm and CMC. Then dispersion was added drop wise through 22-gauze niddle into slightly agitated 100 ml of $AlCl_3$ solution. The beads were removed after 30 min and washed with distilled water and dried at 40°C till constant weight.

Further the beads incubated in $AlCl_3$ solution for 30 minutes, were transferred into 50 ml of pH 2 HCl containing GA for 10 min at 50°C to introduce covalent cross-links. The cross-linked beads were removed and washed with distilled water repeatedly to remove nonreacted gluteraldehyde. Fig.1 shows the images of dry beads.

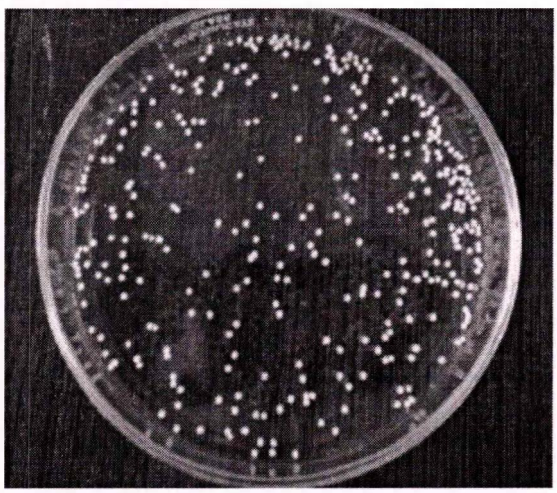

Fig.1 Images of dry beads

4. Fourier Transforms Infrared Spectroscopic Study

FT-IR spectra of pure drug and drug loaded beads were recorded in a FT-IR spectrophotometer (Prestige-21 Shimatzu, Japan) using KBr pellets. The spectra were recorded within 4000-400 cm^{-1} wave number.

5. Differantial Scanning Colorimetry Study

The thermal analysis of drug and drug loaded beads were carried out with thermal analyzer (Pyris diamond, PerkinElmer, Singapore). Differential scanning calorimetry of all the samples was performed up to a temperature of 400°C at 12°C/min.

6. Scanning Electron Microscopic Study

The shape and surface morphology of hydrogel beads were investigated using scanning electron microscopy (JEOL, JSM-6360, UK).

7. Determination of Drug Content

20 mg of beads were crushed with a mortar-pestle and transferred into 200 ml of pH 6.8 phosphate buffer solution. After 3 hours, the suspension was filtered and samples were analyzed with a spectrophotometer (Shimadzu Model: 1800) at 273nm. Entrapment efficiency (%) = (actual drug content/theoretical drug content) × 100[10]

8. Swelling Study

The swelling of the beads was studied in 25ml of pH 1.2 buffer solutions and pH 6.8 USP phosphate buffer solution. The beads were removed at different times by filtration and blotted carefully to remove excess surface water. The swollen beads were weighed. Swelling ratio = (Final weight-Initial weight)/Initial weight [11]

9. In-vitro Drug Release Study

In-vitro drug release study was carried out in pH 1.2 buffer solution and pH 6.8 phosphate buffer solution using USP II dissolution rate test apparatus (Electro lab- TDT-08L). 20 mg dried beads was placed in 500 ml acidic solution for 2 hr then alkaline solution for remaining time maintained at 37±0.5°C. The paddle was rotated at 50 rpm. Aliquot was withdrawn at different times and were analyzed spectrophotometrically at 273nm for acidic solution and 276 nm for alkaline solution.

III. Results And Discussion

When a dispersion of drug and hydrolyzed PAAm-g-LBG graft copolymer was extruded through the needle into the solution containing Al^{+3} cations, the beads were formed instaneously. However, the bead exhibits very poor mechanical strength. In order to improve the mechanical strength, we prepare the beads of hydrolyzed PAAm-g-LBG and CMC by ionotropic gelation process using $AlCl_3$ as a common cross-linking agent for both polymers. As soon as the Al^{+3} are brought in contact with the polymer solution, they form ionic cross-links between two polymer molecules and different parts of the same polymer chain. The exchange of Na^{+} ions of both polymers occurs with Al^{+3}.These Al^{+3} are ionically substituted at the caarboxylated site and a second strand of CMC or hydrolyzed PAAm-g-LBG strands together to form hydrogel beads. The prepared hydrogel beads were spherical in shape having surface folding as evidenced by SEM (Fig.2).

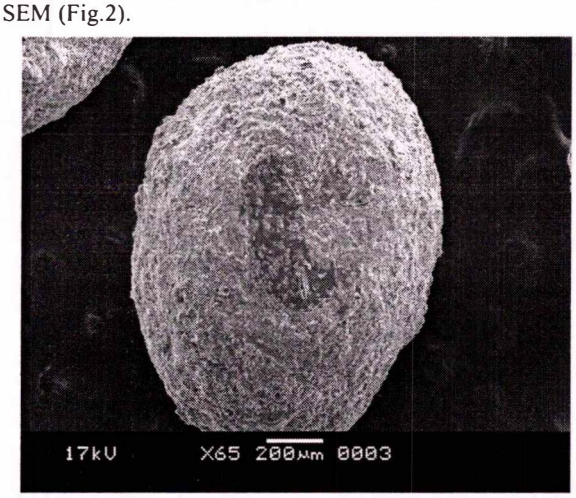

Fig.2 Sem micrograph of hydrogel bead (F5)

The IR spectra of DS (Fig.2) exhibited distinctive peaks at 3387 cm^{-1} (NH stretching of the secondary amine), 1573.91 cm^{-1} (-C=O stretching of the carboxylate functional group),

1305.80 (-C-N stretching) and at 746.45 cm^{-1} (C-Cl stretching) [12]. All the principal peaks of DS were present in drug loaded hydrogel beads (Fig.3) with minor differences in frequencies which confirms that there was no interaction between drug and polymers and reflects the stability of DS in hydrogel beads.

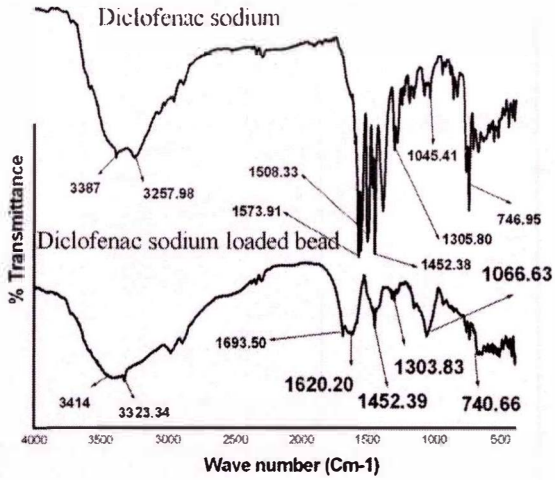

Fig.3 FTIR spectra of diclofenac sodium and diclofenac sodium loaded hydrogel bead (F5)

The DSC thermogram of pure diclofenac sodium (Fig.4) showed two endothermic peaks. The first small endothermic peak at 60.99°C was due to water loss. The second sharp endothermic peak at 288.76°C was due to its melting point. Melting point of the drug was not appeared in drug loaded hydrogel beads (Fig.4). This indicates that most of the drug was uniformly dispersed at the molecular level in the beads.

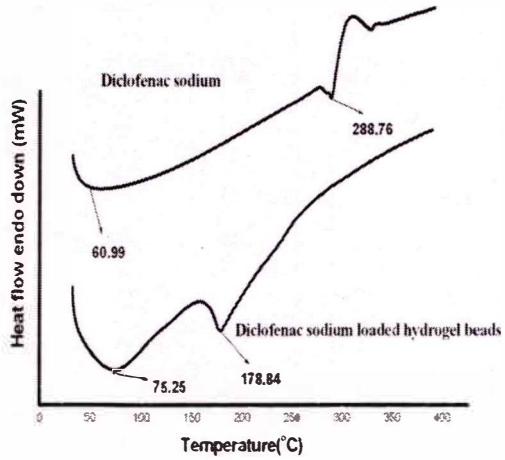

Fig. 4 Differential scanning colorimetry of diclofenac sodium and diclofenac sodium loaded hydrogel bead (F5)

X-ray diffraction pattern of DS showed the important crystallographic reflection at different scattering angle ranges which was due to the crystalline nature of DS (Fig.5). However, these drug peaks were disappeared in the X-ray diffraction pattern of DS loaded hydrogel beads (Fig.5). It was thought that the DS showed its specific crystal peaks when existed in a crystalline form but after drug entrapped into the beads, the drug can be existed as a molecular dispersion in the beads.

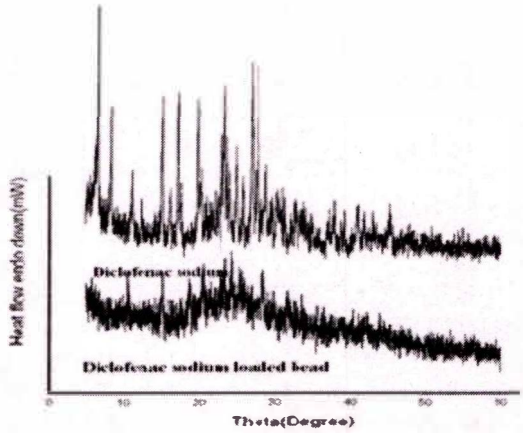

Fig.5 X-ray diffraction patterns of diclofenac sodium and diclofenac sodium loaded hydrogel bead(F5)

Particles were generally spherical in shape with sizes ranging from 803.33-849.33 μm(Table 1). As the concentration of $AlCl_3$ was increased, smaller beads were produced (849.33, 836.67, 823.67 and 803.33 μm for 1, 2, 3 and 4% w/v of $AlCl_3$ respectively). This suggests that during cross-linking, the hydrogel might have undergone rapid shrinkage leading to the formation of smaller and rigid matrix at high cross-linking density [13]. The drug entrapment efficiency of the beads decreased with increasing concentration of $AlCl_3$. The drug entrapment efficiency of the beads decreased from 96.78 to 90.90 with the increase in $AlCl_3$ concentration from 1 to 4% w/v (Table 1). It is assumed that as gelation proceeds water is expelled due to cross-linking. There, the higher the degree cross-linking, the higher is the water loss. The expulsion of water will cause loss of drug from beads. The release of a drug from a polymeric matrix is controlled by the swelling behavior of the polymer. The swelling ratio of the hydrogel beads was very low in acidic solution (pH 1.2), the same property increased considerably in phosphate buffer solution (pH 6.8). The main functional group present in both the polymers that undergoes cross-linking with Al^{+3} ions is -COOH group. In acidic solution, -COOH group remains protonated and exerts insignificant electrostatic repulsive force. As a result, the beads swell to very less extent. At higher pH value, -COOH group undergoes ionization which exerts electrostatic repulsion between the ionized groups, and the results in higher swelling. It was observed that the swelling tendencies of the beads decreased in either of the swelling medium with the increase in $AlCl_3$ concentration. It was estimated that gradual increase in $AlCl_3$ concentration to 4% reduced the swelling ratio by 19.40%. Similarly, in alkaline medium gradual increase in $AlCl_3$ concentration to 4% reduced the swelling

ratio by 15.42%.

TABLE I:
COMPOSITION OF HYDROGEL BEADS

Formulation code	Particle size (μm) (μ±SD, n=3)	Drug content (%)(μ±SD, n=3)	Swelling ratio in pH 1.2 after 1.5 hr (μ±SD, n=3)	Swelling ratio in pH 6.8 after 1.5 hr (μ±SD, n=3)
F1	849.33±6.11	96.78±0.4	0.670±0.020	2.865±0.03
F2	83667±2.52	94.6±0.4	0.647±0.021	2.665±0.01
F3	823.67±3.21	92.57±0.27	0.563±0.025	2.460±0.02
F4	803.33±2.08	90.90±0.67	0.540±0.010	2.423±0.02
F5	785.33±2.08	89.16±0.06	0.190±0.010	0.427±0.03

In vitro drug release profile of the beads has been illustrated in (Fig. 6). The release of drug in pH 1.2 solutions was slower compared with that in pH 6.8 buffer solution. This was due to a higher swelling of beads in alkaline pH condition. It was observed that release rate depend upon the amount of $AlCl_3$ used as a cross-linking agent during the preparation. Release was slower for the beads in which higher amount of $AlCl_3$ was used as compared with those beads in which lower amount of $AlCl_3$ was present. In order to compare the drug release rate, a time point approach was adopted. The values of $t_{50\%}$ were 12.93, 13.48, 13.65 and 13.93 min, respectively in the order of their increasing $AlCl_3$ concentration. This could be due to the fact that at higher cross-linking free volume of the matrix will decrease, thereby hindering the transport of drug molecules through the matrix. This could also reduce the swelling as well as release rate from the matrix. This is in agreement with the previous results [14].

The GA treatment of the beads suppressed the drug release in acidic as well as weakly basic dissolution medium. In addition to ionic cross-links, GA brought about covalent linkages and showed the retarded drug release in both dissolution media than those having ionic linkages only. At higher cross-linking free volume of the matrix will decrease, thereby hindering the transport of drug molecules through the matrix [15].

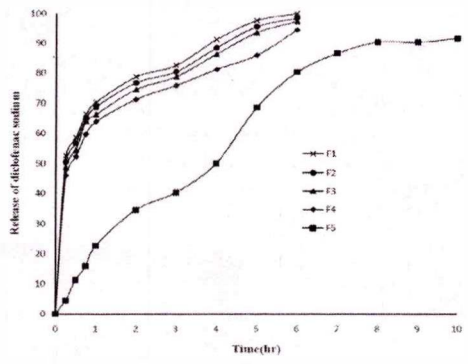

Fig. 6 The release profile of diclofenac sodium from hydrogel beads

IV. CONCLUSION

Hydrogel beads of CMC and hydrolyzed PAAm-g-LBG were prepared successfully by ionotropic gelation and covalent cross-linking method. DSC and XRD studies confirmed the presence of drug mostly in amorphous state and homogeneity of drug dispersion in hydrogel beads. The hydrogel beads showed extended release profile. The results of the study indicate that drug loaded hydrogel beads could be used to minimize the release of diclofenac sodium in stomach and to modulate the drug release in intestine, which would help to minimize the gastric side-effects of diclofenac sodium.

ACKNOWLEDGMENT

The author wants to acknowledge the facilities provided by the NSHM Knowledge Campus, Kolkata Group of Institutions, 124 BL Saha Road, Kolkata-700053, India

REFERENCES

[1] A.Savaser, Y.Ozkan, and A.Isimer, "Preparation and in vitro evaluation of sustained release tablet formulations of diclofenac sodium", Il Farmaco, vol.60, pp.171-177, 2005.

[2] T.K.Giri, C.Choudhary, Ajazuddin, A.Alexander, H. Badwaik, and D.K, "Tripathi. Prospective of pharmaceuticals and biopharmaceuticals loaded microparticles prepared by double emulsion technique for controlled delivery", Saudi.Pharm.J, vol.21,pp.125-141, 2013.

[3] T.K.Giri, K.Kumar, A.Alexander, Ajazuddin, H. Badwaik, and D.K.Tripathi, "A novel and alternative approach to controlled release drug delivery system based on solid dispersion technique", Bulletin. Facult.Pharmacy.Cairo.University, vol.50, pp. 147-159, 2012.

[4] H.Badwaik, M.Singh, D.Thakur, T.K.Giri, and D.K. Tripathi, "The Botany, Chemistry, Pharmacological and Therapeutic Application of Oxalis corniculata Linn– a Review", Int.J. Phytomedicine, vol.3, pp. 1-8, 2011.

[5] T.K.Giri, A.Alexander, and D.K.Tripathi, "Physicochemical classification and formulation development of solid dispersion of poorly water soluble drugs: An updated review", Int.J.Pharmaceutical.Biological. Archives, vol.1, pp.309-324,2010.

[6] S.Hua, H.Ma, X.Li, H.Yang, A.Wang, "pH-sensitive sodium alginate/poly(vinyl alcohol) hydrogel beads prepared by combined Ca2+ crosslinking and freeze-thawing cycles for controlled release of diclofenac sodium", Int.J. Biol.Macromol, vol.46, pp.517-523, 2010.

[7]A.A.K.Ahmed, H.S.B.Naik, B.S.Sherigara, "Synthesis and characterization of chitosan-based pH-sensitive semi-interpenetrating network microspheres for controlled release of diclofenac sodium", Carbohydr.Res, vol.344,pp.699-706, 2009.

[8] Ajazuddin, A.Alexander, J.Khan, T.K.Giri, D.K.Tripathi, S.Saraf, and S.Saraf, "Advancement in stimuli triggered in situ gelling delivery for local and systemic route", Expert. Opinion. Drug. Delivery, vol.9, pp.1573-1592, 2012.

[9] A.Behra, T.K.Giri, D.K.Tripathi, Ajazuddin, and A.Alexander, "An exhaustive review on recent advancement in pharmaceutical bioadhesive used for systemic drug delivery through oral mucosa for achieving maximum pharmacological response and effect", Int.J.Pharmacol, vol.8, pp.283-305,2012.

[10] T.K.Giri, S.Verma, A.Alexander, Ajazuddin, H.Badwaik, M.Tripathy, and D.K.Tripathi, "Crosslinked biodegradable hydrogel floating beads for stomach site specific controlled delivery of metronidazole", Farmacia, vol.533-550, 61, 2013.

[11] T.K.Giri, K.Kumar, A.Alexander, Ajazuddin, H.Badwaik, M.Tripathy, and D.K.Tripathi, "Novel controlled release solid dispersion for the delivery of diclofenac sodium", CurrDrug Deliv,vol.10,pp.435-444, 2013.

[12] D. Kebebe, A. Belete, and T. Gebre- Martin, "Evaluation of two olibanum resins as rate controlling matrix forming excipients in oral

sustained release tablets", Ethiop.Pharm. J, vol.28, pp.95-109, 2010.
[13] T.K.Giri, D.Thakur, A.Alexander, Ajazuddin, H.Badwaik, M.Tripathy, and D.K.Tripathi, "Biodegradable IPN hydrogel beads of pectin and grafted alginate for controlled delivery of diclofenac sodium", J.Mater.Science.Mater.Medicine, vol.24,pp.1179-1190, 2013.
[14] R.V. Kulkarni, and B. Sa, "Evaluation of pH sensitivity and drug release characteristics of (polyacrylamide-grafted-xanthan)-carboxymethyl cellulose based pH sensitive interpenetrating network hydrogel beads", Drug. Dev. Ind .Pharm, vol.34, pp.1406-1414,2008.
[15] A.R. Kulkarni, K.S. Soppimath, and T.M. Aminabhavi, "Controlled release of diclofenac sodium from sodium alginate beads crosslinked with gluteraldehyde", Pharmaceutica. Acta. Helvetiae, vol.74, pp.29-36, 1999.

Thermal Treatment Processes for Increase Lycorine Active ingredient in *Crinum asiaticum* Leaves

Sineenat Laokam, Nattaya Ngamrojnavanich, Somsamai Wejsuthanon, and Nongnuj Muangsin

Abstract*—*Crinum asiaticum has long been used as a traditional folk therapy for various disorders such as inflammation, allergic and cancer. Indigenous people used heated leaves of *Crinum asiaticum* for treatment of aches, arthritis pain, swelling and bruising. However, there are no previously reported about the effect of heat treatment on the ingredients and their activities. Therefore, in this work we focus on the effect of different thermal processes such as steaming (95 °C for 1 hour) and oven dry (160 °C for 10 minutes) processes on the content of lycorine, which is the major active component. The amount of lycorine was evaluated by high performance liquid chromatography (HPLC). We found that thermal processes can increase the lycorine contents.

Keywords*—*Crinum asiaticum, lycorine, thermal process.

I. Introduction

CRINUM asiaticum is distributed on Southeast Asia and has long been used as various disease treatments such as antiinflammation, antiallergic and anticancer [1]. The major biological active alkaloid compounds of *Crinum asiaticum* is lycorine **(Fig. 1)**, which shows strong cytotoxicity against cancer cells and anti-inflammatory activity. It has been reported that lycorine can inhibit DNA synthesis and exert cytotoxic activity against several tumor cell lines such as various type of leukemia, lymphoma, carcinoma and melanoma cell lines [2]. Furthermore, lycorine induces cancer cells to undergo apoptosis such as EL-4 and MOLT-4 cells [3].Moreover, previous study has been reported that lycorine was used for treatment of in chronic and acute inflammatory diseases for carragenan-induced hind paw oedema model and evaluated their anti-inflammatory activity [4].

Sineenat Laokam, Department of Biotechnology, Faculty of Science, Chulalongkorn University, Bangkok 10300, Thailand
Email address: Puimucu@mail.com
Nattaya Ngamrojnavanich, Nongnuj Muangsin· Department of Chemistry, Faculty of Science, Chulalongkorn University, Bangkok 10300, Thailand
Email address: Nnattaya@chula.ac.th, Nongnuj.j@chula.ac.th, Nongnuj.ms@gmail.com
Somsamai Wejsuthanon· [3]Bangbuathong Hospital, Nonthaburi 11110, Thailand

Thermal processes can divide to many methodologies including; (1) Boiling process, is well known that natural nutrients could be significantly lost during the thermal processing due to most of bioactive compounds are relatively unstable to heat. Previous report, curcumin and piperine of turmeric and red pepper were decomposed by the boiling process [5]. (2) Roasting process, Xu and coworker suggest that the content of benzoic acids and cinnamic acids of Citrus Peel was significantly increased after the roasting process [6]. and also the oven dried process caused the loss of gingerol and shogaol in ginger [7]. However, this process is difficultly controlled the temperature and time. Moreover, some biological active compound could be destroyed after roasting process. (3) Steaming process, many researches have been reported the steamed treatment of herbs can increase the active ingredients and hence increase the biological or pharmaceutical activities and new biological compounds in plants such as ginseng [8, 9] to obtain ginsenoside (Rg3, Rh_2) that showed strong antiproliferation against cancer cells such as HCT-116 and SW-480, but this process is difficultly controlled the temperature and time. (4) Oven dried process is a typical process for preserving herbs such as tea, bergamot leaves. Some works have been reported that the oven dried treatment reduced the amount of active ingredients because of decomposition. In contrast, this treatment can increase of the major active ingredients, for example increasing of flavonoids in wheatgrass [10]. Moreover, there are many advantage of this process such as prolonging storage time of products, controlling the temperature and time. So, it is worth to investigate the amount of lycorine after process the oven dried treatment

There are many reported that the heated treatment leaves of *Crinum asiaticum* have been used as traditional Thai folk therapy for treatment of many kinds of inflammation. To date, there are no reported about the effect of thermal processing on the active ingredients of *Crinum asiaticum*. Subsequently, the effect of thermal processes was categorized into 3 groups as following:

1) Fresh leaves; as a un-treatment (group 1)

2) Steamed leaves (group 2), in order to investigate the effect of the steamed treatment on the amount of the lycorine as the major active ingredient, the same amount of leaves used in group 1 was steamed using the following condition steaming at 95 °C for 1h.

3) Oven dried process (group 3) by heating at 160 °C for 10 on the compounds from *Crinum asiaticum*. Moreover, we studied the influence of heating temperature and time (50, 70, 100 and 120°C for 10, 30 and 60 minutes) on the lycorine content in *Crinum asiaticum* leaves were operated using oven dried process, since this process can increase the highest lycorine content.

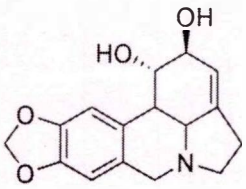

Fig. 1 Chemical structure of lycorine

II. MATERIALS AND METHODS

Heat treatment on *Crinum asiaticum* leaves: The leaves of *Crinum asiaticum* were purchased from Pak Khlong Talat (Bangkok, Thailand), and then were cleaned with water tap, sliced and divided into three groups; in 1)fresh leaves, 2) steamed leaves, and 3) oven dried leaves. Each of group was prepared from 1 kilogram of the fresh leaves. 1) The fresh leaves (untreated) as untreated condition were used immediately without drying. 2)Steamed leaves was performed using steamer, the fresh leaves were steamed in a closed container at temperature approximately 95 °C for 1 h, and then the leaves were dried at room temperature. For 3) oven dried leaves, was operated by oven at temperature 160 °C for 10 minutes. Moreover, heat-processed *Crinum asiaticum* leaves was prepared by oven temperature at 50 °C, 70 °C, 100 °C and 120 °C for 10, 30 and 60 minutes (Each heat treatments were prepared from 100 grams of fresh leaves), which these conditions were chosen by using condition that comprehensive with phase of steaming and oven dried process for searching the optimum condition. Analysis was done in triplicate for each treatments. All heat-processed leaves were grinded with a blender and extracted in the next step.

Extraction of *Crinum asiaticum* leaves: All same weight of the heated leaves of *Crinum asiaticum* (starting material) were extracted and purified from *Crinum asiaticum* leaves using the method modified from a standard procedure reported by [11]. Heat processed leaves were immersed and extracted with 500 mL of methanol for 24 hours and repeated extraction until the solution was cleared, filtered and kept methanol extract layer. Combined methanol extracts were evaporated in a rotary evaporator under reduced pressure, to give a greenish-brown oil of crude extracts. Then, the lycorine contents were determined by high performance liquid chromatography (HPLC).

Determination of lycorine in crude extracts by HPLC: HPLC analysis was carried out using a liquid chromatographic system (Spectra system), instated with a UV variable-wavelength detector (spectra system UV 6000LP), a quaternary pump system (spectra system P4000), vacuum degasser (spectra system SN4000), a manual injector with 100 µL loop (RESTEK SGE syringe 100R-GT-LC-SS), and a chromatographic data processing software (windows 2001). The chromatographic assay for lycorine and crude extracts were operated on Pinnaclell C18 Column (250 mm × 4.6 mm; 5 µm particle size). Crude extracts (10 mg) were dissolved in methanol (1 mL) and injected 20 µL to high performance liquid chromatography (HPLC), eluted with 0.05M KH_2PO_4: CH_3CN (96:4) at flow rate 0.7 mL/min and detected UV at 290 nm. Types of crude were investigated for three internal and external replications. Quantitative determination was carried out by the external standard method based on peak area [4].

Calibration curve of lycorine: A calibration curve was generated to confirm the linear relationship between the peak area (y) and the concentration of lycorine standard (x). Standard lycorine was added to HPLC at concentrations of 0.5, 1.0, 2.0, 4.0 and 8.0 mg/mL. The sample with known amount of lycorine was analyzed by HPLC. The resulting calibration data were $y = 7.4\times10^7x - 4.4\times10^7$ and $R^2 = 0.99$.

Statistical Analysis: Statistical analysis was conducted using one way ANOVA with SPSS.

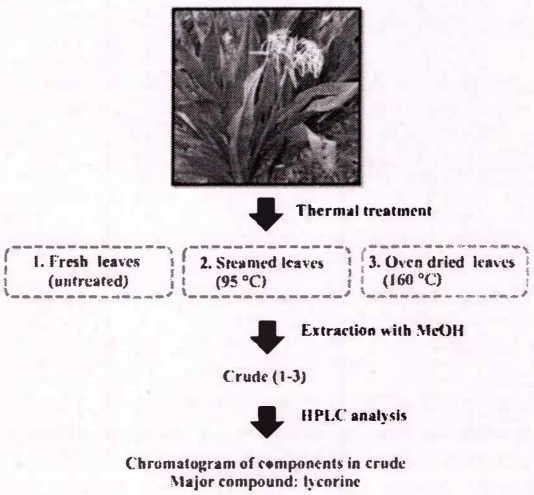

Fig. 2 Thermal treatments on Crinum asiaticum leaves; (1) fresh leaves, (2) steamed leaves (95 °C) and (3) oven dried leaves (160 °C).

III. RESULT AND DISCUSSION

Effect of thermal process on the lycorine compositions: In this work is to study effect of thermal processes, including steaming at 95 °C for 1 hour and oven drying at 160 °C for 10 minutes on the compounds from *Crinum asiaticum* leaves. From 1 kilogram of fresh leaves, to give the yields as crude extract of fresh, steamed and oven dried leaves were 17.22 g (1.72% w/w), 23.82 g (2.38% w/w) and 35.21 g (3.52% w/w), respectively. Crude extract of heated leaves was more than the fresh leaves especially oven dried leaves were highest crudes content. Therefore, When *Crinum asiaticum* leaves were heated process might be increased the kind of compounds that can soluble in methanol. Lycorine content after various heating treatments were analyzed by HPLC.

The chromatograms of standard lycorine, fresh leaves, steamed leaves and oven dried leaves are shown in **Fig 3**. The peaks from chromatograms were confirmed by comparison of retention time with lycorine standard. From the chromatogram in **Fig.3**, the retention time of lycorine standard was 6.77 minutes which is similar to the peak **b** of fresh leaves, steamed leaves and oven dried leaves were 6.79, 6.77 and 6.88, respectively. This result indicated the peak **b** of all crudes was lycorine and lycorine content was determined by comparison peak area with standard curve of lycorine. Thus, amount of lycorine that found in fresh, steamed and oven dried leaves were 2.35±0.09, 3.69±0.04 and 4.48±0.02 mg/mL, respectively (**Table I**).

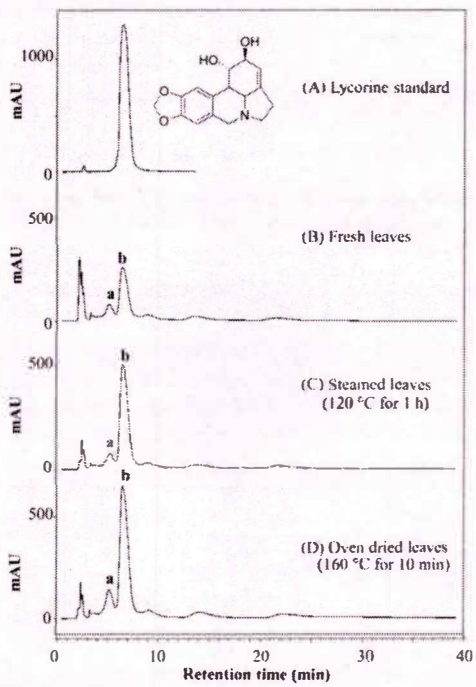

Fig. 3 Representative chromatograms of (A) lycorine standard and crude extracts of (B) fresh leaves (untreated), (C) steamed leaves (95 °C for 1 h) and (D) oven dried leaves (160 °C for 10 min).

For the preliminary, the effect of thermal process on the change of lycorine composition was investigated by using crude of heated leaves at 95 °C for 1 h (steaming) and 160 °C for 10 min (oven dry) compared with untreated *Crinum asiaticum* leaves (**Table I**). Lycorine content of fresh leaves (untreated) was 23.55%. The steamed leaves at 95 °C for 1 h, lycorine content was 36.94% which was greater than the fresh leaves. While oven dried leaves at 160 °C for 10 min had the highest lycorine content was 44.85%, which gave amount more lycorine content than the fresh leave to 2-fold (based on weight of fresh leaves).

TABLE I.
THE CONTENT OF LYCORINE ON THE HEATED *CRINUM ASIATICUM* LEAVES OF DIFFERENCE PROCESS: STEAMED AND OVEN DRIED LEAVES COMPARED WITH THE FRESH LEAVES, DETERMINED FROM FIG. 4.

Type of leaves	Lycorine content (mg/ml)
Fresh leaves	2.35±0.09
Steamed leaves	3.69±0.04
Oven dried leaves	4.48±0.02

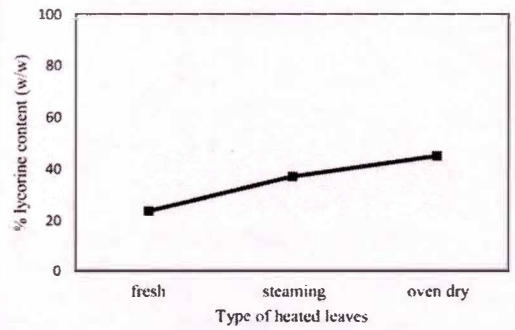

Fig. 4 Percentage of compound a (unknown) and b (lycorine) contain in *Crinum asiaticum* leaves with different heat process.

As we expected, thermal process had effect on constituents of *Crinum asiaticum* leaves especially lycorine content. Increasing temperature could be lycorine-1-0-β-D-glucoside, on further hydrolysis with methanol gave lycorine and D-glucose was confirmed by Ghosal et al. [2]. Thus, the lycorine contents was increased significantly that shown in **Fig. 5**.

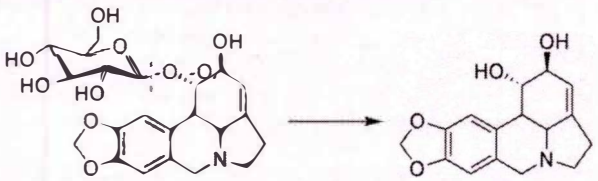

Lycorine-1-0-β-D-glucoside Lycorine

Fig. 5 Proposed mechanism of lycorine was converted from lycorine-1-0-β-D-glucoside.

Effects of temperature on the lycorine constituent: From above preliminary experiment, the thermal process had effect to the lycorine content on *Crinum asiaticcum* leaves. Thus, we studied the influence of heating temperature on the lycorine content in *Crinum asiaticum* leaves were operated by drying oven at various temperature (50 °C, 70 °C, 100 °C and 120 °C) and various time (10, 30 and 60 minutes). From **Fig. 6** showed lycorine content of all heated leaves higher than the fresh leaves, which were significantly differences (p<0.05). The lycorine content of heating condition such as heated leaves of fixed time at 30 minutes for 50 °C, 70 °C, 100 °C and 120 °C that found the highest lycorine content of heated leaves at 50 °C and reduced at 70 °C, 100 °C and 120 °C, respectively. However, all heated condition gave a proximate amount of lycorine. From the result indicated the temperature had effect to the lycorine content on *Crinum asiaticum* leaves.

Effects of time in thermal process on the lycorine constituent: Effect of time heating was shown in **Fig. 6** such as heated *Crinum asiaticum* leaves at 50 °C for 10, 30 and 60 minutes. Compared with untreated leaves, the lycorine content of heated leaves at 50 °C was increased at 10 and 30 minutes, respectively and reduced at 60 minutes, although it was more than the fresh leaves. Moreover, the condition of heated leaves at 50 °C for 30 minutes to give the highest lycorine content. Thus, this is optimum condition of heated leaves at 50 °C for 30 minutes and it may be chosen highest lycorine content. This study concluded that the thermal treatment on *Crinum asiaticum* leaves extracted with methanol is effective for increasing lycorine and other bioactive compound contents.

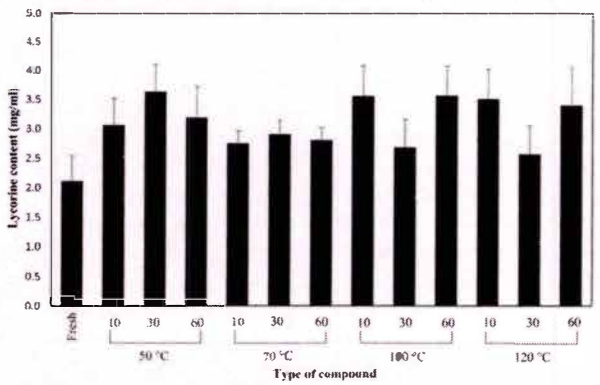

Fig. 6 Lycorine content of fresh *Crinum asiaticum* leaves (untreated) and heated *Crinum asiaticum* leaves at temperature of 50 °C, 70 °C, 100 °C and 120 °C for 10, 30 and 60 minutes.

IV. Acknowledgment

The authors gratefully acknowledge from Ratchadaphiseksomphot Endowment fund of Chulalonkorn University (CU-57-020-FW) to NM and The Department of Biotechnology, Faculty of Science, Chulalongkorn University.

V. Conclusion

We studied the effect of thermal process on *Crinum asiaticum* leaves including heating temperature at 50, 70, 100 and 120 °C for 10, 30 and 60 minutes compared with fresh leaves. This study concluded that thermal process on *Crinum asiaticum* leaves is effective for change lycorine contents. Especially, the heated *Crinum asiaticum* leaves at 50 °C for 30 minutes showed the highest lycorine, and this condition can save time and energy of heat. Thus, thermal process can be useful for increasing lycorine content in *Crinum asiaticum* leaves.

References

[1] J.B. Patel, R.D. Dangar, R.R. Dangar, B.H. Patel, D.R. Parmar, and K.N. Shah, *A Review: Crinum asiaticum*. 2011. Vol. 1. 2011.

[2] S. Ghosal, A. Shanthy, A. Kumar, and Y. Kumar, "Palmilycorine and lycoriside: acyloxy and acylglucosyloxy alkaloids from crinum asiaticum," *Phytochemistry*, vol. 24, no. 11, pp. 2703-2706, 1985.

[3] S. Yui, M. Mikami, M. Kitahara, and M. Yamazaki, "The inhibitory effect of lycorine on tumor cell apoptosis induced by polymorphonuclear leukocyte-derived calprotectin," *Immunopharmacology*, vol. 40, no. 2, pp. 151-162, 1998.

[4] Y.H. Kim, K.H. Kim, C.S. Han, S.H. Park, H.C. Yang, B.Y. Lee, S.Y. Eom, Y.S. Kim, J.H. Kim, and N.H. Lee, "Anti-inflammatory activity of Crinum asiaticum Linne var. japonicum extract and its application as a cosmeceutical ingredient." *J Cosmet Sci*, vol. 59, no. 5, pp. 419-430, 2008.

[5] D. Suresh, H. Manjunatha, and K. Srinivasan, "Effect of heat processing of spices on the concentrations of their bioactive principles: Turmeric (Curcuma longa), red pepper (Capsicum annuum) and black pepper (Piper nigrum)." *Journal of Food Composition and Analysis*, vol. 20, no. 3–4, pp. 346-351, 2007.

[6] G. Xu, X. Ye, J. Chen, and D. Liu, "Effect of Heat Treatment on the Phenolic Compounds and Antioxidant Capacity of Citrus Peel Extract," *Journal of Agricultural and Food Chemistry*, vol. 55, no. 2, pp. 330-335, 2007.

[7] E.S.W. Sukrasno, Irda Fidrianny, "Heating effect of ginger (Zingiber offcinale rosc) content of volatile oil and oleoresin." *Int. J. Res. Pharm. Sci.*, vol. 5, no. 2, pp. 132-136, 2014.

[8] C.Z. Wang, B. Zhang, W.X. Song, A. Wang, M. Ni, X. Luo, H.H. Aung, J.T. Xie, R. Tong, T.C. He, and C.S. Yuan, "Steamed American ginseng berry: ginsenoside analyses and anticancer activities," *J Agric Food Chem*, vol. 54, no. 26, pp. 9936-9942, 2006.

[9] I. Hwang, H. Kim, E. Joung, K. Woo, J. Jeong, K. Yu, J. Lee, and H. Jeong, "Changes in ginsenosides and antioxidant activity of Korean ginseng (Panax ginseng C.A. Meyer) with Heating Temperature and Pressure," *Food Science and Biotechnology*, vol. 19, no. 4, pp. 941-949, 2010.

[10] A. Das, U. Raychaudhuri, and R. Chakraborty, "Effect of freeze drying and oven drying on antioxidant properties of fresh wheatgrass," *Int J Food Sci Nutr*, vol. 63, no. 6, pp. 718-721, 2012.

[11] R.S. MD. Atiar Rahman, MD. Nazim Uddin, Mahbubuzzaman, Sohel Rana, Nazim Uddin Ahmed, "Antinociceptive and antiinflmmatory effect of *Crinum asiaticum* bulb extract," *Asian J Pharm Clin Res*, vol. 4, no. 3, pp. 34-37, 2011.

Nanocrystalline $LaFeO_3$ Perovskite Oxide Prepared at Lower Temperature with Improved Ethanol Gas Sensoring

Wankassama Haron, Anurat Wisitsoraat, Sumpun Wongnawa

***Abstract*—**Nanocrystalline $LaFeO_3$ perovskite oxide were synthesized by the co-precipitation method. The products were characterized with X-ray spectrometer (XRD), an Scanning Electron Microscope (SEM). The XRD patterns confirmed the formation of perovskite phase. The SEM micrographs indicated that perovskite samples were nanosized particles with morphology of likely high concentration of inter particle porosity. The application as ethanol gas sensor was investigated and found from the lower calcinations temperature the $LaFeO_3$ showed great enhancement of sensitivity toward ethanol giving results that were much better than many sensors ever reported.

***Keywords*—**Perovskite, $LaFeO_3$, Co-Precipitation method and Ethanol gas sensor.

I. Introduction

ETHANOL gas sensors may find application in many fields such as the control of fermentation processes, safety testing of food packaging, monitoring drunken drivers, etc. Recently, plastic substrate based ethanol sensors have attracted considerable attention, owing to their attractive characteristics including flexibility, lightness, shock resistance, and softness. However, most plastics will deform or melt at temperature of only 100 – 200 °C causing severe limitations on sensor application as many gas sensors are required to operate at high temperature (> 200 °C) [1].

Perovskite-type oxides (ABO_3; A= a rare earth cation , B = a transition metal cation) constitute an important class of strategic materials due to their outstanding properties such as electrical, mechanical, optical, magnetic, and catalytic properties, hence these materials find numerous technological uses. These oxides have been used in solid oxide fuel cells (as electrode materials), chemical sensors, oxygen-permeating membranes, thermoelectric devices, and as catalyst for combustion of CO, hydrocarbons, and NO_x decomposition . For these applications, it is important to prepare high-quality and homogeneous powders with controlled stoichiometry and microstructure. In most cases, the presence of secondary phases may reduce the functional properties, so the single-phase materials are preferred [2-4].

Many methods of synthesizing nanostructured materials are available: reverse microemulsion nanoreactor method [5], solid state reaction or thermal decomposition [6-7], sol-gel method [8-9], combustion process [10-11], electrospinning method [12-13], biotemplate method [14], glycine nitrate method [15], nanocasting method [16], citrate method [17], polymerizable complex method [18], and co-precipitation method [19-20]. All methods are standout from the efficiency and scale up perspectives.

These techniques, however, have some disadvantages with the preparation of high specific surface area perovskites. The temperature required to induce the perovskite structure in the conventional ceramic methods is usually high. The high temperature can be lowered slightly in the above mentioned methods due to the finely dispersed oxides in the precursors. Nevertheless, this "low" temperature is still high enough (> 600 °C) to enhance grain growth and, hence, to reduce the specific surface area [3].

The aim of this work is to find a simple route to prepare nano-$LaFeO_3$ through low calcination temperature that yields high purity perovskite phase and study for possible application as ethanol gas sensing material. In the first stage, the precursor for $LaFeO_3$ will be synthesized by co-precipitation from metal nitrate and carbonate salts. The precursor then will be calcined at high temperature (conventional method) and at varied lower temperatures to obtain the desired perovskites $LaFeO_3$. The resulting perovskites obtained from the lower temperature treatment exhibited better performance as ethanol sensor than the ones from high temperature. This route has several advantages such as simplicity, low cost, no waste, and no environmental pollution compared with other routes.

II. Experimental

A. Preparations of $LaFeO_3$ Powders by Conventional Method

$LaFeO_3$ perovskites were prepared based on the co-precipitation method reported previously [21] with some modifications. For $LaFeO_3$

, $La(NO_3)_3{\cdot}6H_2O$ and $Fe(NO_3)_3{\cdot}9H_2O$ were used as starting materials. A specific amount of each was dissolved in distilled water to make 1 M solutions. Both solutions (equal volume) were mixed together with vigorous stirring. Then aqueous solution of $K_2CO_3{\cdot}1.5H_2O$ (2 M) – same volume as

Waskassama Haron, Prince of Songkla University, Thailand wankassama@gmail.com,

Dr. Anurat Wisitsoraat, National Electronics and Computer Technology Center (NECTEC), Thailand, anurat.wisitsoraat@nectec.or.th

Assoc.Prof.Dr. Sumpun Wongnawa, Prince of Songkla University Thailand, sampun.w@psu.ac.th, sampun.w@gmail.com

one of nitrate solution – was rapidly added and followed by equal volume of 1M NaOH solution which led to precipitation. After filtering, the precipitate was washed with distilled water several times until the wash water was neutral (pH =7). The product was then dried at 100 °C for 6 h to yield the "precursor" after which it was calcined at 900 °C for 2 h to obtain the $LaFeO_3$ perovskite.

B. Preparations at Lower Calcination Temperatures

The same procedure as above was used to prepare the three precursors then calcinedat other temperatures lower than 900 °C: for $LaFeO_3$ at 600, 700, and 800 °C.

C. Characterization of Products

The structural characterization was carried out by powder X-ray diffraction (XRD) using Cu Kα (λ = 0.154 nm) radiation source in a X'Pert MPD, PHILIPS X-ray diffractometer. The diffraction angle (2θ) ranged between 20 ° and 80 °. The Debye-Scherrer equation was used to calculate the average crystallite size (D),

$$D = \frac{K.\lambda}{B.\cos\theta} \quad (1)$$

where D is the average crystallite size, K is a dimensionless shape factor with a value close to unity. The shape factor has a typical value of about 0.89, but varies with the actual shape of the crystallite. λ is the X-ray wavelength, B is the line broadening at half the maximum intensity (FWHM) after subtracting the instrumental line broadening in radians, θ is the Bragg angle.

The specific surface area and pore size distribution of $LaMO_3$ were determined by nitrogen sorption isotherm using BET method (Coulter, model SA 3100, USA).

D. Sensors Fabrication and Gas Sensing Measurement

The powdered $LaFeO_3$ was mixed with organic binder (mixture of α- terpineal and ethyl cellulose) to make a paste which was dropped onto the alumina substrate (3×2 mm) - with gold interdigitated electrodes - to form films. The $LaMO_3$ film was then annealed at 450 °C for 2 h to remove organic content.

In a gas testing chamber, the electrode of the $LaMO_3$ sensor was connected with the probe on a heating state. Voltage was applied to two Ni-Cr coils and the operating temperature of 350 °C was monitored by thermo couple. For the gas testing, the resistance of the film was measured in air (R_A) then various concentrations of ethanol gas (50, 100, 200, 300, 500, and 1000 ppm) were continuously flowed into the chamber using a mass flow controller and the gas sensor resistance (R_E) was measured. The sensitivity of the LaMO3-based sensor to ethanol gas was expressed in term of response (R) defined as $R = R_E / R_A$.

III. Results and Discussion

A. Preparations by Conventional Method and characterization Of Products

The precursor first obtained was a mixture of $La_2(CO_3)_3$ and $Fe_2(CO_3)_3$ which later was subjected to calcination. As the temperature rose the carbonates decomposed to the corresponding oxides and subsequently merged to form the corresponding perovskite at higher end of calcination temperature. Phase analyses of all samples were studied by powder X-ray diffraction (Fig 1). The XRD pattern of $LaFeO_3$ matched with the JCPDS file number 37-1493 of perovskite having orthorhombic structure.

Using the Debye-Scherrer equation and the XRD peak informations yielded the average crystallite sizes of 79 nm. The appearances of all three XRD patterns are sufficiently clean from other unwanted peaks such that they can be considered as high purity perovskites.

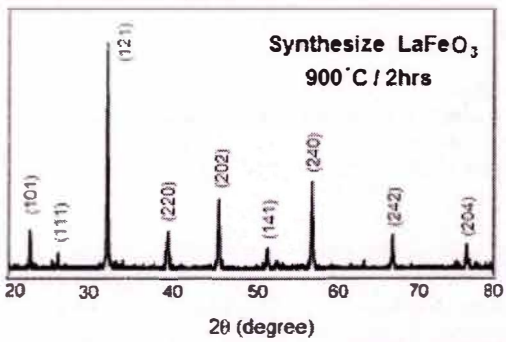

Fig. 1 XRD- Pattern of $LaFeO_3$ Powder after Being Calcined At 900 °C for 2h

B. Morphologies of Products

The scanning electron micrographs of the $LaFeO_3$ sample was shown in Fig.2.The images of $LaFeO_3$ perovskites exhibit distinct grain growth into large particles having and almost-spherical shape for the latter.

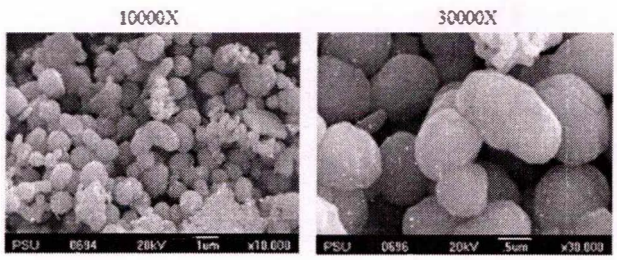

Fig. 2 SEM Image of $LaFeO_3$ Powder After Being Calcined At 900 °C for 2h

The sensitivities of $LaFeO_3$ film-based sensors were tested against some common gases (CO_2, SO_2, H_2, and EtOH) at 350 °C with the gas concentration range 50 - 1000 ppm. All sensors showed no response to CO_2, SO_2, and H_2 gases but exhibited some positive signs with ethanol gas the results of which are shown in Fig.3.The response increased with an increase of ethanol gas concentration. The response exhibited by $LaFeO_3$ film gas was low (response = 1.3 / 1000 ppm) and immeasurable response (~ 0) with CO_2 gas. Wang and co-worker prepared LaFeO3 and measured with CO_2 gas, their result was also low (1.5 / 1000 ppm) but ethanol gas was not mentioned in their report [4]. In other reports for $LaFeO_3$ as ethanol sensor, for example, Sathitwitayakul et al. showed that $LaFeO_3$ prepared from self-propagating high temperature synthesis (> 1000 °C) exhibited response toward ethanol

about 2.6 with 20 ppm ethanol at 550 °C [13], and Chu et al. with the response ~ 10 for 1000 ppm EtOH at 350 °C using $LaFeO_3$ prepared from solid-state reaction [8].

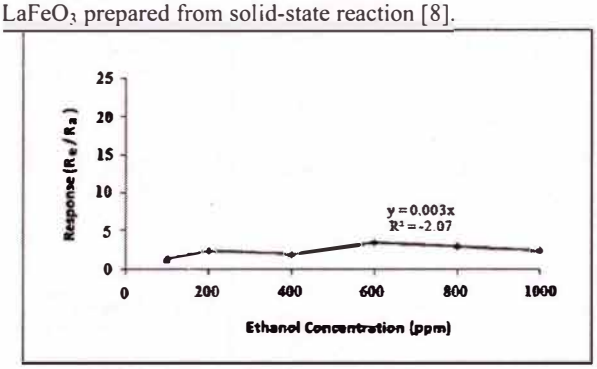

Fig 3 Gas Senser Measurement of $LaFeO_3$ Films

C. Better Products from Lower Calcination Temperatures

C.1. Products Characterization

The desired properties of perovskites believed to exhibit good performance as gas sensors should have high surface area and smaller crystallite sizes compared with those prepared from the conventional method. This is why the lower calcination temperature comes into focus. The high temperature tends to give good crystallinity and larger crystallite sizes which reduces the surface area.

In this part, we attempted to vary the calcination temperatures for the lowest possible temperature to obtain the perovskite structures. The precursors were still prepared by the same method these precursors were then subjected to different calcination temperatures to locate the lowest temperature that each precursor would transform to perovskite phase.

The XRD patterns of $LaFeO_3$ at various temperatures are shown in Fig.4., the product obtained from calcination at 800 °C was indeed $LaFeO_3$ perovskite (matched with JCPDS file no. 37-1493) having orthorhombic structure with particle size of 68 nm. If the calcination temperature was lower than 800 °C, sample powder existed only as mixture of La_2O_3 and Fe_2O_3.

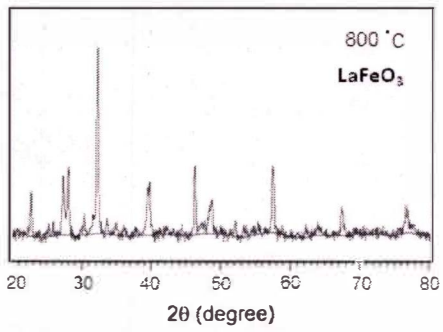

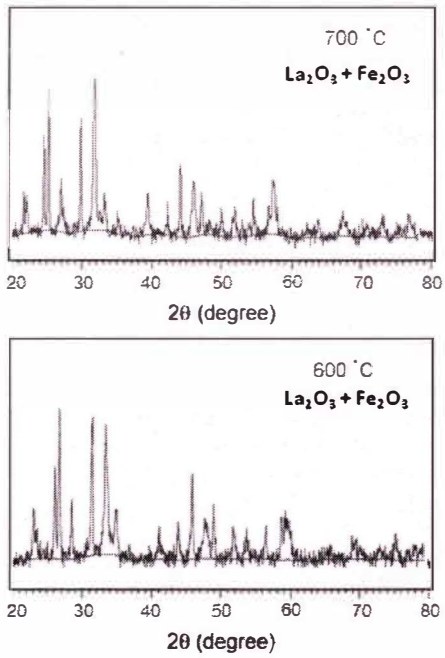

Fig. 4 XRD Patterns of $LaFeO_3$ Perovskites Obtained From Various Temperatures

The SEM images of the two low temperature perovskites revealed markedly different surface morphologies from those obtained at higher temperature (900 °C) (Fig. 3). At higher temperature, small particles developed into larger particles accompanied by smoother surfaces. On the other hand, the low temperature samples exhibit rougher and more irregular surface morphologies which should give them distinct advantage for gas adsorption.

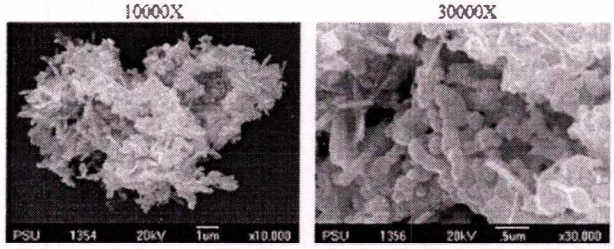

Fig. 5 SEM Image of $LaFeO_3$ Perovskites Obtained At Lower Temperatures; 800 °C.

C.2. Better Gas Sensors

The efficiencies as gas sensors exhibited by $LaFeO_3$ perovskites prepared at lower calcination temperatures (< 900 °C) to ethanol gas are displayed graphically in Fig.6.The responses to EtOH at 2.26, 7.5, 45.50, 52.60, 56.10, 180, and 259 (units of Re/Ra).The experiment was carried out under the same conditions. Comparing Fig. 3 and Fig. 6, one can see that the efficiencies as gas sensors of $LaFeO_3$ were dramatically increased several folds (199 folds for $LaFeO_3$ at 1000 ppm of EtOH) and varied linearly with increasing ethanol concentrations.

One interesting point is that $LaFeO_3$ prepared by this method showed dramatic enhancement of response compared with that prepared at 900 °C (Fig. 4). In all, the two perovskites prepared at temperature below 900 °C in this work are worth being considered as highly sensitive sensors.

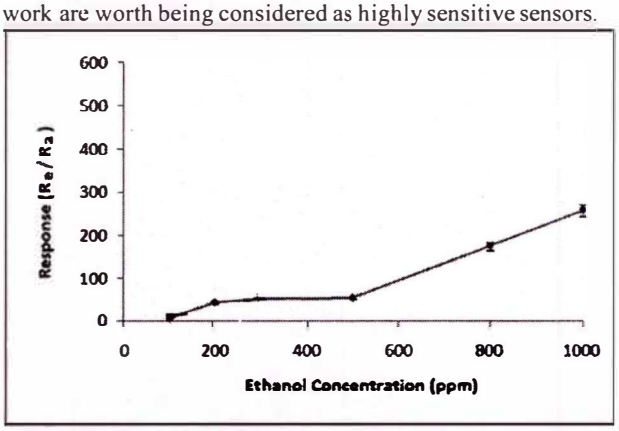

Fig. 6 The Sensor Sensitivity of $LaFeO_3$ Based Sensor From This Work

IV. Conclusion

$LaFeO_3$ perovskite samples in powder form were prepared using the co – precipitation method. XRD, and SEM techniques revealed the significant difference in physical properties of the samples. The responses of $LaFeO_3$ to various concentrations of ethanol gas were measured at 350 °C. From the Lower calcinations temperature the $LaFeO_3$ showed great enhancement of sensitivity toward ethanol giving results that were much better than many sensors ever reported.

Acknowledgment

The authors wish to acknowledge the Office of the Higher Education Commission of Thailand (OHEC) and the Graduate School, Prince of Songkla University, Thailand for financial support of this work.

References

[1] J. W. Fergus, Perovskite oxides for semiconductor –based gas sensors, Sensor and Actuators B 123 (2007) 1169 – 179

[2] X. H. Wu, Y. D. Wang, H. L. Liu, Y. F. Li, Z. L. Zhou, Preparation and gas –sensing properties of perovskite –type $MSnO_3$ (M = Zn, Cd, Ni), Materials Letters 56 (2002) 732- 736

[3] M. Ghasdi and H. Alamdari, CO sensitive nanocrystalline $LaCoO_3$ perovskite sensor prepared by high energy ball milling, Sensor and Actuators B 148 (2010) 478-485

[4] X. Wang, H. Qin, L. Sun, J. Hu, CO_2 sensing properties and mechanism of nanocrystalline LaFeO3 sensor, Sensors and Actuators B 188 (2013) 965–971

[5] W. Kaituo, W. Xuehang, W. Wenxei, L. Yongni, L. Sen, Synthesis of perovskite $LaCoO_3$ by thermal decomposition of oxalates : phase evolution and kinetics of thermal transformation of the precursor, Ceramics International 40 (2014) 5997-6004

[6] X. Chu, S. Zhou, W. Zhang, H. Shui, Trimethylamine sensing properties of nano – LaFeO3 prepared using solid – state reaction in the presence of PEG400, Materials Science and Engineering B 164 (2009) 65-69

[7] M.C. Carotta, M.A. Butturi, G. Martinelli, Y. Sadaoka, P. Nunziante, E. Traversa, Microstructural evolution of nanosized LaFeO3 powders from the thermal decomposition of a cyano –complex for thick film gas sensors, Sensors and Actuators B 44 (1997) 590-594

[8] S.P. Pavunny, R. Thomas, A. Kumar, N.M. Murari, R.S. Katiyar, Dielectric properties and electrical conduction of high –k $LaGdO_3$ ceramics, Journal of Applied Physics 111 (2012) 102811 – 102816

[9] S.P. Pavunny, R. Thomas, T.S. Kalkur, J. Schubert, E. Fachini, R.S. Katiyar, Fabrication and electrical characterization of high – k $LaGdO_3$ thin films and field effect transistors, ECS Trans 35 (2011) 297 – 304

[10] S.P. Pavunny, P. Misra, J.F. Scott, R.S. Katiyar, Advanced high –k dielectric amorphous $LaGdO_3$ based high density metal –insulator – metal capacitors with sub –nanometer capacitance equivalent thickness, Applied Physics Letters 102 (2013) 252905 – 252909

[11] S.P. Pavunny, A. Kumar, P. Misra, J.F. Scott, R.S. Katiyar, Properties of the new electronic device material $LaGdO_3$, Physica status solidi 251 (2014) 131 – 139

[12] K. Rusevova, R. Koferstein, M. Rosell, H.H. Richnow, F.D. Kopinke, A. Georgi, $LaFeO_3$ and $BiFeO_3$ perovskites as nanocatalysts for contaminant degradation in heterogeneous Fenton –like reactions, Chemical Engineering Journal 239 (2014) 322- 331

[13] K. Fan, H. Qin, Z. Zhang, L. Sun, L. Sun, J. Hu, Gas sensing properties of nanocrystalline $La_{0.75}Ba_{0.25}FeO_3$ thick –film sensors, Sensors and Actuators B 171-172 (2012) 302-308

[14] R. Ianos, R. Lazau, S. Borcanescu, R. Babuta, Single –step combustion synthesis of $LaAlO_3$ powders and their sintering behavior, Ceramics International 40 (2014) 7561-7565

[15] W. Li, M.W. Zhuo, J.L. Shi, Synthesizing nano $LaAlO_3$ powders via co –precipitation nmethod, Materials Letters 58 (2004) 365 – 368

[16] W.Y. Lee, H.J. Yun, J.W. Yoon, Characterization and magnetic properties of LaFeO3 nanofibers synthesized by electrospinning, Journal of Alloys and Compounds 583 (2014) 320-324

[17] S.E. Moon, H.K. Lee, N.J. Choi, J. Lee, C.A. Choi, W.S. Yang, J. Kim, J.J. Jong, D.J. You, Low power consumption micro C_2H_5OH gas sensor based on microheater and screen printing technique, Sensors and Actuators B 187 (2013) 598-603

[18] P. Song, H. Zhang, D. Han, J. Li, Z. Yang, Q. Wang, Preparation of biomorphic porous LaFeO3 by sorghum straw biotemplate method and its acetone sensing properties, Sensors and Actuators B 196 (2014) 140-146

[19] P. Song, Q. Wang, Z. Zhang, Z. Yang, Synthesis and gas sensing properties of biomorphic LaFeO3 hollow fibers template from cotton, Sensors and Actuators B 147 (2010) 248-254

[20] K. Kleveland, M.A. Einarsrud, T. Grande, Sintering of $LaCoO_3$ based ceramics, Journal of the European Ceramic Society 20 (2000) 185-193

[21] Z. Tian, W. Huang, Y. Liang, Preparation of spherical nanoparticles of $LaAlO_3$ via the reverse microemulsion process, Ceramics International 35 (2009) 661-664

About Author (s):

Wankassama Haron was born in Pattani, Thailand on August 29, 1981. She completed her undergraduate work in Chemistry (B.Sc. Chemistry) from Thaksin University, Songkhla, Thailand, in Political Science (B.P.Sc. Political Science) from Sukhothai Thammathirat Open University, Nonthaburi, Thailand, and Master degree in Inorganic Chemistry (M.S. Chemistry) from Kasetsart University, Bangkok, Thailand. Presently, she is the Ph.D. candidate majoring in Inorganic Chemistry at Prince of Songkla University, Hat Yai, Songkhla, Thailand. She is studying toward the Ph.D. degree under the scholarship from the Office of the Higher Education Commission of Thailand (OHEC).

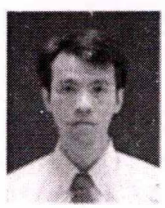

Dr. Anurat Wisitsoraat was born in Bangkok, Thailand. He received B.S. degree in Electrical Engineering from Chulalongkorn University, Bangkok, Thailand, M.S.and Ph.D. in Electrical and Computer Engineering from Vanderbilt University, USA. Presently, he is researcher at Nanoelectronics and MEMS laboratory, National Electronics and Computer Technology Center, Bangkok, Thailand. His research interests are in

Fabrication of Micro-Electro-Mechanical System (MEMSs), Gas and pressure sensors, and Microelectronic devices and Integrated circuits.

Associate Professor Dr. Sumpun Wongnawa was born in Chanthaburi, Thailand, on 3rd February 1950. He received B.S. degree in Chemistry from Michigan Technological University, USA, M.S. and Ph.D. in Inorganic Chemistry from Ohio State University, USA. Presently, he is Associate Professor in Inorganic Chemistry at Department of Chemistry, Faculty of Science, Prince of Songkla University, Hat Yai, Songkhla, Thailand. His research interests are in Metal Oxides and Photocatalysts, Complex Formation between Transition Metals and Herbal Natural Products, Oxalato Complexes of Aluminum and Transition Metals, Nano-materials and Inorganic Chemistry.

Chitosan Scaffold for Wound Healing Application

Priyanka Chhabra, Gaurav Mittal, Aseem Bhatnagar, Amit Tyagi

Abstract:-Chitosan is natural polysaccharide resembles with glycosaminoglycan of Extra Cellular matrix (ECM), which makes it a promising candidate for wound healing application apart from its excellent biocompatibility and biodegradability. In this study we have formulated various types of chitosan gel by dissolving different concentrations of chitosan powder in 100 ml of 2% acetic acid separately. Electrolytes were also added during stirring which was carried out for 5 ±0.5h at 50^0C. Different types of chitosan gel thus obtained were lyophilized for 48 h to remove water and chitosan scaffold were obtained and characterized using Scanning electron microscopy (SEM), FT-IR and swelling test. FT-IR confirms the chemical identity of chitosan in scaffolds. SEM micrographs of polymeric hydrogel scaffolds synthesized using 2% of chitosan was found to be the best in various physiochemical properties. The swelling capacity of 2% Chitosan scaffold was found to be better in comparison to rest of the scaffolds.

Keywords— Chitosan, Histopathology, Wound Healing, Scaffold.

I. Introduction

Chitosan is a partially de-acetylated polymer of glucosamine (GlcN) and N-acetylglucosamine (GlcNAc) residue with β-(1-4) linkage [1], [2]. It possesses many properties like hemostasis, biocompatibility and biodegradability which make it attractive for applications for skin tissue regeneration & wound healing [3], [4]. Chitosan is natural polysaccharide resembles with glycosaminoglycan of Extra Cellular matrix (ECM), which makes it a promising candidate for wound healing application [5], [6]. Chitosan provides a suitable microenvironment for cell activities by behaving like an extra cellular matrix (ECM). [7].It slowly depolarize to release N-acetyl-β-D-glucosamine units which start proliferation of fibroblast cells and stimulation of collagen synthesis [8],[9]. Apart from wound healing it also possess antimicrobial properties which initiates host cell defense and prevent wound from infection which is particularly useful for wound treatment [10],[11].

In present study, an attempt has been made to develop a Chitosan scaffolds with different concentration of Chitosan and hypothesized that Chitosan scaffold with porous surface will provide better microenvironment for wound healing. The physiochemical characterizations of the developed Chitosan scaffolds were evaluated by Scanning Electron Microscopy (SEM), FT-IR and swelling index. The chitosan scaffold with appropriate pore size and swelling index was further used for wound healing application.

Priyanka Chhabra, Gaurav Mittal, Aseem Bhatnagar, Amit Tyagi

INMAS, DRDO,India
Pchhabra188@gmail.com

II. Materials And Methods

Ethics Statement

All the procedures and care managed to the animals has been approved as per the Committee for the Purpose of Control and Supervision of Experiments on Animals (CPCSEA) regulations and the study protocol was approved by the Institutional Animal Ethics Committee of the Institute (INM/IAEC/2012/05), INMAS, DRDO, and Delhi, India.

Chemicals

Chitosan low viscous was procured from Sigma- Aldrich, (USA), Glacial acetic acid and Calcium chloride was procured from Merck India ltd, Mumbai, All other chemicals used were of analytical grade.

Preparation of Chitosan scaffolds.

Different concentration (0.5 -4%) of Chitosan powder was dissolved separately in dilute acetic acid (1% w/v) and the reaction mixtures were kept for 5 ±0.5h at 50^0C under continuous stirring of 250 rpm and 1% w/v of $CaCl_2$ was also added in all the reactions mixtures. The solutions were then poured separately in circular polypropylene pertridishes and kept at -20^0C for 24 hrs. The samples thus obtained were kept overnight for lyophilization. Various types of Scaffolds thus Obtained were stored at 4^0C for further evaluation.

Physiochemical characterization

SEM Analysis

Surface morphology of chitosan scaffolds was observed under scanning Electron Microscope Surface (SEM) (Leo, VP-435, UK).The specimen were cut from the scaffolds and dried overnight at 50^0C and then dried samples were sputter coated with gold particles before observation. In each cross sectional image of the scaffold, the average pore size was calculated.

FT-IR spectroscopy

FTIR analysis of vacuum dried samples of Chitosan and various types of Chitosan scaffolds were recorded on a Perkin

Elmer spectrum one spectrometer in the range of 4000cm^{-1} to 650cm^{1}.

Swelling studies

The swelling characteristics of Chitosan scaffolds were evaluated by weighing the scaffold before and after immersing in distilled water for 3 days at 37^{0}C. At specific interval of time, the scaffolds were taken from the water and excess surface water was removed using filter paper. The swelling ratio (SR) was calculated using the following equation.[9]

$$SR = (W_W - W_d)/W_d$$

Where W_W is the swollen weight of Chitosan scaffold and W_d is the dry weight of scaffold sample.

III. Statistical Analysis

The statistical significance was determined by using one way analysis of variance (ANOVA) by Graph pad prism 5. Statistical significance value was set at $p < 0.05$.

IV. Result and Discussion

Chitosan scaffolds were synthesized for wound healing and fasten blood clotting. Different concentration (0.5-4%) of Chitosan was used in addition to calcium chloride as electrolyte. Calcium chloride was added in the reaction mixture in view of improved blood clotting efficacy of the Chitosan scaffolds. Briefly, Chitosan scaffolds obtained using 0.5% of Chitosan was white color, poor mechanical strength and found to be fragile. Scaffolds obtained using 2% of Chitosan were white color, optimal mechanical properties and surface appeared to be porous. Scaffolds obtained using 3.0 – 4.0 % of Chitosan were of pale white color and lot of cracks were observed over the surface. The intensity of cracks over the surface of scaffolds increases with increase in the concentration of the Chitosan. On the other hand, scaffolds having 0.5% of Chitosan were mechanically very poor strength and cannot be used in wound healing. In view of that, Chitosan scaffolds synthesized using 2% of Chitosan were selected for further studies.

SEM analysis (Fig.1) revealed that chitosan scaffold synthesized using 2% of chitosan showed pore size of 80um to 200um which was randomly distributed throughout the surface of scaffold and found to be the best scaffold. As expected porosity of the chitosan scaffold decreases with increase in concentration of chitosan.

FT-IR measurements (Fig .2) confirmed the presence of Chitosan in Chitosan scaffolds. Characteristic peaks of Chitosan as found at 3253cm^{-1}, 2873cm^{-1}(O-H Stretching),1407cm^{-1},896 cm^{-1},656 cm^{-1} (C-H Bending)1633 cm^{-1},1547 cm^{-1},(C=C stretching) 1069 cm^{-1},1073 cm^{-1} (C-O Stretching). Almost similar peaks were observed in all Chitosan scaffolds formulation.

The propensity of scaffold to retain water is a key aspect to evaluate its property for skin tissue engineering because it not only affects its morphology and configuration but also affect the in growing cells. Swelling characteristic of Chitosan scaffolds of different concentration are shown in Fig.3. It was found that the degree of swelling of Chitosan scaffold increases with increase in concentration of Chitosan in first 2hrs. This rapid increase continues until 6hrs.then the swelling ration of all the samples seemed to stabilize, and slight increase could be observed with time. Chitosan scaffold with 0.5% of chitosan dissolves in water with in 30 min & it was impossible to collect the sample for further readings. The water absorption capacity of 2% Chitosan scaffold was found to be highest which is suitable for skin tissue engineering and wound healing. Swelling index decreases with increase in chitosan concentration probably due to decrease in pore size and complexity of chitosan scaffold.

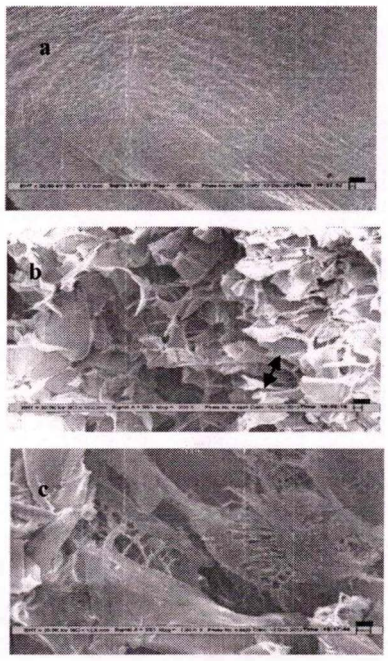

Fig. 1 SEM Micrographs for cross section of the chitosan scaffolds prepared using different concentration of chitosan (n=6).(a) .5% (b) 2% and (c) 4% chitosan

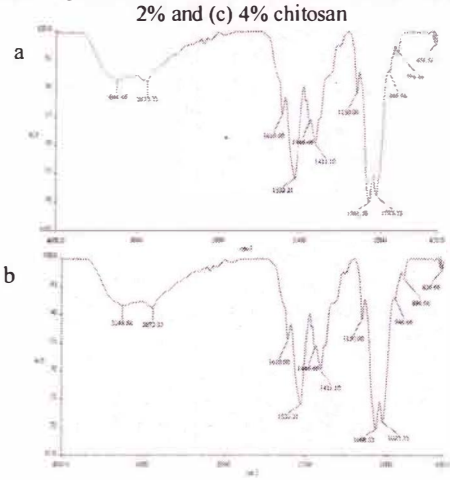

c

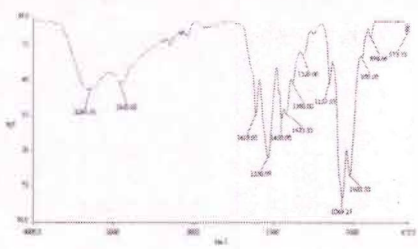

Fig.2. Fourier transform infrared (FTIR) spectra of (a) 0.5%chitosan (b) 2% chitosan scaffold (c) 4% chitosan scaffold

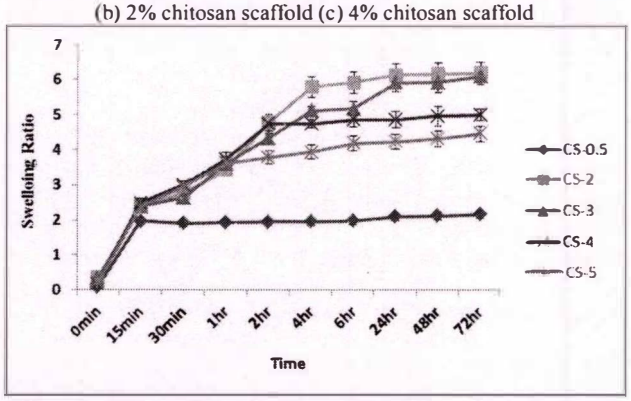

Fig.3. Swelling ratio of chitosan scaffold in water distilled water at 37^{0}C for 3 days. Values are reported as mean ± Standard deviation (SD) (n=3)

V. Competing Interest

The authors declare that they have no competing interest.

VI. Acknowledgment

Authors are greatly indebted to INMAS for providing research support and University Grant Commission (UGC), New Delhi, India whose financial support made this study possible.

References

[1] M. Burkatovskaya, A.P. Castano, T.N. Demidova-Rice, G.P. Tegos "Effect of Chitosan acetate bandage on wound healing in infected and non-infected wounds in mice", *Wound Repair Regen.*, vol. 16(3), pp.425-431, 2008.

[2] B. Yang, X.Y. Li, S. Shi, X.Y. Kong, G. Guo, M. Huang , F. Luo et al, "Preparation and characterization of novel Chitosan scaffold", *Carbohydrate polymer*, vol. 80, pp. 860-865, 2010.

[3] R. Shelma, W. Paul. C. P Sharma. "Chitin nanofibre reinforced thin Chitosan films for wound healing application", *Trends Biomaterial Artif. Organs*, vol. 22(2), pp.107-111, 2008.

[4] H. Ueno, T. Mori, T. Fujinaga, "Topical formulation and wound healing application of chitosan", *Advanced drug delivery reviews*, vol.52 (2), pp. 105-115, 2001.

[5] J.F. Prudden, P.Migel, P.Hanson, L.Friedrich, L.Balassa. "The discovery of a potent pure chemical wound healing accelerator", *Am.J.sur.*,vol. 119, pp. 560-564, 1970.

[6] R.C. Correia, L.S. Moreira-Teixeira, R.L. Reis, C.A.V. Blitterswijk, M. Karperien et al, "Chitosan Scaffold Containing hyaluronic acid for cartilage tissue engineering", *Tissue engineering: Part C*, vol. 17(3), pp.717-730,2011.

[7] W. Paul, C.P. Sharma, "Chitosan and Alginate Wound Dressings: A Short Review", *Trends Biomater. Artif. Organs*, vol. 18 (1), pp. 18-23, 2004.

[8] A.R.C. Duarte, J.F. Mano, R.L. Reis, "Preparation of Chitosan scaffolds for tissue engineering using supercritical fluid technology", *Materials Science Forum*, Vol. 636-637,pp.22-25, 2010.

[9] D. Raafat, K.V. Bargen, A. Haas,H - Sahl, "Insights into the Mode of action of chitosan as an antibacterial compound", *Appl. Environ. Microbiol.* vol. 74 (12), pp. 3764-3773, 2008.

[10] P. Mezzana , "Clinical efficacy of a new chitin nanofibrils based gel in wound healing", *Acta Chir Plast.*, vol. 50(3), pp. 81-84, 2008.

[11] E.I. Rabea, M.ET. Badawy, C.V. Stevens, G. Smagghe, W. Steurbaut, "Chitosan as Antimicrobial Agent: Applications and Mode of Action", *Biomacromolecules*, vol. 4(6), pp. 1457-1465, 2003.

[12] L. Ma, C. Gao, Z. Maoa, J. Zhoua, J.,Shen, X. Hu et al, "Collagen/Chitosan porous scaffolds with improved bio stability for skin tissue engineering", *Biomaterials*, vol.24, pp. 4833-4841, 2003.

Recycling Capability of Multilayer Ag Doped Tio_2/PVA Nanofibers under UV and Solar Irradiation

Norizan Mohammed Lot[1], Siti Nafisah Md Rashid[2], Umi Sara Jais[3], and Mohd Kamil Abd Rahman[4]

***Abstract*—** Pure and Ag doped TiO_2 powder were fabricated to immobilize on the PVA nanofibers and encapsulate in the layers between nanofibers using sol gel and electrospinning technique to form multilayer nanofibers. XRD and FTIR measurement were carried out to confirm the presence of TiO_2 powder inside the PVA nanofibers. The morphology of the multilayer Ag doped TiO_2/PVA nanofibers was observed using FESEM and the image showed that the powder is aligned within the PVA nanofibers. Photocatalytic activity of the multilayer nanofibers has been evaluated using degradation of the MO solution under UV and solar irradiation. Multilayer Ag doped TiO_2/PVA nanofibers exhibited higher rate of degradation where k are 33.4×10^{-3} min^{-1} under UV and 12.8×10^{-3} min^{-1} solar irradiations. The multilayer nanofibers possessed high photocatalytic activity even after 5 cycles of photo-degradation of MO under UV light irradiation.

***Keywords*—**TiO_2, Ag doping, poly (vinyl) alcohol, nanofibers

I. Introduction

TiO_2 is widely known as a superior photocatalyst metal oxide because of its physical and chemical stability, non-toxicity, chemical corrosion, photostability and low cost [1]. Various method and effort have been performed to make TiO_2 powder immobilizes on the substrate as it can be simply detached from the treated water and able to be used for multiple times. Numerous studies have been conducted to immobilize TiO_2 powder on the polymeric nanofibers using electrospinning techniques. Reference [2] used polyacrylonitrile (PAN) to immobilize TiO_2, [3] used a chitosan PVAe nanofibers to immobilize Ag and Nitrogen doped TiO_2 and [4] used Fully hydrolyzed (FH) PVA 99%+ to immobilize TiO_2 and yet less report on the result of this nanofibers for multi-cycle use has been discussed. Therefore, in this study, we design multilayer Ag doped TiO_2/PVA nanofibers to encapsulate the Ag doped TiO_2 powder for multi-cycle usage.

This study provides higher opportunity for TiO_2 powder to fully contact with aqueous organic pollutant [2] as well as increased its surface area on the multilayer nanofibers. Noble metal such as Ag was reported to be less expensive and is capable to increase the efficiency of the photocatalytic activity of TiO_2 by acting as electron trap and subsequently reduced fast recombination rate.

Norizan Mohammed Lot. Universiti Teknologi MARA Malaysia, norizan9021@gmail.com

PVA was chosen due to its economical and eco-friendly aspects. However, FH PVA is found to have high surface tension and thus makes them hardly electrospun [5]. By adding surfactant, the surface tension of the FH PVA can be reduced [6][7].

The higher surface tension of the polymer can influence the form and yield of nanofibers. In this study, non-ionic surfactant of diluted Triton X-100 has been added to reduce the surface tension of the polymer and thus smoothing the electrospinning process. Apart from UV light, solar irradiation has also been used as the light source for photocatalytic activity in this study.

A. Chemicals

Titanium (IV) Butoxide (TTIB), $AgNO_3$, Triton X-100, Polyvinyl Alcohol, PVA (Mw 77000-79000, 99-99.8% fully hydrolysed), Methyl Orange (MO), Ethanol (EtOH), Hydrochloric acid (HCl), deionized water (DI). These chemicals were used without the need for further purifications.

B. Pure and Ag doped TiO_2 powder

The preparation of TiO_2 precursor solution was similar from our previous study. A mixture of 55 ml of EtOH and 5 ml of DI is added drop by drop into 26 ml of TTIB using burette. The solution is left to stir for 4 hours at room temperature. Next, 2.65 ml of 1M of HCl is added to the solution to give pH of the solution is 3.2. Then, the solution is left to stir for another I hour. For the solution with Ag doping, appropriate amount of $AgNO_3$ was added into the precursor solution to give concentration of 0.5wt% of Ag doped TiO_2, then the solution is left to stir overnight to dissolve $AgNO_3$ particle completely. After that, the solution is allowed to be peptized and washed with DI water to remove excess of hydrolysis solution. Subsequently, the gel is dried at 120°C, and its powder is pulverized and heated at 750°C at the rate of 5°C per minutes for 3 hours.

C. Pure and Ag doped TiO_2/PVA solution

For the preparation of nanofibers solution, the powder was dispersed in the DI water using ultrasonic bath for 5 minutes. The sample is stirred and then heated to 90°C using hot plate prior adding 10wt% of the PVA powder and stirring is continued for 4 hours. The sample is then cooled at room temperature before adding 10wt% of diluted non-ionic surfactant of Triton X-100. After stir the solution for 15 minutes at room temperature, the solution is then ready for

electrospinning process.

D. Electrospinning

Before electrospinning is carried out, several trials have been done to obtain suitable parameters. The electrospinning process was set to 0.2 ml/h of the flow rate, 10 cm distance between needle tip and collector and 12 kV of applied voltage. The encapsulation of powder within nanofibers layers were made step by step for every half an hour of electrospinning process. This process is repeated for 3 times, thus formed a sample which contains 3 layers of powder and 4 layers of nanofibers. The obtained sample is then heated to 140°C.

E. Characterization and Degradation of aqueous MO

Structural properties of the sample have been tested by using XRD and FTIR to analyze the chemical bonding between powder and PVA solution. The morphology of the nanofibers and its average diameter has been observed and measured using FESEM and Image J software. The ability of nanofibers with layers of powder for degradation rate of MO in an aqueous solution with concentration of 10mg/L is evaluated based on pseudo-first-order reaction [8] and the expressions of its kinetics as shown in (1)

$$\ln(\frac{Co}{C}) = kt \tag{1}$$

where k is apparent rate constant, Co and C is the initial concentration and concentration at time t of aqueous MO, respectively. The sample was tested under UV and solar irradiation. The spectrum of solar was measured using HR-4000 spectrometer as shown in Fig. 1. The experiments were performed by using 0.1 g of multilayer pure and Ag doped TiO_2/PVA nanofibers immersed in 50 ml of MO (10g/ml) solution. At regular interval, 2 ml of MO has been taken for absorbance analysis using UV-Vis spectrometer. Fig. 2 shows the samples before and after solar irradiation.

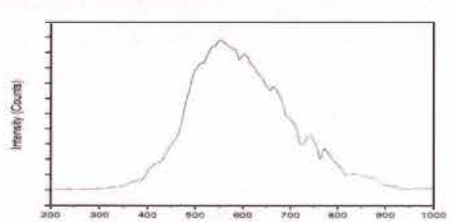

Fig. 1 Spectrum of solar

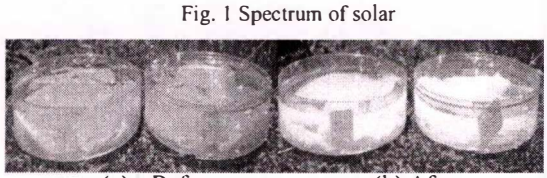

(a) Before (b) After

Fig. 2 Sample before and after solar irradiation

II. RESULTS AND DISCUSSION

A. XRD result

The resulting graph of XRD is analyzed as shown in Fig. 3. The crystallite size can be calculated using Scherrer equation [1] as shown in (2)

$$D = \frac{0.9\lambda}{\beta \cos\theta} \tag{2}$$

where D is average particle size, 0.9 is constant, λ is X-ray wavelength (0.154 nm for Cu Kα), β is the full width at half maximum (FWHM), and θ is Bragg's angle. The crystallite size of pure and Ag doped TiO_2 powder was increased from 33.83 nm to 35.65 nm.

Pure and Ag doped TiO_2 powder exhibited mixed phase of anatase and rutile. The percentage of different phase of TiO_2 was calculated by using Spurr-Myers equation (3)

$$w_A = \frac{1}{1+1.26\frac{I_R}{I_A}}, \quad w_R = \frac{1}{1+0.81\frac{I_A}{I_R}} \tag{3}$$

where w_A is the weight of anatase, w_R is the weight of rutile, I_A and I_R are the relative intensity at the anatase (101) and rutile (110) peaks respectively. Percentage ratio of anatase to rutile of pure TiO_2 was 55:45. For sample Ag doped TiO_2, a small amount of rutile diminished but the amount of anatase is increased with the percentage ratio anatase to rutile is 75:35. This shows the change of structural phase of TiO_2 due to Ag doping. By referring [JCPDS-no 21-1271], the diffraction peak of the anatase are observed at 2θ at 25.3, 37.8, 48.1 and 54.0 correspond to the crystal plane of (101), (004), (200), and (211) respectively. While the diffraction peak of rutile phase are observed at 27.4, 36.1, 38.6 and 55.1 which represent to crystal plane of (110), (101), (112), and (211), respectively [JCPDS-no21-1675].

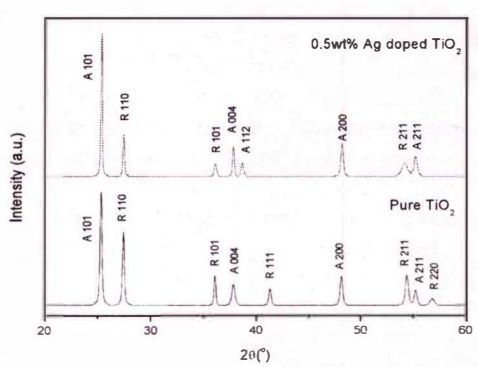

Fig. 3 XRD patterns of Pure and Ag-TiO2 powder

Fig. 4 (a) shows the XRD diffraction peak of PVA nanofibers and Ag doped TiO_2/PVA multilayer nanofibers. The diffraction peak observed at 19.89° represents the superior crystalline properties of PVA nanofibers [4]. From the diffraction peak of multilayer Ag doped TiO_2/PVA nanofibers, Ag doped TiO_2 powder remains their crystalline structure even though high electrostatic force [7] is applied during electrospinning process. The reasons for low doping of Ag with 0.5wt% is used in this project, because as reported by other researchers [9], they found that at elevated temperature of Ag doped TiO_2, the lower concentration of Ag is desired

for higher efficiency of photocatalytic activity.

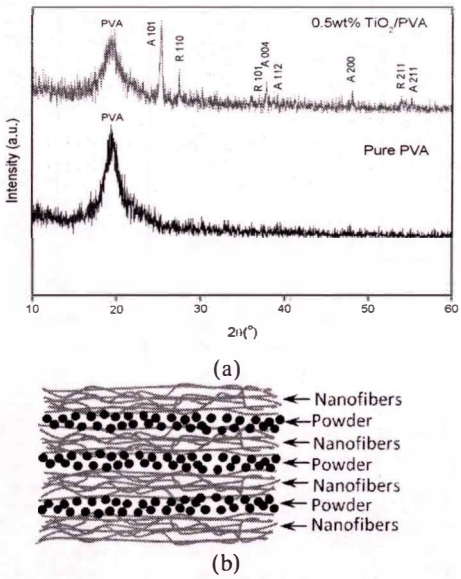

Fig. 4 (a) XRD patterns of pure PVA and multilayer Ag doped TiO2/PVA nanofibers (b) Schematic diagram of multilayer nanofibers

B. *FTIR result*

Fig. 5 shows the FTIR spectra of PVA nanofibers, pure and multilayer Ag doped TiO_2/PVA nanofibers. The broad peak between 3600 cm^{-1} and 3000 cm^{-1} with precise peak appear at 3470 cm^{-1} assigned to the free O-H vibration in PVA. Sharp peak observed at 1260 cm^{-1} and 863 cm^{-1} assigned to the C-C stretching and C-H rocking of PVA. Besides that, the band peak presence at 1474 cm^{-1} belongs to C-H bend of CH_2 in PVA [10],[11]. To observe pure and Ag doped TiO_2 powder immobilize or encapsulated within the PVA nanofibers, peak observed between 800 cm^{-1} to 400 cm^{-1} is presented in PVA nanofibers while the other peaks remain constant [11]. This peak is assigned to the asymmetric stretching and the bending mode of Ti-O-Ti [12].

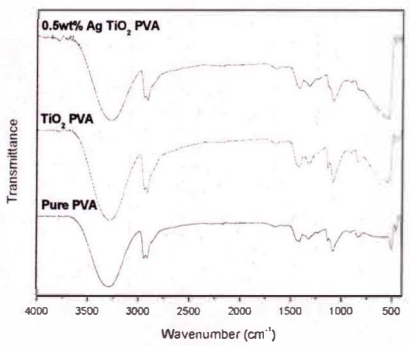

Fig. 5 FTIR spectra of Pure PVA nanofibers, Pure and multilayer Ag -TiO2/PVA nanofibers

C. *Morphology*

Fig. 6a, 6b, 6c show morphology of Ag doped TiO_2 powder, pure PVA nanofibers and multilayer Ag doped TiO_2/PVA nanofibers. Image of Ag doped TiO_2 powder shows the agglomeration of particle shape and it was dispersed and embedded along with PVA direction [2] due to the polarization and orientation of high electric field throughout electrospinning process [4] and hence, increasing diameter of nanofiber. It can be seen from the average diameter nanofibers as shown in Fig. 5a and Fig. 5b, with the average diameter of pure PVA nanofibers and multilayer Ag doped TiO_2/PVA nanofibers is 300-400 nm and 600-700 nm. In addition, irregular morphology with uneven surface is clearly seen by the big agglomeration of the powder. This is because of the aggregation of the powder and the powder also stacking on the surface of the nanofibers [2]. The EDX result also shows the Ag doped TiO_2 powder is well dispersed in the nanofibers with the existence of element C and O from the pure PVA while element Ti and O from the TiO_2 powder. Element Ag cannot be traced due to the lower content in the multilayer nanofibers.

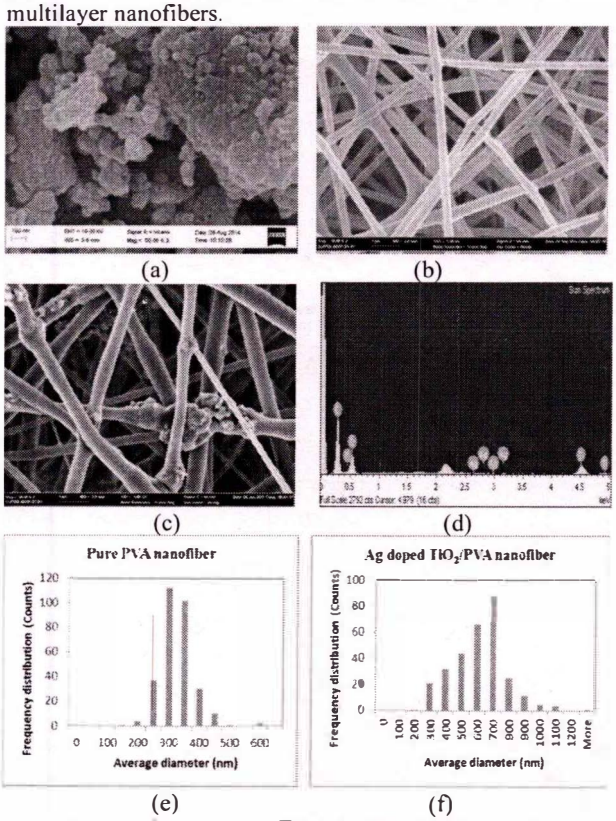

Fig. 6 FESEM images a) Ag-TiO2 powder, b) PVA nanofibers, c) multilayer Ag-TiO2/PVA nanofibers, d) EDX profiles of multilayer Ag-TiO2/PVA nanofibers, Average diameter e) PVA nanofibers and f) multilayer Ag-TiO2/PVA nanofibers

D. *Band Gap*

Band gap of the un-doped and Ag doped TiO_2 powder were analyzed using Kubelka Munk's equation [13] as stated in (4)

$$(\alpha h\nu) = A(h\nu - E_g)^n \quad (4)$$

where A is constant, E_g is the optical band gap which is separation gap among the lowest conduction band and highest valence band, hv is the photon energy and n is the probability of the transition which is ½ and 2 is direct and indirect gap transition, respectively. TiO_2 is indirect band gap [14]and Fig. 7a and 7b showed the relation between $(ahv)^{1/2}$ against photon energy (eV). The estimated band gap is defined by extrapolation of a linear curve. DRS results revealed that the calculated band gap of pure and Ag doped TiO_2 were reduced from 3.03 eV to 2.98 eV.

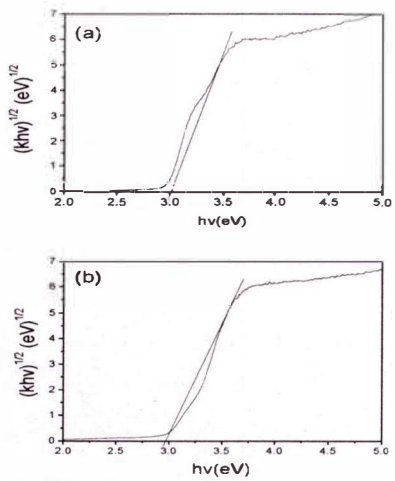

Fig. 7 Band Gap a) Pure TiO2 b) Ag doped TiO2 powder

E. Photocatalytic Activity and Recycle

Fig. 8 shows the degradation activity of pure and multilayer Ag doped TiO_2/PVA nanofibers under UV and Solar irradiation. Table I shows the rate constant value. As can be seen, the degradation rate for sample doping with Ag show better photocatalytic activity under both light source. The percentage degradation of multilayers Ag doped TiO_2/PVA nanofibers under solar and UV within 150 min is 86.52% and 99.62% respectively. It reveals that ability of Ag act as the electron trapped even in the nanofibers/layer formed.

The degradation rate under solar is lower because of the intensity of the UV in the solar region is smaller as shown in Fig. 1. However, the light still be able to utilize for degradation of the dye activity. The degradation activity occurs when the aqueous MO is attached to the sample, the sample absorbed the light and electron is excited from the valence band to the conduction band and hence, the electron at the conduction band was trapped by the Ag particle which prevent fast recombination of the electron and subsequently react with the O from the TiO_2 surface [15][16].

Besides for aiming high efficiency of photocatalyst under UV and solar, because of the design that can be easily separate from the treated water, the multilayer nanofibers was tested again for other 5 cycles to test its performance. Fig. 9 shows that the multilayer Ag doped TiO_2/PVA nanofibers still maintain its performance even though was used for several times.

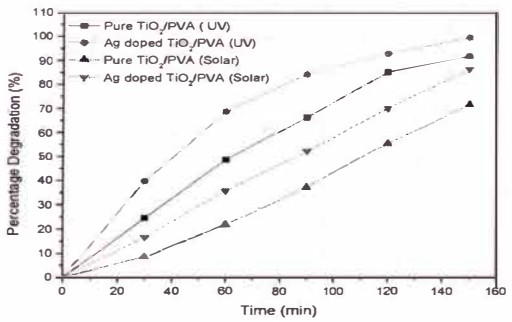

Fig. 8 Percentage degradation of MO using multilayer nanofibers under UV and solar irradiation

TABLE I:
RATE CONSTANT OF MO DEGRADATION ACTIVITY

	Rate Constant, k ($x10^{-3}min^{-1}$)	
Light Source	Pure TiO_2	0.5wt% Ag doped TiO_2
UV	17.3	33.4
Solar	8.3	12.8

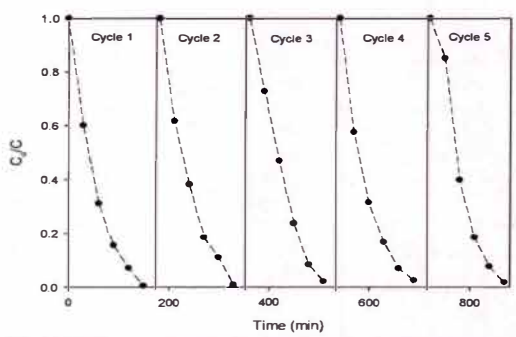

Fig. 9 MO concentration during 5 cycles in the presence of multilayer Ag doped TiO2/PVA nanofibers at 150 min. per cycle under UV irradiation

III CONCLUSION

In present study, multilayer Ag doped TiO_2/PVA nanofibers was successfully fabricated using sol gel and electrospinning technique. XRD and FTIR results show that the Ag doped TiO_2 powder is immobilized and encapsulated within the PVA nanofibers. From the FESEM image, large fiber diameter with irregular size and rougher surface is observed. Photocatalytic behavior in degrading aqueous MO under UV and solar showed the efficiency of Ag dopant is higher than pure TiO_2 based on their high rate constant value. The sample also shows its ability to recycle by observing its degradation activity for 5 cycles. It can be concluded that Ag doped TiO_2 powder still perform its photocatalytic activity even in multilayer nanofibers form and acting electron trapping besides can be recycled photocatalyst.

ACKNOWLEDGMENT

This work was financial supported by RAGS 2013 Grant No. 600-RMI/RAGS 5/3 (21/2013). The author would like to

thank Ministry of Education Malaysia, Research Management Institute UiTM, Faculty of Applied Sciences, and Faculty of Pharmacy Universiti Teknologi MARA for samples characterization facilities and support.

REFERENCES

[1] M. A. Ameen and A. J. Khadum, "Annealing Effect on the Phase Transformation in Sol-Gel Derived Titania Nanostructure," vol. 8, no. 2, 2011.

[2] B. C. Ji, S. S. Bae, M. M. Rabbani, and J. H. Yeum, "Photocatalytic Activity of Electrospun PAN/TiO_2 Nanofibers in Dye Photodecomposition," *Text. Color. Finish.*, vol. 25, no. 2, p. 94, 2013.

[3] A. R. Ocwelwang and L. Tichagwa, "Synthesis and Characterisation of Ag and Nitrogen Doped TiO_2 Nanoparticles Supported on A Chitosan-Pvae Nanofibre Support," vol. 1, no. 2, pp. 28–37, 2014.

[4] N. T. B. Linh, K.-H. Lee, and B.-T. Lee, "Fabrication of Photocatalytic PVA–TiO_2 Nano-fibrous Hybrid Membrane using the Electro-spinning Method," *J. Mater. Sci.*, vol. 46, no. 17, pp. 5615–5620, Apr. 2011.

[5] Q. Gao, J. Takizawa, and M. Kimura, "Hydrophilic Non-wovens made of cross-linked fully-hydrolyzed poly (vinyl alcohol) electrospun nano fi bers," *Polymer (Guildf).*, vol. 54, no. 1, pp. 120–126, 2013.

[6] C. Risdian, H. Rachmawati, and M. Nasir, "Preparation of Electrospun Poly(Vinyl Alcohol) Nanofibers for Ultrafast Release of Protein," vol. 1, no. 3, pp. 91–94, 2014.

[7] E. S. Araújo, M. L. F. Nascimento, and H. P. De Oliveira, "Influence of Triton X-100 on PVA Fibres Production by the Electrospinning Technique," vol. 4, no. 50 ml, pp. 39–43, 2013.

[8] G. Wang, L. Xu, J. Zhang, T. Yin, and D. Han, "Enhanced Photocatalytic Activity of TiO_2 Powders (P25) via Calcination Treatment," *Int. J. Photoenergy*, vol. 2012, pp. 1–9, 2012.

[9] K. Ubonchonlakat, L. Sikong, and K. Kooptarnond, "Effect of Calcinations Temperature on Photocatalytic Activity of Ag-doped TiO_2 Coated on Tile Substrate," vol. 7, pp. 43–50, 2008.

[10] B. K. Avitha, D. D. Asharatham, D. S. Rinivasu, C. H. S. Rinivas, and N. N. Arsimlu, "Synthesis and Characterization of TiO_2 doped Polivynil Alcohol Polymer Composites," vol. 4, no. 4, pp. 155–157, 2011.

[11] P. Lei, F. Wang, X. Gao, Y. Ding, S. Zhang, J. Zhao, S. Liu, and M. Yang, "Immobilization of TiO_2 Nanoparticles in Polymeric Substrates by Chemical Bonding for Multi-cycle Photodegradation of Organic Pollutants," *J. Hazard. Mater.*, vol. 227–228, pp. 185–194, 2012.

[12] M. M. Ba-abbad, A. A. H. Kadhum, A. B. Mohamad, and M. S. Takriff, "Synthesis and Catalytic Activity of TiO_2 Nanoparticles for Photochemical Oxidation of Concentrated Chlorophenols under Direct Solar Radiation," vol. 7, pp. 4871–4888, 2012.

[13] H. Lin, C. Huang, W. Li, C. Ni, S. Shah, and Y. Tseng, "Size dependency of nanocrystalline TiO_2 on its optical property and photocatalytic reactivity exemplified by 2-chlorophenol," *Appl. Catal. B Environ.*, vol. 68, no. 1–2, pp. 1–11, Oct. 2006.

[14] J. Li, T. Ishigaki, and X. Sun, "Anatase , Brookite , and Rutile Nanocrystals via Redox Reactions under Mild Hydrothermal Conditions : Phase-Selective Synthesis and Physicochemical Properties," pp. 4969–4976, 2007.

[15] F. S. R. M. Behpour, S. M. Ghoreishi, "Photocatalytic Activity of TiO_2/Ag Nanoparticle on Degradation of Water Pollutions," *Dig. J. Nanomater. Biostructures*, vol. 5, no. 2, pp. 467–475, 2010.

[16] T.-J. Whang, H.-Y. Huang, M.-T. Hsieh, and J.-J. Chen, "Laser-induced Silver Nanoparticles on Titanium Oxide for Photocatalytic Degradation of Methylene Blue.," *Int. J. Mol. Sci.*, vol. 10, no. 11, pp. 4707–18, Nov. 2009.

Production of Biodiesel from Renewable Biological Sources

D. Raghuveer[1], M.Vijay[2], Dowluru Sreeraulu[3], P.Suman[4], and A.Satish Kumar[5]

***Abstract*—**Biodiesel, an alternative diesel fuel, is made from renewable biological sources such as vegetable oils and animal fats. It is biodegradable and non-toxic has low emission profiles and so is environmentally beneficial. Continued and increasing use of petroleum will intensify local air pollution and magnify the global warming problems caused by CO_2. In a particular case, such as the emission of pollutants in the closed environments of underground mines, biodiesel fuel has the potential to reduce the level of pollutants and the level of potential or probable carcinogens. Fats and oils are primarily water-insoluble, hydrophobic substances in the plant and animal kingdom that are made up of one mole of glycerol and three moles of fatty acids and are commonly referred to as triglycerides. Fatty acids vary in carbon chain length and in the number of unsaturated bonds.

Natural vegetable oils and animal fats are extracted or pressed to obtain crude oil or fat. These usually contain free fatty acids, phospho-lipids, sterols, water, odorants and other impurities. Even refined oils and fats contain small amounts of free fatty acids and water. The free fatty acid and water contents have significant effects on the transesterification of glycerides with alcohols using alkaline or acid catalysts. They also interfere with the separation of fatty acid esters and glycerol.

***Keywords*—**Renewable biological sources, global warming, alternative fuel, transesterification of vegetable oils.

I. Introduction

THE document is a template for *Word (doc)* versions. If you are Biodiesel is defined as mono-alkyl esters of long chain fatty acids derived from vegetable oils or animal fats which conform to American Society for Testing & Materials. It is the name of a clean burning alternative fuel, produced from domestic, renewable resources and animal fats. Today's diesel engines require a clean –burning, stable fuel that performs well under a variety of operation conditions. It is the only alternative fuel that can be used directly in any existing, unmodified diesel engine. Because it has similar properties to petroleum diesel fuel, biodiesel can be blended in any ratio with petroleum diesel fuel. It is simple to use, biodegradable, nontoxic and essentially free of sulfur and aromatics. It is made through a chemical process called transesterification where by the glycerin is separated from the fat or vegetable oil. Fuel-grade biodiesel must be produced to strict industry specifications in order to ensure proper performance. It is better for the environment because it is made from, renewable resources and has lower emissions compared to petroleum diesel. India is rich in renewable resources such as Jatropha, Pongamia etc, which decreases its foreign dependency. Some of the Major and minor renewable biodegradable sources of biodiesel oils such as soya bean, rapeseed, mustard, sunflower, palm and its fractions, coconut, palm kernel, cottonseed, tallow and minor renewable biodegradable sources such as (1) tree-borne seed oils like karanja, mowrah, neem, undi, nahor (2) plant seed oil jatropha (ratanjyot) (3) rice bran (4) water mellon (5) tobacco seed (6) niger seed (7) tea seed (8) jute seed (9) chilli seed oil.

[1,2,4]Assistant Professor, Centurion University of Technology and Management, JITM, Parlakhemundi, Odisha -INDIA
draghuveer@cutm.ac.in, vijay.miditana@gmail.com, suman@cutm.ac.in
[3] Professor, [5]Assistant Professor, Aditya Institute of Technology and Management, Tekkali, AP, INDIA
dowlurusreeram@gmail.com, adapa.satish3@gmail.com

II. Materials And Methods

Out of the available sources palm kernel oil is taken for the present study. The production of Biodiesel from palm kernel, or alkyl esters palm kernel falls in to the below mentioned methods for production of ester from oils.

- Base catalyzed transesterification of the oil with alcohol.
- Direct acid catalyzed esterification of the oil with methanol.
- Conversion of the oil to fatty acids, and then to alkyl esters with acid catalysis.

The majority of the alkyl esters produced today is done with the base catalyzed reaction because it is the most economic for several reasons.

- Low temperature (15^0F) and pressure (20psi) processing.
- High conversion (98%) with minimal side reactions and reaction time.
- Direct conversion to methyl ester with no intermediate steps

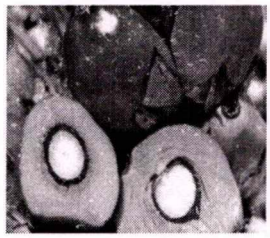

Fig. 1 Palm Kernel Seeds

The productivity and yield of Jatropha and Pongamia was compared with palm kernel in Table 1.

TABLE I:
COMPARISON OF PALM KERNEL SEEDS WITH JATROPHA AND PONGAMIA

S. No	parameter	Jatropha Curcas	Pongamia Pinnate	Palm Kernel Seeds
1	Planting density	1,000 plants per Acre	200 to 250 plants per Acre	60 to 70 plants per Acre
2	Productivity	Starts yielding after 1st year	Starts yielding after 3rd year	Starts yielding from 8th year.
3	Life Span	50 years	100 years	30 years
4	Yield per hectare / year	0.4 to 12 tonnes	6 to 9 tonnes.	18.5 tonnes and 750 kg of seed kernels.

Each tree of Palm Kernel can yield 40 Liters of oil, 120 Kg of fertilizer grade oil cake and 250 Kg of biomass as green manure per year. The expected oil content on whole FFB basis is 25 per cent, oil content in Mesocarp of fruits is 40 per cent, and oil content in kernel (seed) is 10 per cent.

Sources of Vegetable Oils: Palm Kernel oil was obtained and parameters like density, acid value, molecular weights and free fatty acid compositions are determined. The palm kernel seeds can be shown in fig. 1 and the Densities, Acid values and Molecular weights of palm kernel oil are shown in Table-2.

TABLE II
DENSITIES, ACID VALUES AND MOLECULAR WEIGHTS OF PALM KERNEL OIL

Name of the Oil	Density	Acid Value	Mol. Weight
Palm Kernal oil	0.902	4.2	886
Jatropha biodiesel	0.88	3-38	870
Pongamia Pinnate oil	0.88	1.0 to 38.2	886.61

III. EXPERIMENTAL WORK

In the present investigation, experimental work was carried out using different feed stocks of vegetable oils were undertaken. The process development studies are divided into three steps.

- Preconditioning of oil.
- Effect of catalyst concentration and mole ratio of oil to alcohol in transesterification reaction.
- Purification of products and recovery of methanol.

The physical properties such as Kinematic Viscosity, Fire Point, Carbon Residue, p^H, Flash Point, Acid Value are evaluated for the biodiesel samples obtained in the process development work.

The transesterification of the Palm Kernel oil has been carried out using sodium hydroxide as catalyst. These studies include the effect of mole ratio (oil to alcohol) in the range of 1:9 to 1:18 and the effect of catalyst concentrations in the range of 0.5 to 1.0 wt%. The physical properties of the biodiesel samples obtained from experimental analysis have been evaluated for comparison [1].

A. Experimental Setup

The experimental setup was shown in fig. 2 & 3. Three necked flat bottomed glass flask of 500ml capacity was used for transesterification reaction. A double coiled reflux condenser was fitted to a neck of the glass flask for condensing methanol vapors during the reaction. Ice cooled water was circulated through coils of the condenser. A thermo-well was fitted to the second neck of the flask. Thermo-well was filled with a thermometric liquid (Ethylene Glycol). A glass thermometer of 0-100^{0}C range was placed in the thermo-well to measure the temperature of the reaction mixture. A plate heater with a magnetic stirrer was used for uniform heating of the contents of the flask. Oil, methanol and other chemicals were transferred through the third neck of the flask at the start of each experimental run using glass funnel and was stoppered during the reaction. A constant temperature bath was provided to maintain the temperature of the contents in the flask in the range 60-63^{0}C.

Description of the experimental setup:

Apparatus: The important apparatus are Hot plate with magnetic stirrer (220/230 V 50 ~ 1 ϕ AC Amperes 1.8), Magnetic element, Three necked flat bottom flask with neck size of 24/29 and 500 ml (made of Borosil glass), Reflux coil condenser (Joint size 24/29), Thermo-well filled with thermometric liquid (Ethylene Glycol), Thermometer of 0-100°C range. Transesterification setup as shown in fig. 2 of 500 ml (made of Borosil glass) and separating funnels as shown in fig. 3 below

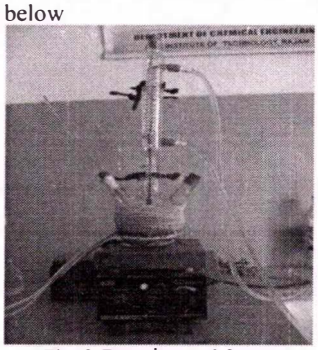

Fig. 2 Experimental Setup

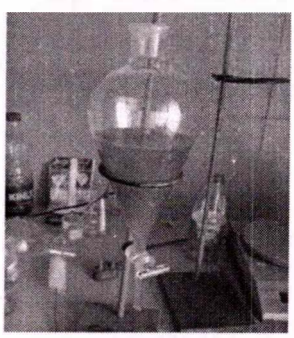

Fig. 3 Separating funnel

B. Experimental Procedure

Preconditioning of oil: Preconditioning of oil involved the removal of the moisture and neutralization of Free Fatty Acids (FFA).Usually refined oils consist less than 5% of FFA but they need to be neutralized as they result in the formation of soap.For determination of FFA present in the oil taken, we titrated the oil sample with 0.1N KOH solution with Phenolphthalein as indicator. Volume in ml of 0.1N KOH required to neutralize one gram of oil is called acid value. And with this we determined the amount of KOH needed to neutralize the FFAs in the oil. Thus by adding calculated amount of KOH, FFAs are removed in the form of soap. Removal of moisture involved heating the oil sample upto105-110 ^{0}C and maintaining it there for few minutes so that all moisture gets evaporated if required vacuum pump arrangement is used to remove the moisture present [2].

Transesterification Reaction: The most common derivatives of agricultural oil for fuels are methyl esters. These are formed by transesterification of the oil with methanol in the presence of a catalyst (usually basic) to give methyl ester and glycerol. Sodium hydroxide (NaOH) is the most common catalyst, though others such as potassium hydroxide (KOH) can also be used and is shown in fig. 4.

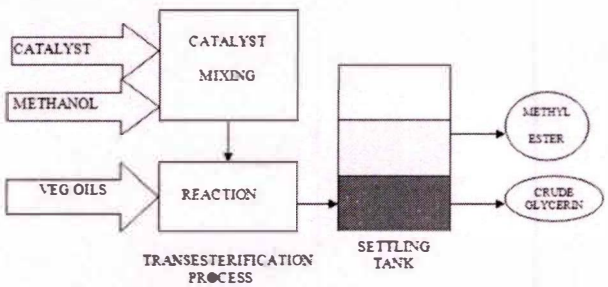

Fig. 4 100 kg oil+24 kg methanol+2.5 kg NaOH a 100 kg biodiesel+26 kg glycerine

Calculated amount of oil sample is taken in thee necked flat bottom flask and it is put over the flat plate heater and heated to this methanol taken in 9:1 mole ratio (alcohol to oil) is gently added such that no amount of methanol gets evaporated. The condenser is readily fitted to one of the neck of the three necked flask. To the other neck, thermometric well is fixed and the third neck is closed with a stopper. Now the stirrer is put on, and the whole batch of oil and methanol are thoroughly mixed to attain uniform reaction. The temperature of the bath is maintained in the range of 60-63 ^{0}C and the reaction is carried out for one hour. After the reaction time is over, the batch is withdrawn from the heater and cooled to room temperature on cooling formation of two layers are observed. This whole batch is poured into a separating funnel and allowed for at least 5 hour. To get clear separation of ester and glycerine. Glycerine formed at the bottom is taken out as a by-product. The obtained ester is subjected to further purification. The Trans-Esterification process (Reaction) is shown in fig. 5.

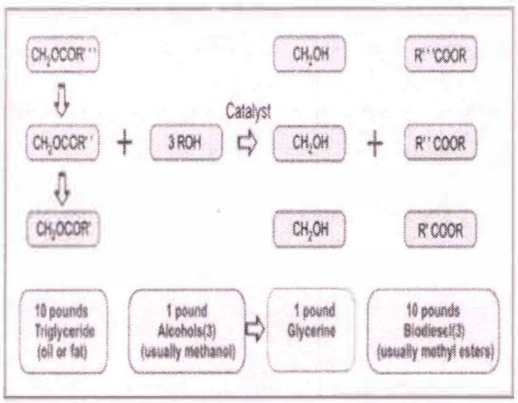

Fig.5. Trans-Esterification process (Reaction)

The methanol and NaOH are premixed and added to the oil, mixed for a few hours, and allowed to gravity settle for about 8 hours. The glycerine settles to the bottom, leaving biodiesel on the top. The physical and chemical properties of the resulting biodiesel (Jatropha methyl esters) are presented in the following Table alongside those for petroleum diesel and European Union standards for biodiesel [1].

Purification of products and recovery of methanol: For removing the catalyst present in the ester small amount of glacial acetic acid is added to get a neutral ester and then it is washed with hot distilled water to remove any traces of catalyst present. Washing is done with distilled water at 50 ^{0}C, 65 ^{0}C and 80 ^{0}C to remove traces of methanol or catalyst. Thus ester obtained is dehydrated to remove traces of moisture present in it and it is heated to 60-110^{0}C remove excess methanol present in it. Thus obtained ester is almost 100% pure. Yields of esters: The yields of methyl Palm Kernal ester at 0.5, 0.75 and 1.0 wt% of sodium hydroxide catalyst were taken

IV. Results And Discussion

As observed from results, the yields of Palm Kernel ester, ranged from 90% to 99.6%. Irrespective of different mole ratios and catalyst concentrations, the yields were more or less same with about 3-9% variation. In case of methyl Palm Kernel ester, at 1:9mole ratio and 0.5, 0.75 &1 wt% of catalyst (NaOH) the % yield was 98.5%, 98% & 87.5% respectively.

A. Effect of Mole Ratio on pH

The values of pH are in increasing trend when the mole ratio is increased from a value of 1:9 to 1:18 in Palm Kernel ester. The variation of pH with mole ratios is shown in fig. 6.

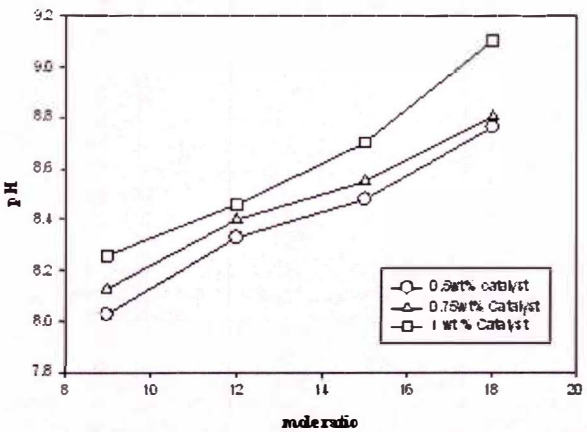

Fig. 6 Mole ratio Vs pH at various catalyst concentrations for methyl palm kemal easter with NaOH catalyst

B. Effect of Mole Ratio on kinematic viscosity

The values of kinematic viscosity are also in decreasing trend when the mole ratio is increased from a value of 1:9 to 1:18 in Palm Kernel ester. The variation of kinematic viscosities with mole ratios was shown in fig. 7.

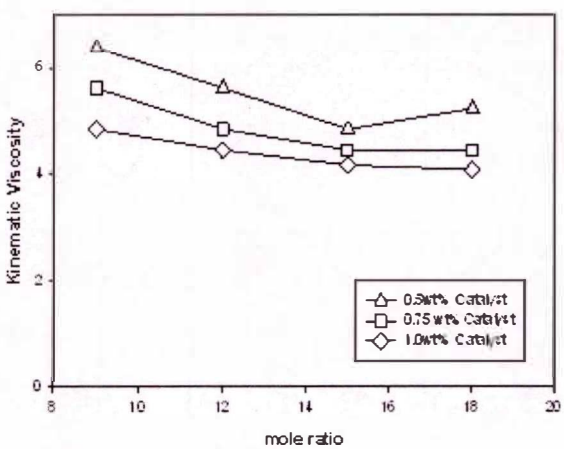

Fig.7 Mole ratio Vs kinematic viscocity at various catalyst concentrations for methyl palm kemal oil with NaOH catalyst

C. Effect of catalyst concentration on kinematic viscosity

The effect of catalyst concentration on kinematic viscosity is shown in fig. 8. The values of kinematic viscosities decreased when the catalyst concentration is raised from 0.5% to 1.0%. It is clear from these results that the conversion of oil to ester is low even the concentration of the catalyst at 0.5%. At the 1.0% catalyst concentration, the values of kinematic viscosity of the ester are significantly reduced indicating the fact that the minimum catalyst concentration should be in the vicinity of 1.0%. Obviously higher values of density are recorded for the Palm Kernel ester because of low conversion of oil to ester.

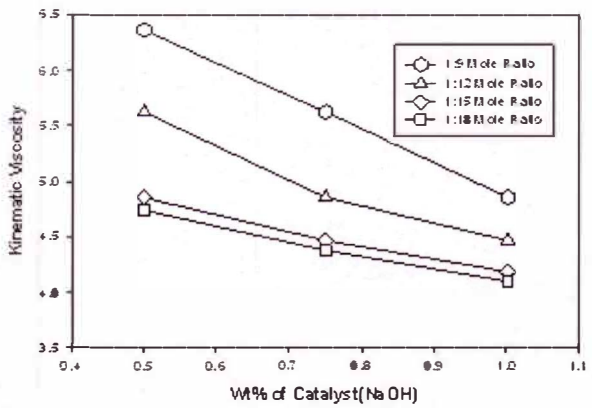

Fig.8 Catalyst concentration Vs kinematic viscocity at various catalyst concentrations for methyl palm kemal oil with NaOH catalyst

D. Effect of mole ration on flash point

The values of flash points gradually decreased for Palm Kernel ester as the mole ratio was increased. This sudden decrease in the flash points may be because that the esters at greater mole ratios become very volatile and because of which it is producing sufficient vapors at its volatile temperature which is very low compared to the esters which were less volatile. The variation of flash points with change in mole ratios is shown in fig. 9[3].

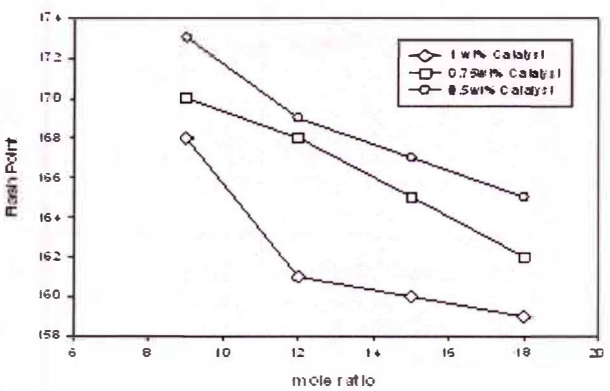

Fig.9 Mole ratio Vs Flash poiny at various catalyst concentrations for methyl palm kemal oil with NaOH catalyst

E. Effect of mole ratio on fire point

The values of Fire Points are also in decreasing trend when the mole ratio is increased from a value of 1:9to 1:18 in Palm Kernel ester. The variation of Fire Points with mole ratios is shown in fig. 10 [4].

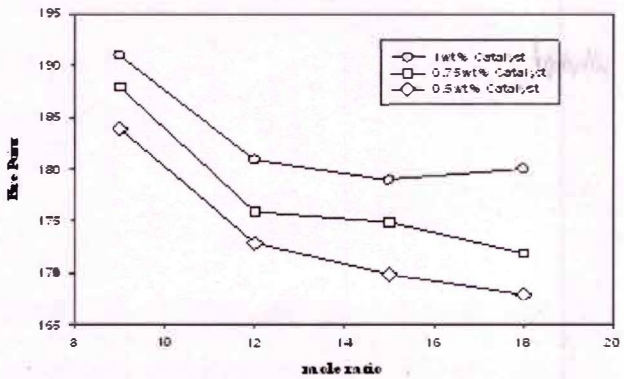

Fig.10 Mole ratio Vs Fire poiny at various catalyst concentrations for methyl palm kernal oil with NaOH catalyst

F. Performance of Biodiesel

Successful alternative fuels fulfill environmental and energy security needs without sacrificing operating performance. Operationally, biodiesel performs very similar to low sulfur diesel in terms of power, torque, and fuel without major modifications of engines or infrastructure. Biodiesel offers similar power to diesel fuel. Biodiesel has a higher cetane number than diesel fuel. In over 15 million Miles of in-field demonstrations biodiesel showed similar fuel consumption, horsepower, torque, and haulage rates as conventional diesel fuel. Biodiesel provides significant lubricity improvement over petroleum diesel fuel. Lubricity results of biodiesel and petroleum diesel using industry test methods indicate that there is a marked improvement in lubricity when added to conventional diesel fuel [5,6].

Biodiesel contains no sulfur or aromatics, and use of biodiesel in a conventional diesel engine results in substantial reduction so unburned hydrocarbons, carbon monoxide and particulate matter. Biodiesel can be manufactured using existing industrial production capacity and used with conventional equipment, is provides substantial opportunity for immediately addressing our energy security issues. Increased utilization of renewable biofuels results in significant microeconomic benefits to both the urban and rural sectors.

V. Conclusions

Biodiesel is safe to handle because it is biodegradable and non-toxic. Biodiesel reduces all the emission. Biodiesel can be used alone or mixed in any amount with petroleum diesel fuel. Biodiesel runs in any conventional, unmodified diesel engine. No engine modifications are necessary to use biodiesel and there is no "engine conversion". Increased utilization of renewable biofuels results in significant microeconomic benefits to both the urban and rural sectors, and the balance of trade. It is clear that more can be done to utilize domestic surpluses of vegetable oils while enhancing our energy security. Because biodiesel can be manufactured using existing industrial production capacity, and used with conventional equipment, it provides substantial opportunity for immediately addressing our energy security issues.

There are several advantages of biodiesel produced from Palm Kernel oil. As biodiesel is more viscous, its lubricity is more. Settling of two layers at separation stage is faster for Palm Kernel oil, so separation is easy and faster. The biodiesel obtained from non-edible oils is cheaper than that from edible oils. Finally it can be concluded that the biodiesel is a better alternative fuel when compared to conventional diesel [7]. Waste/arid lands can be utilized for growing trees like jatropha, mahua, castor etc. There will be substantial employment generation mainly in the rural areas which will help in the overall development of these areas. [8]

References

[1] Peterson, Charles L., Feldman, M., Korus, R., and auld, D.L ., "Batch type transesterification process for winter rape oil", *ASAE paper*, St.Joseph, 1991, MI 49085- 9659.

[2] Nicaragua Bringi, N.V., "Non-Traditional Oilseeds and Oils in India", *the Biomass Project, Curcas Oil Methyl Ester,* Oxford & IBH Publishing Co. Pvt. Ltd. New Delhi, India, 2000, pp 143-166.

[3] Cole, G. Mattney, "Assessment and remediation of petroleum contaminated sites and test guidelines, aerobic aquatic bio degradation", *publishers 1982 test guidelines chemical fate-aerobic aquatic bio degradation,* 2003

[4] Shaine Tyson nrel golden, U.S.Department of energy, Colorado, USA, Biorefinery. 2003.

[5] Das, "Performance evaluation and emission characteristics of a compression ignition engine using esterified Biodiesels" *CES, IIT Delhi,* 1996.

[6] LM Das, "Biodiesel development and characterization for use as a fuel in compression ignition engine", Journal of engineering for gas turbine and power (ASME Transaction journal), vol.123, 2001, pp440-447.

[7] Pitter, Pavel and Chudoba "biodegradability of organic substances in the aquatic environment", *CRC press,* 1990, pp167.

[8] Jeffrey L. Rosenblum, "Feasibility of Biodiesel for Rural Electrification in India", *Carnegie Mellon University*

Nanotechnology for Human Hematological Malignancies Treatment

Marin Gustavo H., and Mansilla Eduardo

Abstract: The main problem of anti-neoplasic drugs is the damage normal cells while controlling tumors. We used biodegradable nanoparticles (BNP) as carriers for drugs. *Materials and Methods*: We investigated the effect of BNP on B-chronic lymphocytic leukemia (B-CLL) and normal cells in vitro. BNP coated with monoclonal antibodies (mAbs) towards malignant cells antigens in surface, encapsulated either hydroxylchloroquine (HDQ), or chlorambucil (CLB) which are toxic drugs when used alone. Viability and apoptosis were evaluated at 24-48h.
Results: mAbs BNP with HCQ or CLB resulted in significant penetration of leukemia cells compare to controls or to BNP without antibodies ($p < 0.001$). After 24h both HCQ/CLB-BNP induced 85% of apoptosis and 70% of mortality in malignant cells compared to normal cells (17%-10% respectively, $p<0.0001$).
Conclusion: Our data indicate that nanoparticles are suitable for selective drug delivery to leukemia cells and produce a strong apoptotic effect when loaded with antineoplasic agents.

Keywords: Chronic Leukemia; nanoparticles; drug delivery, monoclonal antibodies.

I. Introduction

ALTHOUGH development anti-neoplasic drugs initiated in the middle of the XX siècle. These drugs had all the same problem: they were able to eliminate the malignant cells but with severe damage to normal cells that could compromised patients life a cause of their toxicity.

This new siècle brought the discovery of new molecules that focused to specific tumours cell targets. This is the case of some haematological malignancies like Chronic Myeloid Leukaemia where Imatimib changed its prognosis. However, these benefits are limited to very few diseases and today many the illnesses remain incurable. This is the case of mature lymphoid malignancies like B-Chronic Lymphocytic Leukemia (B-CLL) or Multiple Myeloma that continues to be incurables progressive clonal diseases [1]. Developing new therapeutic effective modalities are still difficult aims to be attained [2]. Along these lines, old strategies like alkilant agents (clorambucil, melphalan) are good alternatives, capable to control the diseases at high doses but with the risk of severe toxicity for the host. In general, the standard initial therapy for B-CLL has been single-agent chemotherapy typically employing the drug, Chlorambucil (CLB) at limitated doses because of its toxics effects to normal cells [3]. In the last decade, Fludarabine has been incorporated as the frontline treatment for B-CLL [4]. Various monoclonal antibodies such as anti-CD20, (Rituximab) [5], anti-CD52, (Alemtuzumab) [6], have shown promise for addressing B-CLL treatment. At least 60% of the patients may transient respond these therapies, but eventually all patients finally become resistant to these agents4. Traditional, anti-CLL agents such as CLB are transported by carrier-mediated systems into cells and generally alkylate to DNA, RNA, and proteins [6]. Ordinarily, CLB-resistant B-CLL lymphocytes are 5 to 6 fold more resistant in vitro, using the MTT assay, as compared to sensitive lymphocytes (IC50 CLB of $\leq$ 61.0 µmol/L can be considered sensitive) [7]. Other alternatives like hydroxychloroquine (HCQ), original an anti-rheumatic drug, were assay to treat on malignant B-cells with interesting results related to apoptosis induction via activation of Caspase-3. However, the level of drug concentration needed to this induction is very difficult or impossible to reach in vivo with common oral or parenteral administration [8]. Again toxicity limited the expectative of a good anti-neoplasic agent. Unfortunately, for one cause of another, all patients finally relapse from original disease and died a cause of it or its complications.

Overcome these pharmacokinetic obstacles or specifically deliver effective amounts of drugs straight into the targeted B-CLL cells, may improve the overall survival and decrease treatment-associated morbidity.

We report in this paper an innovative technology based on biodegradable nanoparticles that could avoid these problems and introduce a new way of treatment modality for cancer diseases.

II. Methods

Biodegradable Nanoparticles (BNPs): Seven different types of BNPs made of polyethylene glycol were used for

Gustavo H. Marin, National University La Plata – CUCAIBA-CONICET Argentina. gmarin2009@gmail.com
Eduardo Mansilla, National University La Plata – CUCAIBA, Argentina

testing (Table 1). The drugs HCQ sulfate (ACROS, Geel Belgium) and Chlorambucil (CLB) (SigmaAldrich, St Louis, Mo) were encapsulated at a concentration of 165 µg per mg of polymer inside BNPs. HCQ-BNPs or CLB-BNPs surface were modified with monoclonal antibodies of either anti-human CD19, or anti-human CD19 and anti-human CD20.

TABLE I:
SUMMARY OF NANOPARTICLES PROPERTIES

Particle Name	Monoclonal Antibody	Flurophore Tag	Tag Attachment	Encapsulated Agent
BNP1	Anti-CD19	FITC	MoAb	HCQ
BNP2	Anti-CD19/anti-CD20	FITC/Alexa-Fluor	MoAb	HCQ
BNP3	none	FITC	PLGA	HCQ
BNP4	Anti-CD19	FTIC	MoAb	CLB
BNP5	Anti-CD19/anti-CD20	FITC/Alexa-Fluor	MoAb	CLB
BNP6	none	FITC	PLGA	CLB
BNP7	Anti-CD19/anti-CD20	FITC/Alexa-Fluor	MoAb	none

The anti-CD19 and anti-CD20 monoclonal antibody concentration was 5.75 and 5.38 µg, respectively, per mg of polymer. A fluorescent marker was attached to each monoclonal antibody; FITC conjugated anti-CD19 (fluorescein isothiocyanate exhibits excitation at 495 nm and emission at 525 nm) and Alexa-Fluor conjugated anti-CD20 (excitation at 696 nm and emission at 719 nm). An additional HCQ or CLB-BNPs system was produced with a fluorescent polymer (PEG-FITC) and no antibody. Others BNPs were coated with anti-CD19/FITC or CD20/Alexa-Fluor antibodies but without active drugs. All BNPs were suspended in PBS with 10% Bovine Serum Albumin at a final total mass concentration of 900 µg/ml. Aliquot of 0.5µl from these solutions was used for all experiments.

B-CLL cells and Normal B lymphocytes: Two types of heparinized blood were obtained after informed consent from a healthy volunteer and from B-CLL patient Rai-IV B-CLL patient. The primary tumour B cells were positive for CD5+, CD19+, CD23+, CD20+, CD38+ and ZAP70+ and unmutated for Ig genes and p53 mutations. The mononuclear cell fractions were isolated by centrifugation on Ficoll-Hypaque gradients. Cells were purified at 99%.

Cell Culture with BNPs: The freshly isolated cells were incubated for all experiments at 37°C and 5% CO2. 4 x 10^5 cells, both from the CLL patient and the healthy control, were incubated in triplicate in 0.5 ml of AIM V medium. The cells were cultured in plastic sterile tubes in the presence of 0.5µl of each BNPs solution.

BNPs cell penetration: In order to test if BNPs loaded with HCQ or CLB penetrated either in normal or malignant cells we used Confocal Microscopy and Fluorescence Correlation Spectroscopy method. Confocal Imaging combined with Fluorescence Correlation Spectroscopy (FCS) was performed on all our BNPs after incubation with cells at 4 hours. All Fluorescence Correlation Spectroscopy measurements were acquired using a standard Alba FCS spectrometer (ISS, Champaign, IL) and a Nikon microscope Model TE2000-E, equipped with a water immersion, NA=1.2, 60X objective. Acquisition of the fluorescence by filters allowed separation of two bands: 500-550 nm (channel one) and 700-750 nm (channel two). All cell samples were also observed with an Olympus Laser Confocal Fluorescence Microscope, evaluated for BNPs cell penetration and photographed with an Olympus digital camera after 4 hours incubation period. Images were analyzed with FluoView software, Version 3.3. For the confocal observations, laser excitations were at 525 nm (green) and 719 nm (red), and the cross correlation was also provided. DAPI (4',6-diamidino-2-phenylindole) nuclear staining of the cells cultured with the different BNPs was done and observed in blue for laser excitation at 461 nm.

Cell Viability Testing: We analyzed the percentage of living and dead cells in each sample at 0, 24 and 48 hours of incubation with each of the BNPs systems using Ethidium Bromide/Acridine Orange staining and immune-fluorescence microscopy counting.

Apoptosis Analysis: Measurement of cell apoptosis using annexin-V and propidium-iodide by FACS analysis, was made at 0, 24 and 48 hours of incubation with each type of the BNPs systems.

Statistical analysis: The statistical significance of differences among groups was assessed using Student's t test with a 5% limit for statistical significance. Correlation analysis was performed using a regression test.

III. RESULTS

FCS analysis provided the lifetimes of the anti-CD19 and anti-CD20 markers coated on the BNPs. These markers had distinguishable lifetimes which were monitored spatially and temporally. The spatial characteristics of the anti-CD19 and anti-CD19/anti-CD20 BNPs demonstrated rapid cell internalization for both systems after 4 hours of incubation (Fig.1) with anti-CD19 having more rapid internalization than the anti-CD20. BNPs formulated with monoclonal antibodies resulted in significant penetration after 4 hours of incubation in both normal lymphocytes and B-CLL cells compared to BNPs without antibodies ($p < 0.001$).

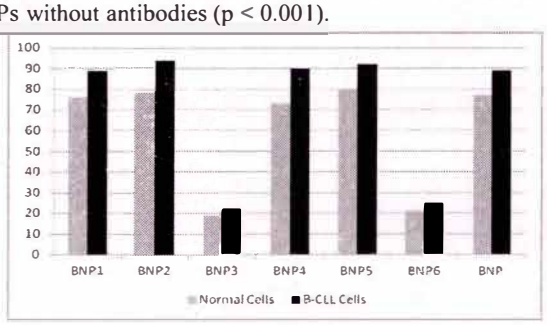

Fig. Icellular uptake of nanoparticle into normal and b-cll
Cellular uptake of nanoparticles into normal and B-CLL cells after 4 hours of incubation ($p<0.001$).

All HCQ- and CLB loaded anti-CD19, and anti-CD19/anti-CD20 coated BNPs efficiently induced apoptosis of malignant human B-CLL cells in vitro. At 0.5 µl concentration, both HCQ and CLB -antiCD19-BNPs induced more apoptosis in malignant B-CLL cells compared to normal lymphocytes ($p < 0.001$) (Fig 2). When HCQ and CLB-BNPs were simultaneously coated with both antibodies and injected at the same concentration (0.5 µL), the most effective apoptotic effect was over 4-fold more pronounced on B-CLL cells compared to normal lymphocytes (Fig.2).

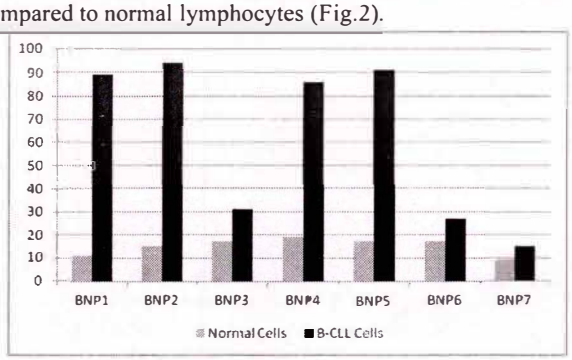

Fig. 2 apoptosis induction in normal and leukemia cells according to bnp used

Cellular apoptosis induced by BNP nanoparticles in normal and B-CLL cells; (BNP at 0.5ul concentration; incubation time = 24 hrs).

Reductions of living B-CLL cells were observed in vitro at 24 and 48 hours for injections of all concentrations of monoclonal antibodies coated nanoparticles loaded with HCQ and CLB. Loss of viability in human CLL cells correlated with early induction of apoptosis. HCQ- and CLB-BNPs with monoclonal antibodies both induced a decrease in cell viability in a dose and time-dependent manner (Fig.3). In leukemic cells, the nanoparticles reduced cell viability in doses and times significantly lower than in normal lymphocytes. In vitro treatment of drug resistant B-CLL cells with these HCQ-loaded BNPs (BNP1, BNP2, BNP3) or CLB-BNPs (BNP4, BNP5, BNP6) showed to be significantly more effective ($p < 0.001$) than BNPs without drug (BNP7) indicating that treatment with empty BNPs had little impact on cell viability. BNPs encapsulated with HCQ or CLB but without monoclonal antibodies (BNP3 and BNP6) had significantly less impact on in vitro cell viability ($p < 0.001$).

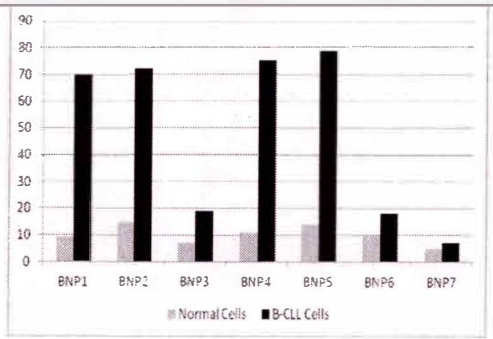

Fig. 3 cellular mortality of b-cll and normal cells induced by nanoparticles after 48 hours of incubation

FITC-conjugated anti-CD19 and Alexa-Fluor-conjugated anti-CD20 antibodies suspended in PBS with 10% Bovine Serum Albumin (BSA) in AIMV medium alone without BNPs produced no significant apoptotic effect in B-CLL or normal lymphocytes.

IV. Discussion

Although during the last decades some In clinical oncology, especially for the treatment of CLL, the development of new anticancer agents with different modes of action is of key importance for overcoming therapy resistance. The hydroxychloroquine is defined as antiproliferative compounds in the National Cancer Institute database [9] and Clorambucil is the gold standard for classic CLL treatment [10]. These drugs can stimulate cell differentiation at growth inhibitory concentrations as well as inhibition of histone deacetylase (HDAC) activity in vitro, and DNA damage and apoptosis in tumour lines respectively [11]. Maximum HCQ blood concentration in healthy volunteers receiving a 800 mg dose of hydroxychloroquine sulphate orally ranged from 135-422 ng ml-1 and time to maximum (tmax) was 1.5-7.0 h. Higher serum levels are toxic for many tissues and for long period of times since HCQ half-life and mean residence time is long (around 40 days) and has large volumes of distribution (5,522 L from blood, 44,257 L from plasma). Sequestration into the tissues is an important feature of the disposition of HCQ. However, concentrations on B-CLL lymphocytes high enough to cause effective apoptosis as seen in vitro are impossible to reach in the in vivo setting by oral administration of HCQ [12]. Hence, BNP drug delivery could be a solution to reach anti-neoplasic concentrations in tumour cells avoiding toxic effect in other cells. Protein expression values for CD19 and CD20 in leukemic B cells can differ from those of normal blood B lymphocytes and provide promising targets for attachment and intracellular entry into B-CLL cells [13]. Analysis of HCQ-CLB loaded/antibody-coated BNPs effects on B-CLL cells clearly showed that these particles are potent inducers of tumour cell death for in vitro applications. Furthermore, HCQ-CLB loaded BNPs efficiently induced CLL cell apoptosis with little effect on the viability of normal B cells in vivo at the same concentrations.

The data presented here suggests that HCQ-CLB-BNPs trigger a selective, apoptotic response in B-CLL cells at low concentrations when specific monoclonal antibodies like anti-CD19 and/or anti-CD20 are coated on their surface and that apoptosis shifts to necrosis at higher concentrations. Our system offers a new powerful and less toxic therapy for B-CLL and other malignancies.

CONFLICT OF INTEREST: The authors of this paper have no conflict of interest related to this paper.

REFERENCES

[1]. Reed, J. C. Molecular biology of chronic lymphocytic leukaemia. Semin Oncol 25(1):11-8; 1998.

[2]. Vicent, M. J. & Duncan, R. Polymer conjugates: nanosized medicines for treating cancer. Trends Biotechnol. 24:39-47; 2005.

[3]. Dighiero, G., Maloum, K., Desablens. B. Chlorambucil in Indolent Chronic Lymphocytic Leukemia. N Eng J Med. 21, 338:1506-1514; 1998.

[4]. Rai, K. R., Peterson, B. L., Appelbaum, F. R. Fludarabine compared with chlorambucil as primary therapy for chronic lymphocytic leukemia. N Engl J Med 343:1750–8; 2000.

[5]. Huhn, D., von Schilling, C., Wilhelm, M. Rituximab therapy of patients with B-cell chronic lymphocytic leukemia. Blood 98, 5: 1326-1331; 2001.

[6]. Fraser, G., Smith, C. A., Imrie, K., Meyer, R. Alemtuzumab in chronic lymphocytic leukemia: a clinical practice guideline. Toronto (ON): Cancer Care Ontario (CCO) 14: 32-5; 2006.

[7]. Silber, R., Degar, B., Costin, D.. Chemosensitivity of lymphocytes from patients with B-cell chronic lymphocytic leukemia to chlorambucil, fludarabine, and camptothecin analogs. Blood 84(10):3440-6; 1994

[8]. Carmichael, S. J., Charles, B., Tett, S. E.. Population pharmacokinetics of hydroxychloroquine in patients with rheumatoid arthritis. Ther Drug Monit 25(6):671-81; 2003.

[9]. Martirosyan, A. R., Rahim-Bata, R., Freeman, A. B., Clarke, C. D., Howard, R. L., Strobl JS. Differentiation-inducing quinolines as experimental breast cancer agents in the MCF-7 human breast cancer cell model. Biochem Pharmacol. 68(9):1729-38; 2004.

[10]. Raphael B, Andersen JW, Silber R, et al. Comparison of chlorambucil and prednisone versus cyclophosphamide, vincristine, and prednisone as initial treatment for chronic lymphocytic leukemia: long-term follow-up of an Eastern Cooperative Oncology Group randomized clinical trial. J Clin Oncol. 1991;9(5):770-6.

[11]. Zhou, Q., McCracken, M. A. Strobl, J. S. Control of mammary tumor cell growth in vitro by novel cell differentiation and apoptosis agents. Breast Cancer Res Treat. 75(2):107-17; 2002.

[12]. Munster, T., Gibbs, J. P., Shen, D. Hydroxychloroquine concentration-response relationships in patients with rheumatoid arthritis. Arthritis Rheum. 46(6):1460-9; 2002.

[13]. Huh, Y. O., Keating, M. J., Saffer, H. L., Jilani, I., Lerner, S., Albitar, M. , , Higher levels of surface CD20 expression on circulating lymphocytes compared with bone marrow and lymph nodes in B-cell chronic lymphocytic leukemia. Am J Clin Pathol 116(3):437-43; 2001.

Preliminary Study in Seulimeum fault, Aceh Besar (Indonesia) using Gravity and Magnetic Methods

M.M. Nordiana, Rosli Saad, Muhammad Syukri, I.N. Azwin and Andy Anderson Bery

***Abstract*—**The study explores the use of the gravity and magnetic method for Seulimeum fault detection conducted in Krueng Raya, Banda Aceh (Indonesia). The spacing between stations for gravity survey was 200-500 m randomly while for magnetic was 50-300 m randomly. The gravity and magnetic data was processed by utilizing Microsoft excels and Surfer8 software. The local gravity value covers -33 to 21 mGal. The gravity results shows the trend pattern of low gravity value at northwest part and high gravity value at south-east part of Krueng Raya which was indicated as fault system. The local magnetic value covers -700 to 650 nT. The magnetic results showed the trend pattern of low residual value at north part and a lot of spotted high residual value surrounds Krueng Raya which was indicated as fault zones. Gravity and magnetic results are well correlated which indicated that the area is bounded by major faults.

***Keywords*—** Aceh, fault, gravity, magnetic, Seulimeum,

I. Introduction

MANY geophysical methods had been constructed to determine the faults distribution. In this study, gravity and magnetic survey were chosen as preliminary study and alternative measurement device for fault detection.

Located in Krueng Raya, Aceh Besar (Indonesia), Seulimeum fault is one of the fault segment included in Sumatra fault zone (SFZ). Furthermore, due to the gravity density and magnetic susceptibilities contrast, this region offers a unique pattern of gravity and magnetic surveys in delineating shallow features.

II. Sumatra Fault Zone

Krueng Raya is located in Banda Aceh district which is one of the areas affected by tsunami disaster and precisely at the line of Sumatra fault system. The Sumatra fault zone (SFZ) is the most active fault in Indonesia as a result of strike-slip component of Indo-Australian oblique convergence. With the length of 1900 km, Sumata fault was divided into 20 segments starting from the southernmost Sumatra Island having small slip rate and increasing to the north end of Sumatra Island as shown in Fig. 1 [1].

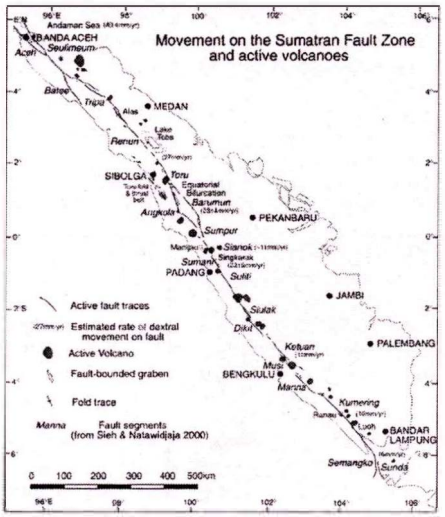

Fig. 1 The great Sumatra fault zone (SFZ) is; a trench parallel, right-lateral strike-dip fault and divided into 20 fault segments [1]

III. Theory

A. Gravity

Gravity measurements are used to detect geological formations with different densities. The density contrasts leads to a different gravitational force which is measured in mGal or 10^{-3} cm/s^2. Density of the rocks mainly depends on the composition and porosity, but partial saturation of the rocks may also influence the values. Generally, sedimentary rocks are lighter than crystalline rocks. The raw data needs to be corrected for several factors. The results are usually presented in Bouguer maps based on the Bouguer anomaly (Δg_B) where corrections have been done on the measured value (g_M) for tidal effects, elevation, local topography, latitude and drift for the gravimeter [2].

B. Magnetic

The magnetic method measures the intensity of the natural magnetic field. This includes contribution from the earth's core and crust, as well as any secondary magnetic field induced in magnetic geological bodies, which locally creates positive and negative magnetic field anomalies. Those

M.M. Nordiana, School of Physics, Universiti Sains Malaysia Malaysia. mmnordiana@usm.my
Rosli Saad, School of Physics, Universiti Sains Malaysia Malaysia. rosli@usm.my
Muhammad Syukri, Faculty of Sciences, Syiah Kuala University, Indonesia,m.syukri@unsyiah.ad.ic
I.N. Azwin, School of Physics, Universiti Sains Malaysia Malaysia. nurazwinismail@yahoo.com

anomalies are the target of a magnetic survey for geological purposes.

IV. General Geology

The regional geology of Banda Aceh Quadrangle has been mapped by [3] (Fig. 2). The Krueng Raya lithology is dominated by Lam Tuba volcanic, composed of andesitic to dacitic volcanics, pumiceous breccia, tuffs, agglomerate and ash flows which intruded of the Seulimeum formation composed of tuffaceous and calcareous sandstones, conglomerates and minor mudstones [3]. The prospect area is near the Raya mount and le se uem hotspring. It forms a topographic depression, occupied by alluvial flat and low, flat-topped hills within the Barisan range; a rugged mountain range that runs along the entire western edge of the Sumatera Island. Following closely the crest of the Barisan range is a continuous system of axial valleys, including the Kr. Tangse valleys, which marks the outcrop of the main fault line of the Sumatran fault system. This is essentially a right lateral fracture system [4] and [5]. The area is controlled by two main faults system, with orientation NW to SE. The topographic morphology of the Krueng Raya is subdued because the rocks are strongly fractured and altered.

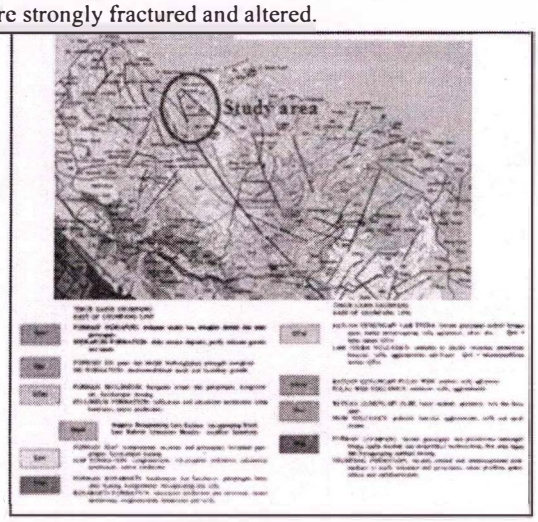

Fig. 2 Geology map of the study area

V. Study Area

The study was carried out in the area of Krueng Raya, Banda Aceh (Indonesia) with area of 6 km x 8 km (Fig. 3). The gravity and magnetic survey was carried out with random moving station. The distance for gravity station was set at 200-500 m (Fig. 4) while for magnetic station was set at 50-300 m to cover the survey area (Fig. 5).

Fig. 3 The magnetic survey at Krueng Raya, Banda Aceh (Indonesia) [6]

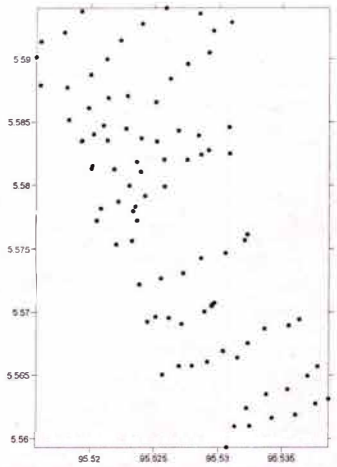

Fig. 4 Gravity stations of Krueng Raya area

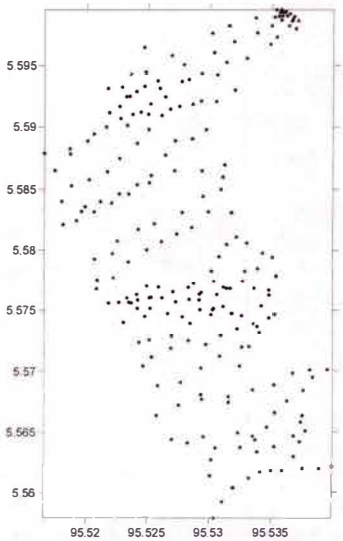

Fig. 5 Magnetic stations of Krueng Raya area

VI. Methodology

A. Gravity

The gravity measurement was applied at all moving station scattered around the study area with station interval of 200-500 m, in order to identify subsurface structure. A local base station was located at one place where one repeats a gravity reading in the morning and in the afternoon after finishing

survey line for each day. The repeated readings are performed because even the most stable gravity meter will have their reading drift with time due to elastic creep within the meter's springs and also to help remove the gravitational effects of the earth tides. The instrument drift is usually linear and less than 0.01mGal/hour under normal operating conditions. The gravity survey covered most of the area, except some locations due to thick jungle.

The observed gravity readings obtained from the gravity survey reflect the gravitational field due to all masses in the earth and the effect of the earth's rotation. To interpret gravity data, one must remove all known gravitational effects not related to the subsurface density changes. These include latitudinal variations, elevation changes, topographic changes, building effects and earth tides [7]. The field survey usually removes the earth tidal effect during the drift curve determination and use latitudinal correction. To take into account, the vertical decrease of gravity with increase of elevation from a predetermined datum plane (usually sea level) and the gravitational field of the mass between the datum plane and a gravity station, a free-air and Bouguer corrections are applied to the observed gravity data. The Bouguer correction requires an average density value (Bouguer reduction density) of the mass, which is usually assumed to be 2.67 gm/cm^3. The final form of the processed gravity data is called a complete Bouguer gravity anomaly. Once corrections were done, the data were exported into a grid file to the Surfer8 software to perform gravity contour map.

B. Magnetic

The magnetic survey was carried out with scattered moving station with interval of 50 m to 300 m interval in order to detect the subsurface structure. The used system is designed to measure the total field and/or gradient field, and is essentially proton precession devices. The measured independent grid was later combined to form a single master grid. The master grid provided a full magnetic map for easy display of the anomalies and allows the data to be processed using Surfer8 software. A base station with magnetic homogeneity was selected within the study area to recorded magnetic readings at a time interval of 1 minute to correct the diurnal variation effects of the earth's field from survey measurements. The magnetic survey covered most of the area, except some locations due steel fancies and thick jungle in the area. Base station data was used to correct the moving data, and finally, a total intensity magnetic anomaly map was produced, reflecting the subsurface structure. Magnetic data alone gives a general idea about the subsurface structures affecting the study area. Processing the magnetic data enhances and sharpens the anomalies and trends of the data and helps in the interpretation. In this work, we will apply two techniques in order to estimate the locations of the subsurface faults. First step in magnetic processing was inspecting raw data for spikes, gaps, instrument noise or any irregularities in the data. The next step involved diurnal variation correction and IGRF correction to produce magnetic residual. Once corrections were done, the data were exported into a grid file to the Surfer8 software. After calculating a grid from xyz data in Surfer8, magnetic residual was carried out to compare the difference between a grid value and the new data at any definite location of the site.

VII. Results And Discussions

A. Gravity

Fig. 6 shows the bouguer anomaly contour map. It consists of two gravity anomalies which may be related to the Seulimeum fault where it is located at northwest part and south-east part. The local gravity values cover -33 to 21 mGal. The low values are distributed on the northwest part while the high values are distributed on the south-east part. Fig. 6(b) shows the lateral view of the faulting system which runs from northwest to south-east in the study area. The bouguer anomaly contour map shows the same trend as geological map based upon [3] as it bends slightly to the west-east.

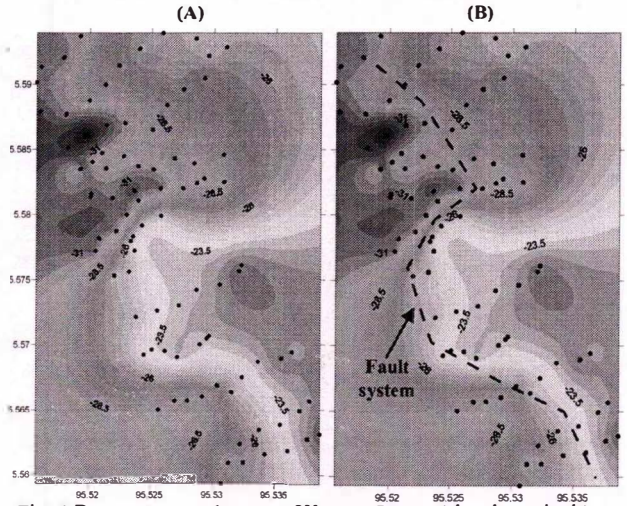

Fig. 6 Bouguer anomaly map of Krueng Raya; a) local gravity b) fault system

B. Magnetics

Ground magnetic data can more easily overemphasize shallow features the data may suggest the presence of faults when instead the anomaly is being produced due to variations in magnetic susceptibility. Thus, it is important to evaluate the results of these profiles in conjunction with other data types. Whereas depth estimates cannot be generated from these data, an analysis of these profiles can help determine the horizontal location of possible magnetic contrast.

The data was plotted as a contour map using Surfer8 software and was displayed in nanoteslas (nT). Magnetic results show lateral view of the faulting system in the study area (Fig. 7). The local magnetic value covers -700 to 650 nT. The total intensity magnetic anomaly map of Krueng Raya, Banda Aceh (Indonesia) was characterized by low magnetic anomalies over northern part and high magnetic anomalies spotted surrounding of the area, which indicate the presence of fault covering these parts. Potential faults location are depicted as linear nortwest to southeast trending features due to the the trend pattern of lower magnetic values than the surrounding

(black dashed lines). From the magnetic maps, several of the anomalies can be clearly correlated with geological map.

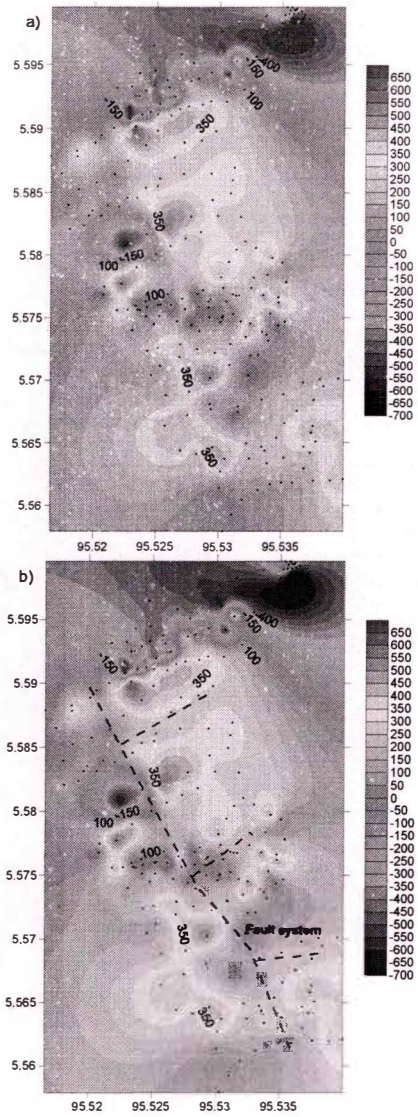

Fig. 7 Magnetic anomaly in Krueng Raya a) local residual and b) fault system

VIII. Conclusion

Data collection, processing, contouring and interpretation of the gravity and magnetic data provide increased understanding of the shallow structures associated with the Seulimeum fault system. The gravity and magnetic results supported with geological map suggested the existence of several small faults in the study area. It is clear that the main trend of the Seulimeum faults in Krueng raya is in the NW-SE direction. The application of gravity and magnetic survey are well correlated and can be easily determine the fault zones for preliminary study at the study area. Detail investigation using other geophysical methods should be apply for further investigation.

Acknowledgment

M.M. Nordiana thanks the member of Geophysics group, Universiti Sains Malaysia (USM), Penang, Malaysia, students and staffs of Faculty of Sciences and Faculty of Engineering, Syiah Kuala University (UNSYIAH), Banda Aceh (Indonesia) who helped acquire the geophysical field data.

References

[1] L. Prawirodirdjo, Y. Bock, J. F. Genrich, S. S. O. Puntodewo, J. Rais, C. Subarya, and S. Sutisna, "*One century of tectonic deformation along the Sumatran fault from triangulation and Global Positioning System surveys*," Journal of Geophysical Research, Vol. 105, No. 28, 2000, pp 343–28, 363.

[2] L. S. Georgson, "Geophysical Methods Used In Geothermal Exploration," Presented short course IV on Exploration for Geothermal Resources, organized by UNU-GTP, KemGen and GDC, at Lake Naivasha, Kenya, November 1-22, 2009.

[3] J. D. Bennett, D. McC Bridge, N. R. Cameron, A. Djunuddin, S. A. Ghazali, D. H. Jeffrey, W. Kartawa, W. Keats, N. M. S. Rock, S. J. Thomson and R. Whandoyo, *Geologic map of the Banda Aceh Quadrangle, Sumatra*, 1981.

[4] J. Katili and F. Hehuwet "*On the occurrence of large transcurrent faults on Sumatra Indonesia: Osaka, Japan*", Osaka City University Journal of Geoscience, Vol. 10, 1967, pp 1-17.

[5] B. G. N. Page, J. D. Bennett, N.R. Cameron, D. Bridge, D. H. McC Jeffery, W. Keats and J. Thaib, "*A review of the main structural and magmatic features of northern Sumatra*," Journal of Geological Society of London, Vol. *1*, 36, 1979, pp 569-579.

[6] Google earth, 2013.

[7] T. R. LaFehr, "Standardization in gravity reduction", Geophysics, Vol 56, 1991, pp 1170-1178.

About Author (s):

Muztaza M. Nordiana was born in Johor Bahru, Malaysia, on January 25, 1986. She was graduated BSc (2008) and MSc (2010) in Applied Science (Geophysics) at Universiti Sains Malaysia (USM), Malaysia. She is lecturer at the same university. She is also conducting and teaching undergraduate and postgraduate students in their final year and research projects.

She has experienced working in field that involves engineering and environmental projects including slope, engineering and groundwater in all Peninsular Malaysia including Sarawak, Labuan and Brunei. Her research interest is about Geophysics in mineral exploration, engineering and environmental study.

Dr. Nordiana is a member of European Association of Geoscientists & Engineers (EAGE) and Geological Society of Malaysia. She was obtained fellowship from USM. She was a recipient of the Student Travel Grant Saint Petersburg 2012 sponsor by EAGE Student Affairs. She has published several journals and refereed proceeding papers. She was also received best paper award, best presenter and 3rd prize for national three minutes thesis competition 2014.

S. Rosli (rosli@usm.my) was born in Penang, Malaysia, on 28th February 1960. He is a senior lecturer in Geophysics section, School of Physics, Universiti Sains Malaysia (USM). He obtained his B.Sc from Universiti Sains Malaysia in 1984, M.Sc from USM in 2004 and was awarded a PhD in 2009 from USM. He has served at USM since year 1985.

Prior joining USM, he worked as Tutor in Matriculation Centre USM and School of Physics, USM. His current research activities are Engineering

and Environment. He expertise is in Electrical method (2D/3D resistivity/ IP/ SP), Seismic (Refraction and Reflection), Ground Penetrating Radar, Magnetic and Gravity.

Dr. Rosli is a registered member of Institute of Geology Malaysia, Committee member of 2002 One day Geophysics Conference and secretary of 2006 Geophysics conference. He has published several books and more than 80 journals and conference papers.

M. Syukri was born Medan, Indonesia, in 1970. He received the B.Sc. degree in Physics from the Sepuluh November Institute of Technology (ITS), Surabaya, Indonesia, and M.Eng. in Applied Geophysics from Bandung Institute of Technology (ITB) Indonesia, and received Ph.D. degree in Geophysics Section, School of Physics, Universiti Sains Malaysia (USM), Malaysia, in 2006. In 1993, he joined the Department of Physics, Faculty of Sciences, Syiah Kuala University (SKU), as a Lecturer.

He is responsible for carrying out teaching and research duties. He lectures Environmental Physics, Thermodynamics, Introductory Geophysics, and Environmental and Engineering Geophysics at the university. He is involved in the administration of degree and postgraduate courses as well as responsible for organizing lectures and supervising final project, seminars and tutorials.

Dr. Syukri current research interests include applied and environmental geophysics. He is a member of the Indonesian Geophysics Association (IGA) and Indonesian Physics Association (IPA).

Ismail N. Azwin was born in Kedah, Malaysia, on 25th September 1987. She is currently a post-graduate student in Universiti Sains Malaysia (USM) pursuing her PhD in seismic and electromagnetic wave propagation characteristics. She graduated from USM in Master of Science (Geophysics) in September 2011 regarding the application of geophysical methods in engineering and environmental problems. She obtained her BSc from same university in August 2009.

She has field work experiences concerning geophysics-related in engineering and environmental projects including slope stability, groundwater exploration, constructions and also in archaeological research. Her research interest is about Geophysics in engineering and environmental study.

Ms. Nur Azwin is a member of European Association of Geoscientists & Engineers (EAGE) and Geological Society of Malaysia. She has attended few conferences and published some refereed proceeding papers.

Andy Anderson Bery was born in Kuala Lumpur, Malaysia. He received his B.App.Sc in Geophysics (2008) and M.Sc in Physics (2012) from Universiti Sains Malaysia. He is currently a PhD candidate at the School of Physics, Universiti Sains Malaysia. His research interests is mainly in high resolution in electrical tomography methods. He has been awarded the best paper award (Technologies of Environmental Engineering). He is a member of EAGE, SEG and Geological Society of Malaysia (GSM).

Analysis of Biofilter and Microbial Community Change under the Treatment of Ammonia and Toluene

Beomsoo Kim, Jingyu Kim, Daekeun Kim, and Joonho Park†

***Abstract*—**There are many methods to treat Ammonia and Toluene. BioFilter has many advantages. But Because of cytotoxicity of ammonia and toluene, we need microorganisms suitable for ammonia and toluene. Therefore, we study microbial community change under the treatment of Ammonia and/or Toluene. The Genus *Pseudofulvimonas* and *Pusillimonas* are increased under the treatment of Ammonia and Toluene.

***Keywords*—**Biofilter, Metagenomics, *Pseodofulvimonas,*

I. Introduction

AMMONIA and Toluene and malodorous substance[1].There are many methods to treat toluene and ammonia (Chilling, Absorption, Adsorption, Combustion and ECT) [2], Biofilter system using microorganisms is one of the potential solutions for removal ammonia and toluene. Biofilter has many advantages (Low cost, Low byproduct and ETC). To improve Biofilter efficiency, it is important to find microorganism suitable for ammonia and toluene [3] (or any other pollutants). We need other microorganisms suitable for ammonia and toluene .especially, because of cytotoxicity of ammonia and toluene [4]-[5]. We studied change of microorganism community under treatment of ammonia and toluene using Metagenomics sequencing of 16s rRNA gene. Additionally, we studied Biofilter efficiency.

II. Method

A. Bioreactor

We collect return sludge (namely, S) at sewage treatment plant in Uijeongbu-si, Gyeonggi-do, Korea. The Sludge mixing with nutriments was injected into Bioreactor [Fig 1] under aerobic control. Also, gas mixing with pure air was injected into Bioreactor. There are Polyurethane foam (1cm X 1cm X 1cm) in Bioreactor. The culture control was shown at [Table 1].

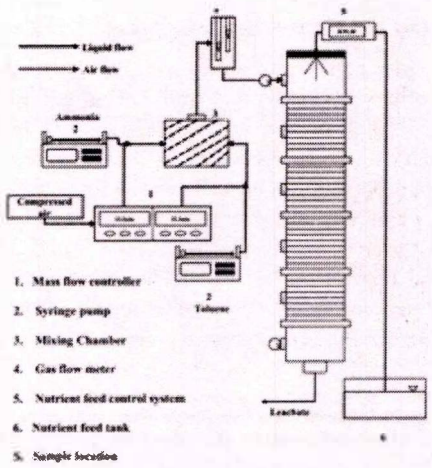

Fig 1. Schematic of Biofilter

TABLE I
CONDITION OF BIOFILTER

pH	8~8.3
Dissolved Oxygen(DO)	7 mg/L
Temperature	28~32 ℃

B. Analysis of Ammonia and Toluene

Ammonia gas (namely, A) or Ammonia + Toluene gas (namely, AT) was respectively injected into bioreactor. Ammonia and Toluene were injected at 100ppmv and 590.95ppmv. After 2 month, ammonia gas from Biofilter was collected by indophenol method. After 1 hour, absorbance was analyzed at 640nm using UV-Spectrophotometer. Toluene gas was analyzed using gas chromatography equipped Flame ionization detector (FID)

C. Analysis of Microorganisms

1. Extraction of DNA

We brought 3 Piece of Polyurethane foam adhere by Microogranimsms from bioreactor after 30days. The Polyurethane foam was put into Tris-Buffered saline (20mM Tris, 150mM NaCl). After 25 minutes, the Tris-Buffered Saline

Beomsoo Kim, Fine chemistry, Seoul National university of Science and Technology, Seoul , Republic of Korea
e-mail : redbp@naver.com
Jingyu Kim, Fine chemistry, Seoul National university of Science and Technology, Seoul , Republic of Korea
e-mail : medal12@naver.com
Daekeum Kim, Enviromental eng, Seoul National university of Science and Technology, Seoul , Republic of Korea
e-mail : kimd@seoultech.ac.kr
Joonho Parkm, Fine chemistry, Seoul National university of Science and Technology, Seoul , Republic of Korea
e-mail : jhpark21@seoultech.ac.kr

C. Analysis of Microorganisms

1. Extraction of DNA

We brought 3 Piece of Polyurethane foam adhere by Microogranimsms from bioreactor after 30days. The Polyurethane foam was put into Tris-Buffered saline (20mM Tris, 150mM NaCl). After 25 minutes, the Tris-Buffered Saline was centrifuged at 11000rpm. After 15minutes, pellet was collected. Using NucleoSpin Soil Kit (Macherey-Nagel GmbH & Co. KG, Duren, Germany), we extracted DNA

2. Sequencing Analysis

DNA (extracted at C.1) was purified by PCR purification kit. Using GS_FLX_454 Titatnium sequencer, we carried out metagenomics.

III. Result and Conclusion

A. Ammonia and Toluene degradation

The performance of biofilter with respect to ammonia and toluene removal is shown in Figure 1. During the experimental runs up to 200 days, ammonia removal was observed with consistent removal efficiency up to 100%. For toluene removal, the second operation, phase II, was recognized as a start-up period, which demonstrates the acclimation period to remove toluene. Phase III was conducted under a toluene loading of 20 ppm, and Phase IV under a toluene of 50 ppm. The overall toluene removal efficiency reached up to 95% level after a certain period each experimental phase.

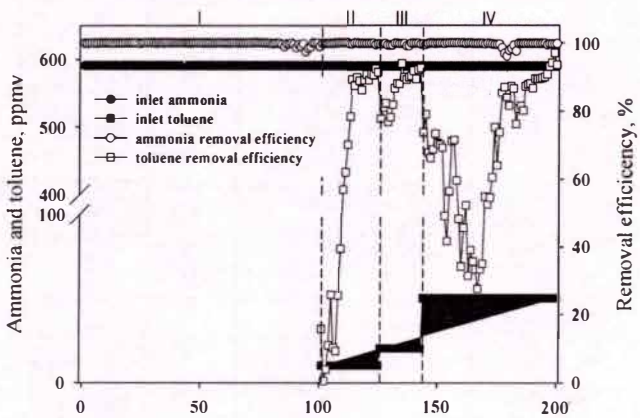

Fig. 2 BioFilter performance with respect to ammonia and toluene removals.

B. Metagenomics Analysis

The microbial populations in the media sample of the bio filter were analyzed by Metagenomic analysis. [Fig 3].1.5% or more percent microorganisms were only shown. Under the treatment of Ammonia (A), *Nitrosomonas* (37.44%) and *Pseudofulvimonas* (27.30%) species were most abundant [Fig 4]. *Nitrosomonas* were well known species as an oxidation of ammonia [6]. Under the treatment of Ammonia and Toluene (AT), *Pseudofulvimonas* (21.59%) and *Pusillimonas* (13.32 %) species were most dominant [Fig 3].

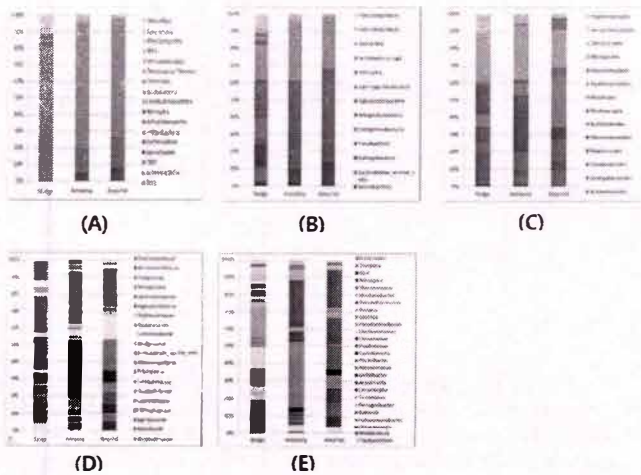

Fig. 3 Sequence composition of the 16s rRNA gene is presented at (A) phylum, (B) order, (C) family, (D) class and (E) genus.

Acknowledgment

This study was supported by the Research program funded by the Seoul National University of Science and Technology.

References

[1] Smeets, M. A., P. J. Bulsing, S. van Rooden, R. Steinmann, J. A. de Ru, N. W. Ogink, C. van Thriel and P. H. Dalton. "Odor and Irritation Thresholds for Ammonia: A Comparison between Static and Dynamic Olfactometry." Chem Senses 32, no. 1 (2007): 11-20.

[2] Mehdizadeh, S. N., M. R. Mehrnia, K. Abdi and M. H. Sarrafzadeh. "Biological Treatment of Toluene Contaminated Wastewater by Alcaligenese Faecalis in an Extractive Membrane Bioreactor; Experiments and Modeling." Water Science and Technology 64, no. 6 (2011): 1239-1246.

[3] Riesenfeld, C. S., Schloss, P. D., & Handelsman, J. (2004). Metagenomics: genomic analysis of microbial communities. Annu. Rev. Genet., 38, 525-552.

[4] Mrowiec, B. "Toluene in Sewage and Sludge in Wastewater Treatment Plants." Water Science and Technology 69, no. 1 (2014): 128-134

[5] Dange, A. D. and V. B. Masurekar. "Toluene Toxicity - Effects of Sublethal Levels on Enzyme-Activities in Seawater Adapted Tilapia (Sarotherodon-Mossambicus Peters)." Journal of Biosciences 3, no. 2 (1981): 129-134p

[6] Berube, P. M., & Stahl, D. A. (2012). The divergent AmoC3 subunit of ammonia monooxygenase functions as part of a stress response system in Nitrosomonas europaea. Journal of bacteriology, 194(13), 3448-3456.

Activated Neem Bark as a Potential Low-Cost adsorbent for the Removal of Cr(VI), Cu(II) and Zn(II) from Wastewater

Utkarsh Maheshwari, and Suresh Gupta

***Abstract*—**In the era of industrialization and urbanization, there is a huge increase in the use of metals in the industries.The effluents from these industries contains heavy metals in their effluents which leads to the deterioration of the water quality. This guide to a need for finding efficient ways for its purification and treatment.Among all the available methods, Adsorption proves to be an efficient and effectual means to handle the industrial effluents when high concentration, multiple pollutants are the main concern. The adsorption process can be made more economical by utilizing a low cost alternative to the commercial adsorbent.

In the present study, a low cost adsorption is developed using neem bark as the raw material. The bark is chemically treated with H2SO4 in a ratio of 1:1 on the weight basis while the physical treatment is given by keeping it at 50°C for 24 hours. The performance of the developed adsorbent in tested on the removal of multiple metal ions i.e. Cr(VI), Cu(II) and Zn(II) by performing equilibrium experiments. The Langmuir isotherm model satisfactorily describes the adsorption behavior and supports the monolayer adsorption during the three processes. The maximum adsorption capacity for the removal of Cr(VI), Cu(II) and Zn(II) are found to be 18.52, 19.23 and 11.49 mg g^{-1} respectively

***Keywords*—** Activation, Adsorption, Heavy Metals, Multiple Metal Ions

I. Introduction

CLEAN water is a primary concern in the present scenario of pollution. Increase in industries using metals in their processes are the primary factor of the pollution. The effluents from these industries are containing heavy metals which are much above the permissible limits and too are really harmful. This leads to a demand of finding new ways for the treatment of the effluents. Among the various methods available, adsorption is one of the methods proven to be more economical and efficient at the multiple level of pollution. Identifying a low cost material as an adsorbent for multiple metal removal can be an added advantage to the process [1-5].

The neem bark is taken as the raw material for the development of adsorbent in the present study. The performance of the developed adsorbent is evaluated by performing equilibrium experiments for the removal of various heavy metals (chromium (Cr(VI)), copper (Cu(II)) and zinc (Zn(II))). Langmuir and Freundlich isotherm models are utilized to study the adsorption behavior of the process.

Utkarsh Maheshwari (Author), Birla Institute of Technology and Science(BITS), Pilani, India
utkarsh@pilani.bits-pilani.ac.in, utkarshmaheshwari13@gmail.com
Suresh Gupta (Author), Birla Institute of Technology and Science(BITS), Pilani, India, sureshg@pilani.bits-pilani.ac.in

II. Experimental Methods

The neem bark collected from the Birla Institute of Technology and Science (BITS)-Pilani, India locality are used for the preparation of the adsorbent. The bark is further crushed and sieved to obtain the required sized (≈1.20 mm) pieces. The bark particles are further chemically treated with sulfuric acid in a proportion of 1:1 on the weight basis and later physically treated at 50°C for 24 h. The activated bark is further washed to get rid of the free acids available on the surface before using it as an adsorbent. Initially, the 1000 mg L^{-1} of stock solutions of Cr(VI), Zn(II) and Cu(II) are prepared using Potassium dichromate, Copper sulfate and Zinc sulfate respectively. The stock solution is further diluted to 5-200 mg L^{-1} of the initial concentration for the equilibrium experiments on the removal of Cr(VI), Cu(II) and Zn(II). The other parameters such as mass of adsorbent, pH and time of contact are kept constant at 6 g L^{-1}, 2.70 and 48 h respectively. The experiments are performed in the 100 ml conical flask and the proper agitation is provided using rotary shaker.

The amount of the adsorbate left in the solution is determined using Atomic Absorption Spectrophotometer (AAS) (Model: AA-7000, Shimadzu). The solid phase concentration of the metal is determined using (1) [5].

$$q_e = \frac{(C_i - C_e)V}{W} \quad (1)$$

where, q_e is the amount of metal adsorbed by the adsorbent (mg g^{-1}), C_i represents the initial concentration of sample (mg L^{-1}), C_e is concentration of metal sample at equilibrium (mg L^{-1}), V is the initial volume of the solution (L) and W is the weight of the adsorbent (g).

III. Results

The effect of the initial concentration on the removal of Cr(VI), Cu(II) and Zn(II) is studied in the present work. The

effect of the initial concentration on the removal of Cr(VI), Cu(II) and Zn(II) is shown in Fig. 1, 2 and 3 respectively.

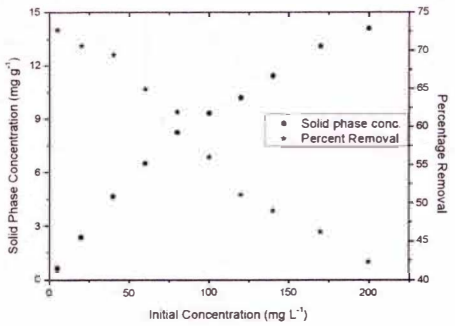

Fig. 1 Effect of initial concentration on the removal of Cr(VI)

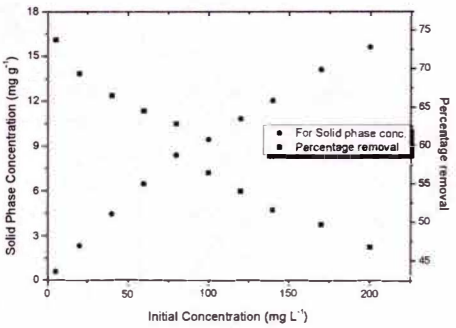

Fig. 2 Effect of initial concentration on the removal of Cu(II)

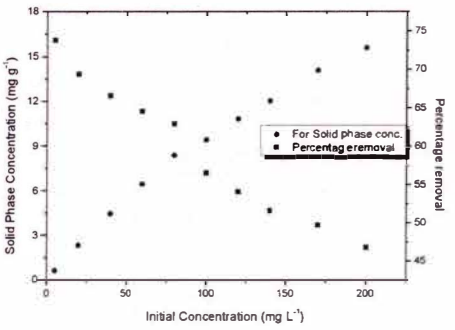

Fig. 3 Effect of initial concentration on the removal of Zn(II)

From the Fig. I, it is seen that the removal percentage of Cr(VI) decreases from 77 to 46%, while the solid phase concentration increases from 0.5 to 15 mg g^{-1} when the initial concentration varies from 5 to 200 mg L^{-1} respectively. Also, from the Fig. 2, it can be inferred that the solid phase concentration increases from 0.5 to 15 mg g^{-1} while the removal percentage of Cu(II) decreases from 74 to 44% for the increase in the initial concentration from 5 to 200 mg L^{-1} respectively. Similarly from the Fig. 3, it is seen that the removal percentage of Zn(II) decreases from 53 to 36%, while the solid phase concentration increases from 0.5 to 11 mg g^{-1} for the increase in the initial concentration from 5 to 200 mg L^{-1} respectively.

The reduction in the percentage removal is due to the availability of more amount of the adsorbate in comparison to the same quantity of the adsorbent dosage available for adsorption. This also leads to an increase in the adsorption capacity.

IV. Isotherm Study

Isotherm models are an important mode of explaining the adsorption behavior of the process, especially when the adsorbents are new in the system. The isotherm models help in understanding the relationship between the solid and liquid phase concentrations. There are a number of adsorption models available in the literature. In the present study, Langmuir and Freundlich isotherm models are utilized for understanding the behavior of the process.

A. Langmuir Isotherm Model

Langmuir isotherm is one of the simplest isotherm, which is used by a number of researchers to explain the behavior of their adsorption systems [1-5]. Langmuir isotherm is based on the assumption of having monolayer adsorption of the adsorbate on the adsorbent surface. The linear form of the isotherm is presented below in (2).

$$\frac{C_e}{q_e} = \frac{1}{bq_m} + \frac{C_e}{q_e} \tag{2}$$

where q_m is representing the maximum adsorption capacity while b is the Langmuir isotherm coefficient.

The linear plot for the Langmuir isotherm model for the removal of Cr(VI), Cu(II) and Zn(II) are presented in Fig. 4. The parameters evaluated are given in Table I.

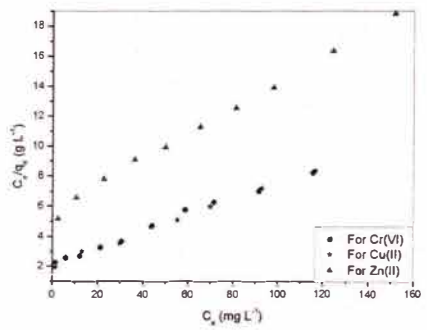

Fig. 4 Langmuir isotherm plot for the removal of Cr(VI), Cu(II) and Zn(II)

B. Freundlich Isotherm

The Freundlich isotherm model is another model used by a number of researchers. It is assumed to follow heterogeneous adsorption phenomena [1-3,7]. The linearized Freundlich model is represented by (3).

$$\log(q_e) = \log(K_F) + \frac{1}{n_F}\log(C_e) \tag{3}$$

where n_F and K_F are representing the Freundlich isotherm constants. The linear plot of Freundlich isotherm for the removal of Cr(VI), Cu(II) and Zn(II) is presented in Fig. 5. The parameters are evaluated and tabulated in Table 1.

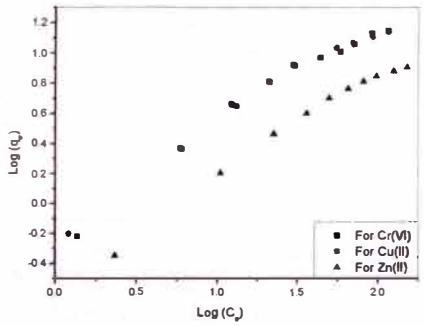

Fig. 5 Freundlich isotherm plot for the removal of Cr(VI), Cu(II) and Zn(II)

TABLE I:
ISOTHERM CONSTANTS FOR THE REMOVAL OF CR(VI), CU(II) AND ZN(II)

		Cr(VI)	Cu(II)	Zn(II)
Langmuir	q_m	18.52	19.23	11.49
	b	0.024	0.022	0.016
	R^2	0.990	0.995	0.996
Freundlich	K_F	0.649	0.676	0.294
	n_F	0.691	0.628	0.697
	R^2	0.967	0.976	0.983

From the correlation coefficient, it is clear that the adsorption removal of Cr(VI), Cu(II) and Zn(II) are best described by the Langmuir isotherm model. This supports the formation of monolayer on the surface of the adsorbent i.e. activated neem bark during the adsorption process.

V. CONCLUSION

In the present work, neem bark is used for the development of the adsorbent. The bark is further treated chemically and physically to make it use for the removal of multiple metal ions. The performance of the developed adsorbent is analyzed for the removal of Cr(VI), Cu(II) and Zn(II) by performing equilibrium experiments. The activated neem bark is found suitable for the removal of the three metal ions. Also it is found that the adsorption removal of all the three i.e. Cr(VI), Cu(II) and Zn(II) is well defined by the Langmuir isotherm model supporting the monolayer adsorption during the process. The maximum adsorption capacity obtained for the removal of Cr(VI), Cu(II) and Zn(II) using activated neem bark is found to be 18.52, 19.23 and 11.49 mg g^{-1} respectively.

ACKNOWLEDGEMENT

The authors would like to thank the University Grants Commission (UGC), New Delhi and the Department of Science & Technology (DST), New Delhi for financial assistance.

REFERENCES

[1] B. V. Babu and S. Gupta, "Removal of Cr(VI) from wastewater using activated tamarind seeds as an adsorbent" in J Environ Eng Sci, vol. 7 (5), 2008, pp. 553-557.

[2] S. Gupta and B. V. Babu, "Removal of toxic metal Cr(VI) from aqueous solutions using sawdust as adsorbent: Equilibrium, kinetics and regeneration studies" in Chem Eng J, vol. 150 (2–3), 2009. pp. 352-365.

[3] S. Gupta and B. V. Babu, "Utilization of waste product (tamarind seeds) for the removal of Cr(VI) from aqueous solutions: Equilibrium, kinetics, and regeneration studies" in J Environ Manage, vol. 90 (10), 2009, pp. 3013-3022.

[4] U. Maheshwari and S. Gupta, "Kinetic and Equilibrium Studies of Cr (VI) Removal from Aqueous Solutions using Activated Neem Bark" in Research Journal of Chemistry and Environment, vol. 15 (2), 2011, pp. 939-943.

[5] K. K. Panday, G. Prasad and V. N. Singh, "Copper(II) removal from aqueous solutions by fly ash" in Water Research, vol. 19 (7), 1985, pp. 869-873.

[6] S. Gupta and B. V. Babu, "Experimental, kinetic, equilibrium and regeneration studies for adsorption of Cr(VI) from aqueous solutions using low cost adsorbent (activated flyash)" in Desalination and Water Treatment, vol. 20 (1-3), 2010, pp. 168-178.

[7] R. J. Bhargavi, M. Utkarsh and G. Suresh, "Synthesis and Use of Alumina Nano-Particles as an Adsorbent for the Removal of Zn(II) and CBG Dye from Wastewater" in International Journal of Industrial Chemistry, vol. 2014.

Removal of Organic Constituents from Treated Wastewater using Nanotechnology and Advanced Oxidation Processes

Mahad S. Baawain, Hajar Al-Balushi, Abdulsalam Al Zakwani

***Abstract*—** Water is subjected to pollution with impurities and contaminations as a result of increasing urbanization, industrial activities and population growth. Consequently, more technological treatments are needed to eliminate/reduce the pollutants from water. In this study, photocatalytic degradation (nanomaterials of Zinc Oxide (ZnO) and Titanium Dioxide (TiO_2) activated with ultraviolet radiation (UV)) and advanced oxidation processes (O_3 and O_3/UV) were used to degrade organics from water samples. A known amount of Potassium Hydrogen Phthalate with two different concentrations (1,000 mg/L and 500 mg/L) were injected in synthetic water samples. The synthetic water samples were treated with ZnO/UV, TiO_2/UV, O_3 and O_3/UV at different loads. Optimum removal efficiency of TOC and COD was found to be at 15 mg/mL of TiO_2 and 30 mg/mL of ZnO. It was found that the removal efficiency of TOC using O_3 and UV combination is higher than O_3 alone. Also, the TOC removal efficiency increased as the ozonation time increased. Treated wastewater sample, collected from a local wastewater treatment plant, was treated with 15 mg/mL of TiO_2. The removal efficiency for TOC and COD were found to be 31 % and 83%, respectively.

***Keywords*—** Organic constituents, treated wastewater, nanotechnology, advanced oxidation.

I. Introduction

IT is important to keep the water fresh, clean and free from contaminants for human uses [1]. The pollution due to organic contaminants is very risky due to their hazardous and toxic nature [2]. The organics in water are indicated by Chemical Oxygen Demand (COD), Biological Oxygen Demand(BOD), and Total Organic Carbon (TOC). Some methods in removing organics from water are advanced oxidation processes, electrolysis, reverse osmosis, electro-dialysis, ion exchange, membranes, adsorption, electrochemical and nanotechnology [1-6].

Nanotechnology is described by the use of materials lesser than 100 nm which are called nanoparticles or nanomaterials [1, 7]. This technology has general applications in industrial, agricultural and environmental sectors [8]. Therefore, it has the future to become a major industry over the next 10-15 years [5]. The advances in nanotechnology applications provide opportunities to overcome the different problems and challenges in water system.

Moreover, advance oxidation processes (AOPs) are among the best alternatives to degrade the organic pollutants. AOPs are chemical oxidation processes with hydroxyl radicals, which are very reactive and short-lived oxidants. The radicals need to be produced on site, in a reactor where the radicals can react with the organics in the water or wastewater. Hydroxyl radicals may be produced in systems using: Ozonation (O_3), Ultraviolet Light (UV), Hydrogen Peroxide (H_2O_2), Photocatalysis, and Ozone in combination with UV (UV/O_3), ozone plus hydrogen peroxide (O_3/H_2O_2), and Hydrogen Peroxide and Ultraviolet Light (H_2O_2/UV) [9].

This paper discussed the importance of nanotechnology and AOPs applications in wastewater treatment. It aims at evaluating the removal of organic constitutes from treated wastewater by using nanotechnology and AOPs. The removal efficiency will be evaluated by measuring chemical oxygen demand (COD), and total organic carbon (TOC).

II. Background

A. Applications of Nanotechnology in Wastewater Treatment

Nanomaterials have a great scope to improve wastewater treatment, due to their features concourse with present treatment technologies such as ultraviolet (UV) disinfection. In future, nanotechnology will bring a broad change in wastewater technologies [1, 6, 8]. For a material to be used for water disinfection, it must show a strong antimicrobial activity whereas lasting harmless to humans. There are factors to be considered for suspended nanoparticles that affect its capability as a disinfectant. These factors are; the existence of salts that encourage precipitation and coagulation, conflicting species that consume Reactive oxygen species (ROS), and natural organic matter that coats on nanoparticles and shrinks their bioavailability [6].

The unique properties of nanomaterials can be exploited to yield enhanced adsorbents, reactive or photocatalytic

Mahad S. Baawain, Hajar Al-Balushi, Abdulsalam Al Zakwani, Department of Civil and Architectural Engineering, Sultan Qaboos University
Oman. msab@squ.edu.om

materials, and improved membranes. The present cost of nanomaterials is excessively high except for nano-TiO_2, nanoscale iron oxide, and polymeric nanofibers. This can be solved by using low purity nanomaterials. However the cost-effectiveness can be enhanced by retaining and reusing nanomaterials [1].

B. Applications of AOPs in Wastewater Treatment

Ozone has long been used for disinfection, taste and odor management, and color removal in water treatment facilities. Ozone reacts with natural organic matter (NOM) by an electrophilic addition to double bonds. This reaction is very selective. In addition to direct reaction of ozone with NOM, non-selective and fast reaction occurs with OH radicals that are formed when ozone decomposes in water. Compared to AOPs, the OH radical formation potential is much lower. The oxidation potentials for ozone and OH radical are 2.42 and 2.86 eV, respectively. There are several solutions to promote the OH radical production in ozonation process. The easiest and cheapest solution to convert a conventional ozonation process into AOP is the addition of H_2O_2. Another alternative is the combination of ozone with UV irradiation or the combination of all three [10].

III. Methodology

The experiments of nanotechnology and AOPs were conducted on a batch mode. In order to evaluate the performance of the treatment systems to degrade the organic content, influents and effluents from each system were analyzed for chemical oxygen demand (COD) and total organic carbon (TOC). The conducted tests were based on Standard Methods for Examination of Water and Wastewater [11].

IV. Results and Discussion

A. Nanotechnology Results

Table I shows that the maximum removal efficiencies in TOC and COD were 10.5 % and 24.69%, respectively when using 10 mg/mL of TiO_2 load. The minimum removal in TOC and COD was 3.61% and 13.2 %, respectively, were obtained when 300 mg/mL of TiO_2 was used. Therefore, 10 mg/mL of TiO_2 is the best among the different loads.

Table II shows that the maximum TOC removal (35.2%) accorded with the lowest amount of Potassium Hydrogen Phthalate (5 mL).The removal kept decreasing with the increase of Potassium Hydrogen Phthalate amount. It reached the lowest percentage (4.04%) at 20 mL of Potassium Hydrogen Phthalate. Furthermore, the maximum COD removal (45.21%) was obtained at 10 mL of Potassium Hydrogen Phthalate and the minimum removal percentage (6.99%) was at 25 mL of Potassium Hydrogen Phthalate. It can be concluded that, with the increase in Potassium Hydrogen Phthalate (concentration = 1,000 mg/L) amount; the removal efficiency of Titanium Dioxide decreases. This may be due to the high concentration of Potassium Hydrogen Phthalate that coat the nanomaterial and thus lower its removal efficiency.

TABLE I
TOC AND COD REMOVAL FOR FIXED $C_8H_5KO_4$ (1,000 MG/L) WITH VARIED TiO_2 LOADS

TiO_2 (mg/mL)	TOC Removal (%)	COD Removal (%)
10	10.50	24.69
50	9.92	20.45
100	5.71	15.01
200	6.30	21.13
300	3.61	13.20

TABLE II
TOC AND COD REMOVAL FOR 10 MG/ML TiO_2 WITH VARIED $C_8H_5KO_4$

$C_8H_5KO_4$ (mL)	TOC Removal (%)	COD Removal (%)
5	35.20	36.94
10	15.96	45.21
15	14.41	32.47
20	4.04	15.77
25	0	6.99

Table III shows that the maximum removal in TOC and COD (7.89 % and 16.46%, respectively) when using 30 mg/mL of ZnO load. The COD results were quit consistent with TOC results and the maximum was at 30 mg/mL of ZnO. Therefore, 30mg/mL of ZnO is the best among the different loads.

TABLE III
TOC AND COD REMOVAL FOR FIXED $C_8H_5KO_4$ (1,000 MG/L) WITH VARIED ZNO LOADS

ZnO (mg/mL)	TOC Removal (%)	COD Removal (%)
10	5.55	6.85
20	2.41	9.76
30	7.89	16.46
40	2.43	10.97
50	4.63	16.05

Table IV shows that the maximum removal of TOC and COD, 7.62 % and 53.97 %, respectively, corresponding to 10 ml of Potassium Hydrogen Phthalate (concentration = 1,000 mg/L). It can be observed that the removal decreases continuously when Potassium Hydrogen Phthalate amount increases.

TABLE IV
TOC AND COD REMOVAL FOR 30 MG/ML TNO WITH VARIED $C_8H_5KO_4$

$C_8H_5KO_4$ (mL)	TOC Removal (%)	COD Removal (%)
5	-	23.03
10	7.62	53.97
15	4.32	26.62
20	5.03	7.28
25	2.07	1.40

B. AOPs Results

Two samples of distilled water and tap water mixed with Phenol were tested using O_3 and O_3/UV at different ozonation times (5, 10, 15, 20 and 30 min) separately. Table V shows the TOC removal efficiency for distilled water and tap water mixed with phenol. It was found that the combination of O_3 and UV has higher removal efficiency than O_3. However, the

TABLE V
TOC REMOVAL FOR DISTAL WATER AND TAP WATER MIXED WITH PHENOL

Sample	Ozonation Time (min.)	TOC (mg/L)		TOC Removal (%)	
		O3	O3+UV	O3	O3+UV
Distilled water + phenol	0	117	117	0	0
	10	105	102	10.2	12.6
	20	102	87.0	12.6	25.4
	30	99	96.0	15.2	17.5
Tap Water + phenol	0	97.89	97.9	0	0
	5	83.18	71.4	15.0	27.0
	10	78.01	66.2	20.3	32.4
	15	77.44	65.5	20.9	33.1
	20	75.58	66.5	22.8	32.0
	30	62.1	67.0	36.6	30.8

The ozonation time that achieved the best removal (20 min) was fixed against variable amounts of phenol initial concentrations in water samples (Table IV). It can be seen that the removal efficiency decreases as the organic content (i.e. TOC) in the sample increases.

TABLE VI
TOC REMOVAL EFFICIENCY WITH FIXED OZONATION TIME FOR DIFFERENT PHENOL CONCENTRATIONS

Sample	Ozonation Time (min.)	TOC (mg/L)		TOC Removal (%)
		Before	O_3+UV	
Tap water + phenol	20	60.1	38.13	36.5
	20	110	78.8	28.1
	20	168	130	22.7
	20	219	153	30.4

V. CONCLUSIONS

Zinc Oxide and Titanium Dioxide were used to remove organic matter in treated wastewater and their removal efficiency was evaluated. Known amounts of Potassium Hydrogen Phthalate were injected in synthetic water samples and were treated with different loads of Zinc Oxide and Titanium Dioxide. TOC and COD were performed for samples before and after treatment. Optimal removal efficiency of TOC and COD were found to be at 30 mg/mL of ZnO and 15 mg/mL of TiO_2.

Furthermore, the AOPs experiments were conducted by using O_3 and a combination of O_3 and UV. It was found that the removal efficiency of TOC using the combination of O_3 and UV combination is higher than O_3 alone. Also, the TOC removal efficiency increased as the ozonation time increased.

ACKNOWLEDGMENT

The authors would like to acknowledge the financial support received form The Research Council (TRC) of Oman under the grant number RC/ENG/CAED/11/01.

REFERENCES

[1] Qu, X., P. J. J. Alvarez. (2013). "Applications of nanotechnology in water and wastewater treatment." *Water Research* 47(12): 3931-3946.
[2] Ali, I., M. Asim. (2012). "Low cost adsorbents for the removal of organic pollutants from wastewater." *Journal of Environmental Management* 113(0): 170-183
[3] 14. Xu, P., G. M. Zeng. (2012). "Use of iron oxide nanomaterials in wastewater treatment: A review." *Science of The Total Environment* 424(0): 1-10.
[4] Mook, W. T., M. H. Chakrabarti. (2012). "Removal of total ammonia nitrogen (TAN), nitrate and total organic carbon (TOC) from aquaculture wastewater using electrochemical technology: A review." *Desalination* 285(0): 1-13.
[5] Rejeski, D. and E. S. Michelson (2009). "Chapter 33 - International Governance Perspectives on Nanotechnology Water Innovation." Nanotechnology Applications for Clean Water, William Andrew Publishing, pp 509-519.
[6] Mahendra, S., Q. Li, et al. (2009). "Chapter 12 - Nanotechnology-Enabled Water Disinfection and Microbial Control: Merits and Limitations." Nanotechnology Applications for Clean Water, William Andrew Publishing, pp 157-166.
[7] Reijnders, L. (2006). "Cleaner nanotechnology and hazard reduction of manufactured nanoparticles." *Journal of Cleaner Production* 14(2): 124-133.
[8] Brar, S. K., M. Verma. (2010). "Engineered nanoparticles in wastewater and wastewater sludge – Evidence and impacts." *Waste Management* 30(3): 504-520.
[9] Esplugas, S., J. Giamenez, S. Contreras. (2001). "Comparsion of different advanced oxidation processes for phenol degradation." *Water Research* 36: 1034-1042.
[10] Matilainen, M., A. Sillanpää. (2010. Removal of natural organic matter from drinking water by advanced oxidation processes. *Chemosphere*, 80(4): 351–365.
[11] Eaton D., Clesceri S. and Greenberg E. 1995. Standard Methods for the Examination of Water and Wastewater, American Public Health Association and Water Environment Federation.

SECTION-II

International Conference on Biotechnology, Nanotechnology and Environmental Engineering (ICBNE'15)

Eco-Friend Flame Retarding High Temperature Poly(Cyclohexylene Dimethyl Terephthalate) For Led Packaging Application

Jinhwan Kim, H.Y. An

Abstract— Partly aromatic polyesters such as poly(ethylene terephthalate) (PET) or poly(1,4-butylene terephthalate) (PBT) are made by reacting terephthalic acid with aliphatic diol and widely used as engineering plastics in electric and electronic applications. Recently, lots of attention have been paid to another type of partly aromatic polyester, poly(cyclohexylene dimethylene terephthalate) (PCT), having higher heat resistance and hygrothermal stability compared to PET and PBT. The structural formula of PCT is shown in Fig. 1. When the thermal properties of three polymers are determined by a differential scanning calorimetry (DSC), the crystalline melting temperature (T_m) of PBT, PET, and PCT are 227, 243, and 289 °C, respectively. PCT possesses the highest T_m and is suitable for high temperature electric and electronic applications. PCT's high T_m and good hygrothermal stability coming from its inherent cycloaliphatic structural unit find its application as an adequate material for the "reflector", the molded part of LED devices such as high power lightenings. Since PCT is used in electric and electronic applications, the impartment of flame retardancy is essential and the development of effective halogen-free system is very demanding. However, no publication has been reported on this subject. In this study, the pyrolysis and flame behavior of PCT are investigated by employing the metal (Aluminum) complex of alkyl phosphinate as a main FR. Moreover, Melamin cyanurate(MC) and Melamin Polyphophate (MPP) are used as synergists to understand the combustion mechanism. The results are compared with the flame retardancy behavior of PBT system. The flame retarding performances of various formulations are studied by Underwriters Laboratories test (UL-94) and thermogravimetric analysis (TGA). The charred residues are investigated by FT-IR (ATR) spectrophotometry and scanning microscope (SEM). A decomposition mechanism is also postulated on the basis of experimental results.

Keywords— Poly(cyclohexylene dimethylene terephthalate), LED devices, Flame retardancy, Decomposition mechanism

Jinhwan Kim, Sungkyunkwan University, Korea (South), jhkim@skku.edu
H.Y.An, Sungkyunkwan University, Korea (South)

Highly-Efficient Semitransparent Solar Cells with Good Transparency, Color Perception, and Rendering Properties

Chih-Yu Chang*

***Abstract*—**Polymer solar cells are of great interest as an alternative renewable energy source to typical silicon-based photovoltaic cells due to their potential for cost-effective large-area manufacturing, light-weight, and mechanical flexibility. Semitransparent (ST) solar cells, in particular, have great potential for power-generating window applications, which permits daylight to pass through while generating electricity. In this study, we demonstrate highly-efficient ST solar cells through the development of innovative materials and device structures. Two polymers are used in this study, including a novel fluoro-containing low bandgap polymer poly[2,6-(4,4-bis(2-ethylhexyl)-4H-cyclopenta[2,1-b;3,4-b']dithiophene)-alt-4,7-(5-fluoro-2,1,3-benzothia-diazole)] (PCPDTFBT) and a medium bandgap polymer poly(indacenodithiophene-co-phananthrene-quinoxaline) (PIDT-phanQ). Considering the major absorption of PCPDTFBT locates at the near infrared region and most of the visible light is unutilized, the semitransparent cell based on PCPDTFBT exhibits a PCE of 5.0% and an average visible transmittance (AVT) of 47.3%, which represents the highest value reported for ST cells with similar transparency. In addition, we also employed a novel tandem structure to improve the light absorption for better energy conversion in a ST cell. The resulting ST cell based on PIDT-phanQ exhibits a high PCE of 7.4%, which is the highest value reported so far for a ST solar cell. The nearly identical current density between the measured value and the predicted value from optical simulation indicates that there is no significant electrical loss in the device. More importantly, this ST cell also possesses a desirable AVT (~40%) and an excellent color rendering index (~100), which enables its use for power generating window applications.

***Keywords*—** polymer solar cell, tandem solar cell, semitransparent cell, organic electronics, efficiency.

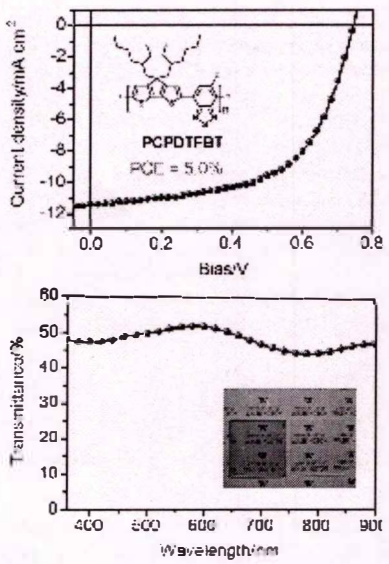

Fig. 1 *J-V* characteristics and AVT of a ST cell based on PCPDTFBT (inset: a photograph of a ST cell).

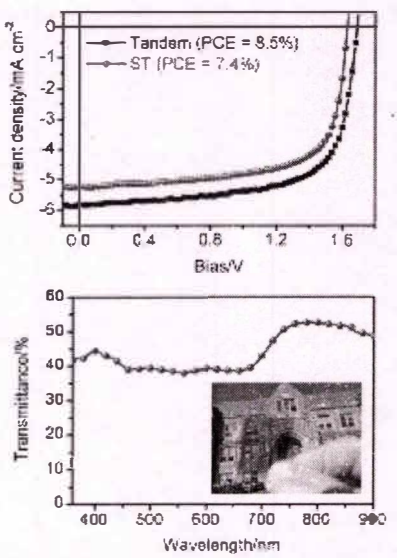

Fig. 2 *J-V* characteristics and AVT of a ST cell based on PIDT-phanQ (inset: a photograph of a ST cell).

Department of Materials Science and Engineering, Feng Chia University, Taichung, TAIWAN
*No. 100, Wenhwa Rd., Seatwen, Taichung, TAIWAN 40724; changcyu@fcu.edu.tw.

Preparation and Characterization of Photoluminescent Electrospun Nanofiber of Carbon Quantum Dots and Polyacrylonitrile

Cho-Hye Lee, Al-Mahmnur Alam, Mira Park, and Hak-Yong Kim

Abstract—In this study, novel photoluminescence (PL) nanofibers consist of carbon quantum dots (CQDs) and polyacrylonitrile (PAN) were fabricated by the electrospining process. The CQDs containing nanofibers were characterized by field-emission scanning electron microscopy (FESEM), transmission electron microscopy (TEM), fourier transform infrared spectroscopy (FTIR), X-ray photoelectron spectroscopy (XPS) and confocal microscopy. CQDs are familiar to emit blue, green and red color depending on the excitation. The PAN/CQDs nanofibers were found to be exhibited PL properties similar to CQDs. Therefore, blue, green and red color was observed under confocal microscope from the nanofibers membrane while the sample was excited by 405 nm, 488 nm and 543 nm lasers.

Keywords—Electrospinning, Carbon quantum dots, Polyacrylonitrile

Cho-Hye Lee/BIN Fusion Technology
Chonbuk National University, South Korea
thmxum@naver.com
Hak-Yong Kim/BIN Fusion Technology
Chonbuk National Technology, South Korea
khy@jbnu.ac.kr

Polyacrylonitrile Composite Nanofibers Encapsulated with Ag_2CO_3 Nanoparticles: A Study on the Effect of Photocatalytic Performances of Composite Nanofibers Electrospun at Different Applied Electric Voltages

Tae-Hee An, Gopal Panthi, Mira Park, Soo-Jin Park, and Hak-Yong Kim

Abstract—polyacrylonitrile (PAN)/Ag_2CO_3 composite nanofibers were fabricated via simple and versatile technique: electrospinning of colloidal solution of PAN and Ag_2CO_3 nanoparticles at different applied electric voltages. Synthesis of Ag_2CO_3 nanoparticles was carried out by ion exchange reaction between $Ag(NH_3)_2^+$ and $NaHCO_3$ in aqueous solution. FESEM and TEM analysis revealed that Ag_2CO_3 nanoparticles were completely encapsulated within PAN nanofibers in all formulations, which can be helpful to avoid the photocorrosion and separation difficulty of photocatalyst in large scale application. Photocatlytic efficiency of the introduced composite nanofibers was evaluated by photodegradation of methylene blue (MB) and rhodamine B (RhB) under visible light irradiation. On the basis of experimental results composite nanofibers obtained at applied electric voltage of 18 kV (PAN/Ag_2CO_3-18) was found to be more superior towards the photodegradation of organic contaminants. Overall, this sort of composite material may represent a new promising alternative with wide range of potential application in the field of water treatment.

Keywords— Electrospinning; Photocatalyst; Visible light; Silver carbonate; Organic contaminants

[1]

Tae-hee An/BIN fusion technology, Chonbuk national university, South Korea
ath624@naver.com
Hak-Yong Kim/BIN fusion technology, Chonbuk national university, South Korea, khy@jbnu.ac.kr

Preparation of Pt Impregnated Boron Doped Graphene Catalyst for High-Temperature Proton Exchange Membrane Fuel Cells

H.N. Yang, K.W. Park, and W.J. Kim*

Abstract—Graphene is composed by one-atom thick sheet of hexagonal arrangement of carbon atoms and is the base of all graphitic forms of carbon materials, which has high mechanical strength, feasible electro conductivity and high surface area. Recently, many researches have focused on the enhancement of electrochemical properties of graphene through heteroatom doping such as boron and nitrogen. Especially, boron doped graphene (B-Gr) shows lower electron transfer resistance toward redox probe and higher carrier concentration than graphene.

Graphene or modified graphene has been gradually used as a catalyst supporting materials while Nafion has been most widely used as a membrane in polymer electrolyte membrane fuel cell (PEMFC) under low temperature condition. Nafion membrane, however, has some problems such as high fuel crossover, low conductivity at low humidity, difficult water and heat management. In order to overcome these problems, a high temperature PEMFC (HT-PEMFC) to be operated above at 100 ℃ has been studied. As the part of developing HT-PEMFC, cost effective and thermally stable membranes have been developed. Poly [2, 2-(m-phenylene)-5,5-bibenzimidazole](PBI) is considered to be the best candidate high temperature membrane due to its excellent thermal, oxidative, chemical and hydrolytic stability under operation conditions. As of now, however, Pt-B-Gr has not been reported as a catalyst in HT-PEMFC.

In this study, B-Gr was prepared by pyrolytic synthesis of boric acid and graphene oxide (GO) with different doping levels (from 1 to 5 times). GO was synthesized by modified hummers method from graphite. Pt nanoparticles were then impregnated using microwave method. As-prepared Pt-B-Gr was characterized by XRD, SEM and FT-IR, TGA, TEM, and XPS. Electrochemical properties of Pt-B-Gr with various doping levels was confirmed by CV, the single cell test of membrane electrode assembly(MEA) using PBI membrane was conducted with 0.5 mg/ cm^2 of Pt loading both at anode and cathode, respectively. Finally, the effects of boron doping levels of catalyst layer fabricated on the cell performance were studied at 150 ℃.

Keywords—Graphene, doping level, PBI, High-temperature PEMFC.

Heena Yang, Konkuk university, Republic of Korea
gmlsk29@konkuk.ac.kr
Kyungwoo Park, Konkuk university, Republic of Korea
park9681@konkuk.ac.kr
Whajung Kim, Konkuk university, Republic of Korea
whajungk@konkuk.ac.kr

Electrochemical Properties of Cathode Catalyst with Dual Pore Structures Based On Pt-CB and Mesoporous CMK-3 as a Supporting Layer in Polymer Electrolyte Membrane Fuel Cell

K.W. Park, H.N. Yang, W.H Lee, B.S Choi, and W.J. Kim

Abstract— Mesoporous carbon molecular sieve, CMK-3 is synthesized from silicate template (SBA-15) and sucrose as the carbon source. CMK-3 is a carbon molecular sieve with mesoporous structure. In this study, the electrochemical properties of cathode catalyst based on Pt-CB and mesoporous CMK-3 as a supporting layer are evaluated and the MEA using this dual layer at cathode was tested in polymer electrolyte membrane fuel cell. In addition, the effect of thickness of supporting layer on the cell performance is investigated. The cell performance of dual layer catalyst shows the enhancement, depending on the thickness of mesoporous supporting layer. It is attributed to the facilitation of mass transfer due to the facile water removal from the cathode due to capillary force exerted from mesoporous supporting layer by CMK-3 as well as the prevention of Pt loss into the gas diffusion layer (GDL).

Keywords— PEMFC, capillary force, mesoporous carbon, cell performance.

Kyungwoo Park, College of engineering , Konkuk University, Republic of Korea, park9681@konkuk.ac.kr
Heena Yang, College of engineering , Konkuk University, Republic of Korea, gmlsk29@konkuk.ac.kr
Woonghee Lee, College of engineering , Konkuk University, Republic of Korea, whlee202@hanmail.net
Beomseok Choi, College of engineering , Konkuk University, Republic of Korea, bschoi8375@naver.com
Whajung Kim, College of engineering, Konkuk University, Republic of Korea, whajungk@konkuk.ac.kr